iScience

CellPress
OPEN ACCESS

Article

From *Tg*O/GABA-AT, GABA, and T-263 Mutant to Conception of *Toxoplasma*

Joseph Lykins, Matthew J. Moschitto, Ying Zhou, Ekaterina V. Filippova, ..., Hernan A. Lorenzi, Richard B. Silverman, Rima L. McLeod

efilippova@uchicago.edu (E.V.F.)
hernan.lorenzi@nih.gov (H.A.L.)
r-silverman@northwestern.edu (R.B.S.)
rmcleod@uchicago.edu (R.L.M.)

Highlights

*Tg*O/GABA-AT uses GABA or ornithine as a substrate

Co-crystallized inactivators elucidate structure with selective inactivators identified

Increased in merozoites/ sporozoites, regulated by MORC is un-essential for oocysts

Sequencing clone incapable of zygote formation reveals mutated related genes

Lykins et al., iScience 27, 108477
January 19, 2024
https://doi.org/10.1016/j.isci.2023.108477

iScience

CellPress
OPEN ACCESS

Article

From *Tg*O/GABA-AT, GABA, and T-263 Mutant to Conception of *Toxoplasma*

Joseph Lykins,[1,18,26] Matthew J. Moschitto,[2,19,26] Ying Zhou,[3,26] Ekaterina V. Filippova,[4,20,26,*] Hoang V. Le,[2,21,26] Tadakimi Tomita,[5] Barbara A. Fox,[6] David J. Bzik,[6] Chunlei Su,[7] Seesandra V. Rajagopala,[8,22] Kristin Flores,[4] Furio Spano,[9] Stuart Woods,[10] Craig W. Roberts,[10] Cong Hua,[3] Kamal El Bissati,[3] Kelsey M. Wheeler,[3,23] Sarah Dovgin,[3,24] Stephen P. Muench,[11] Martin McPhillie,[12] Colin W.G. Fishwick,[12] Wayne F. Anderson,[4,13] Patricia J. Lee,[14] Mark Hickman,[14] Louis M. Weiss,[5,15] Jitender P. Dubey,[16] Hernan A. Lorenzi,[8,25,*] Richard B. Silverman,[2,13,*] and Rima L. McLeod[3,17,27,*]

SUMMARY

***Toxoplasma gondii* causes morbidity, mortality, and disseminates widely via cat sexual stages. Here, we find *T. gondii* ornithine aminotransferase (OAT) is conserved across phyla. We solve *Tg*O/GABA-AT structures with bound inactivators at 1.55 Å and identify an inactivator selective for *Tg*O/GABA-AT over human OAT and GABA-AT. However, abrogating *Tg*O/GABA-AT genetically does not diminish replication, virulence, cyst-formation, or eliminate cat's oocyst shedding. Increased sporozoite/merozoite *Tg*O/GABA-AT expression led to our study of a mutagenized clone with oocyst formation blocked, arresting after forming male and female gametes, with "Rosetta stone"-like mutations in genes expressed in merozoites. Mutations are similar to those in organisms from plants to mammals, causing defects in conception and zygote formation, affecting merozoite capacitation, pH/ionicity/sodium-GABA concentrations, drawing attention to cyclic AMP/PKA, and genes enhancing energy or substrate formation in *Tg*O/GABA-AT-related-pathways. These candidates potentially influence merozoite's capacity to make gametes that fuse to become zygotes, thereby contaminating environments and causing disease.**

[1]Pritzker School of Medicine, University of Chicago, Chicago, IL 60637, USA
[2]Department of Chemistry, Department of Molecular Biosciences, Chemistry of Life Processes Institute, Center for Molecular Innovation and Drug Discovery, and Center for Developmental Therapeutics, Northwestern University, Evanston, IL 60208-3113, USA
[3]Department of Ophthalmology and Visual Sciences, The University of Chicago, Chicago, IL 60637, USA
[4]Center for Structural Genomics of Infectious Diseases and the Department of Biochemistry and Molecular Genetics, Northwestern University, Feinberg School of Medicine, Chicago, IL 60611, USA
[5]Division of Parasitology, Department of Pathology, Albert Einstein College of Medicine, Bronx, NY 10461, USA
[6]Department of Microbiology and Immunology, Geisel School of Medicine at Dartmouth, Lebanon, NH 03756, USA
[7]Department of Microbiology, University of Tennessee, Knoxville, TN 37996, USA
[8]Department of Infectious Diseases, The J. Craig Venter Institute, 9704 Medical Center Drive, Rockville, MD 20850, USA
[9]Department of Infectious Diseases, Istituto Superiore di Sanità, Rome, Italy
[10]Strathclyde Institute of Pharmacy and Biomedical Sciences, University of Strathclyde, Glasgow Scotland, UK
[11]School of Biomedical Sciences and Astbury Centre for Structural Molecular Biology, The University of Leeds, Leeds, West York LS2 9JT, UK
[12]School of Chemistry and Astbury Centre for Structural Molecular Biology, University of Leeds, Leeds, UK
[13]Department of Pharmacology, Northwestern University, Chicago, IL 60611, USA
[14]Division of Experimental Therapeutics, Military Malaria Research Program, Walter Reed Army Institute of Research, 503 Robert Grant Avenue, Silver Spring, MD 20910, USA
[15]Division of Infectious Diseases, Department of Medicine, Albert Einstein College of Medicine, Bronx, NY 10461, USA
[16]Animal Parasitic Diseases Laboratory, Beltsville Agricultural Research Center, Agricultural Research Service, United States Department of Agriculture, Beltsville, MD 20705, USA
[17]Department of Pediatrics (Infectious Diseases), Institute of Genomics, Genetics, and Systems Biology, Global Health Center, Toxoplasmosis Center, CHeSS, The College, University of Chicago, Chicago, IL 60637, USA
[18]Present address: Department of Emergency Medicine, Chobanian & Avedisian School of Medicine at Boston University, Boston, MA 02118, USA
[19]Present address: Department of Medicinal Chemistry, Rutgers University, Piscataway, NJ 08854, USA
[20]Present address: Department of Biochemistry and Molecular Biology, The University of Chicago, Chicago, IL 60637, USA
[21]Present address: National Institute on Drug Abuse, National Institutes of Health, North Bethesda, MD 20852, USA
[22]Present address: Division of Infectious Diseases, Department of Medicine, Vanderbilt University Medical Center, Nashville, TN 37232, USA
[23]Present address: Massachusetts General Hospital, Boston, MA 02114, USA
[24]Present address: Case Western Reserve University, Cleveland, OH 44106, USA
[25]Present address: National Institute on Diabetes, Digestive and Kidney Dieseases, National Institutes of Health, North Bethesda, MD 20852, USA
[26]These authors contributed equally
[27]Lead contact
*Correspondence: efilippova@uchicago.edu (E.V.F.), hernan.lorenzi@nih.gov (H.A.L.), r-silverman@northwestern.edu (R.B.S.), rmcleod@uchicago.edu (R.L.M.)
https://doi.org/10.1016/j.isci.2023.108477

INTRODUCTION

The Apicomplexan parasite, *Toxoplasma gondii*, is a major cause of morbidity and mortality worldwide, with toxoplasmosis being one of the leading causes of death attributed to food-borne illness in the United States.[1–3] Globally, this parasite infects between 30 and 50% of the population, which means that approximately two billion people have this parasite living within their brains, with largely unknown consequences. Infection with *T. gondii* typically occurs via inadvertent ingestion of oocysts in food or water contaminated by cat excrement.[4] Indeed, it has been estimated that the number of infectious oocysts per square foot of soil in the US ranges from 9 to 434.[5] Ingestion of a single oocyst is capable of inducing infection. An acutely infected feline excretes upwards of 500 million oocysts over the approximately two weeks of acute infection, and oocysts persist in moist soil or water for up to a year.[6–8] Comprising a public health threat, toxoplasmosis results in a wide range of serious health problems, including loss of sight and significant neurological disease in congenital infection and severe meningoencephalitis in immunocompromised persons.[9–12] Current therapeutics for this parasitic infection have some limitations, including toxicity, hypersensitivity reactions, and an inability to eliminate the latent bradyzoite stage of the parasite.[13–17] For these reasons, new therapeutic approaches and the development of safe and effective vaccines are needed.

To address this issue, a variety of molecular targets have been identified. One such target, ornithine aminotransferase (OAT) was chosen for its position as a key node in several biochemical pathways,[18] with demonstrated importance to cell viability.[18] In fact, OAT is at the intersection of pathways that produce amino acids, neurotransmitters, purines, as well as play key roles in the urea cycle, TCA cycle, the polyamine pathway, and in the production of glutamate (Figure 1A). Glutamate has been reported to be an alternative energy source in *Plasmodium*, a related Apicomplexan.[19] *T. gondii* OAT (*Tg*OAT) was selected by the Center for Structural Genomics of Infectious Disease at Northwestern University (Chicago, IL) for further study on the basis of its contribution to several key metabolic pathways, as well as its computed drugability, phylogenetic data, assayability, and the predicted feasibility to solve its three-dimensional structure. *Tg*OAT was initially deposited into and selected from the Tropical Disease Resource (TDR) Targets Database by Agüero and colleagues in 2008.[20,21]

OAT is a pyridoxal-5′-phosphate-dependent enzyme that catalyzes the conversion of L-ornithine and α-ketoglutarate to glutamate-γ-semialdehyde (which spontaneously cyclizes to pyrroline-5-carboxylate) and L-glutamate to prevent toxic accumulation of ornithine in mammalian cells[22] (Figure 1B). In protozoans, ornithine is the starting point for the polyamine pathway, which has been the subject of therapeutic interest for some time.[23–26] The long-term lack of OAT results in hyperornithinemia, leading to gyrate atrophy of the choroid and retina, a genetic disorder in humans.[27,28] OAT and γ-aminobutyric acid aminotransferase (GABA-AT) are members of subgroup II of the aminotransferase family of enzymes.[29] GABA-AT has been an extensively studied enzyme, the substrate of which, GABA, is the key inhibitory neurotransmitter in the brain (Figure 1C; [30]). Vigabatrin, which is approved for the treatment of infantile spasms, and CPP-115 (**1**, Figure 2A), which has completed a successful Phase I clinical trial for the treatment of epilepsy and is being used to treat infantile spasms,[31,32] are examples of inhibitors of GABA-AT. Because of the similarity in the active sites of both OAT and GABA-AT, it is difficult to design inhibitors that will selectively inactivate OAT; CPP-115, for example, inhibits both GABA-AT and human OAT (*h*OAT). In 2015, the Silverman group reported the first selective inhibitor (**2**, in Figure 2A) for *h*OAT over GABA-AT,[33] and its selectivity was hypothesized to derive from a novel mechanism of inactivation, which is not seen in GABA-AT,[34] and its overall size.

The crystal structures and kinetic characterization of *human*GABA-AT and OAT complexed with the aforementioned inhibitors, as well as gabaculine, L-canaline, and 5-fluoromethylornithine, have provided a basis for structural characterization of each enzyme.[35–38] Structural characterization of OAT homologues in other Apicomplexans, including *Plasmodium falciparum* and *Plasmodium yoelii*, has also been reported.[39,40] OAT functions as a dimer, in which monomers share a typical α/β structural fold known to be a feature of subgroup II of the aminotransferase family members. The crystal structure of OAT dimer from *T. gondii* in complex with cofactor PLP has been studied in our previous work.[41] Similar to its homologous structures, each monomer in the *Tg*OAT dimer consists of three domains and resembles a conserved cofactor-binding site.

Beyond a study on the spectroscopic analysis of catalytic characteristics,[18] *Tg*OAT had not been characterized, structurally or functionally to identify selective inhibitors, nor studied for its potential as a molecular target in this parasite.[18] Somewhat surprisingly, this paper suggested that the enzyme, referred to as *Tg*OAT, in fact, had enhanced substrate specificity for GABA relative to ornithine, implicating it in the metabolism of GABA and suggesting that it can also function as a GABA-AT. This metabolic activity would be of potential importance to the recently described GABA shunt, shuttling carbon from GABA into the TCA cycle to meet the energetic needs of the parasite, particularly under conditions of limited nutrient availability and the concomitant stress this causes to the parasite.[42] Nutrient abundance, and its compartmentalization, could influence flux through and substrate utilization in these pathways. Astegno et al. suggested that selective inhibitors might have a role in the treatment of infection with *T. gondii* in humans.[18] To date, no selective inhibitors of *Tg*OAT have been identified to target any of the parasite life cycle stages. Even if *Tg*OAT were not critical for tachyzoites or bradyzoites, targeting the formation of the environmentally resistant oocyst life cycle stage could have a significant impact on disrupting the chain of transmission and, thereby, decrease consequent morbidity and mortality. Furthermore, inhibition of OAT in *P. falciparum* also is of interest because *P. falciparum* causes malaria, and there are particular problems with resistance to available antimalarials. The same compounds that are effective against *T. gondii* are sometimes also effective against *Plasmodia* because of their phylogeny as related Apicomplexan parasites. Because of the recently reported use of GABA as a substrate by *Tg*OAT,[18] hereafter we will refer to this enzyme as *Tg*O/GABA-AT, recognizing its potential dual biologic function.

The comprehensive characterization of *Tg*O/GABA-AT, presented herein, includes an analysis of the gene with phylogeny. Further, transcriptional and proteomic analyses led to production of the enzyme and use of the enzyme to produce antibodies, kinetically characterize putative inhibitors/inactivators, and solve and analyze the structure in complex with selected inhibitors. In addition, the antibody was used

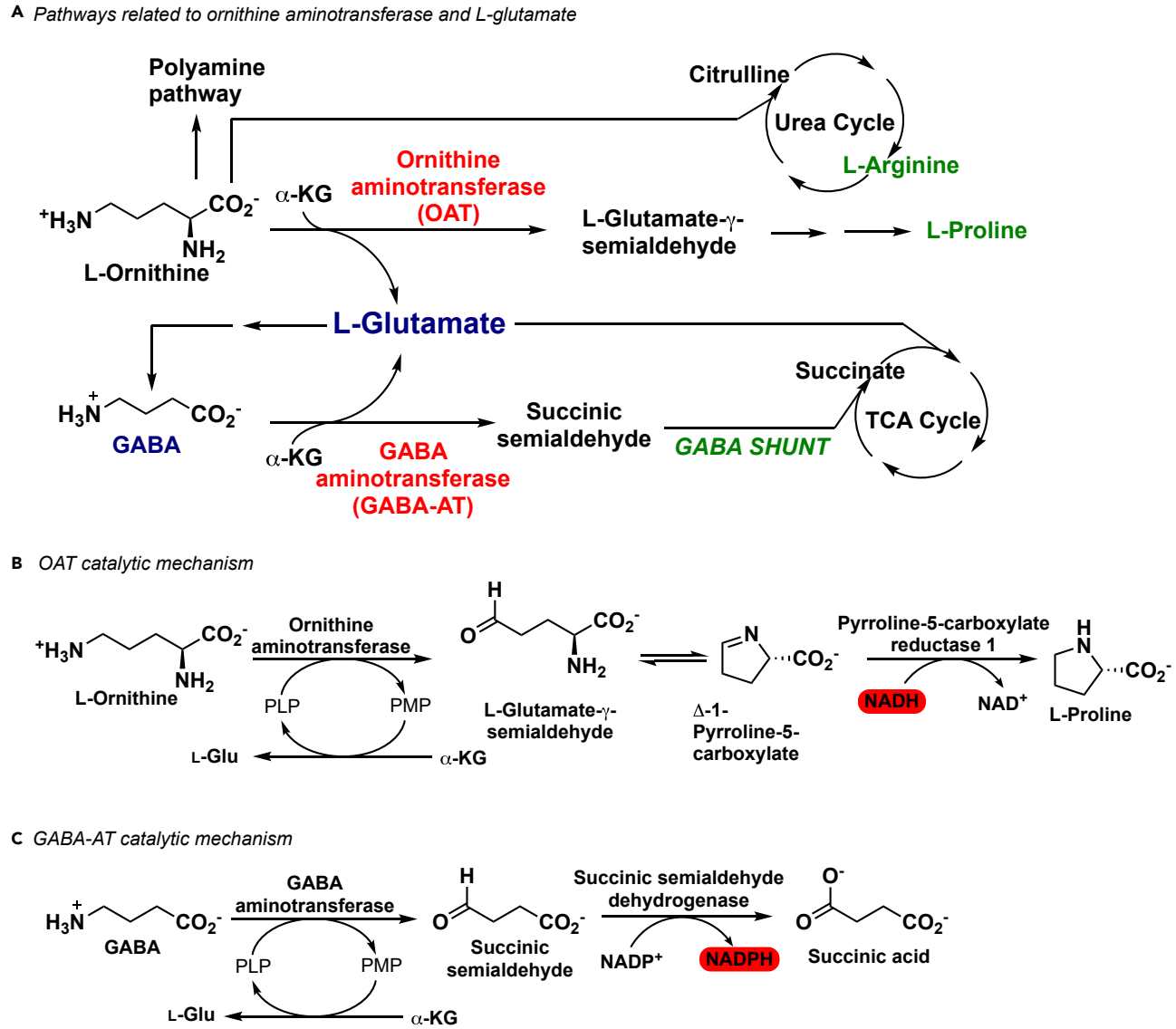

Figure 1. Enzyme pathways involving ornithine aminotransferase, GABA amino transferase, and glutamate

(A) Ornithine aminotransferase (OAT), GABA aminotransferase (GABA-AT) and glutamate play a central role in numerous important biological pathways including the polyamine pathway, urea cycle, and TCA cycle.

(B) OAT catalyzes the conversion of ornithine to L-glutamate 5-semialdehyde, which when coupled with pyrroline-5-carboxylate reductase, allows for conversion to be monitored by NADH disappearance.

(C) GABA-AT converts GABA to succinic semialdehyde with concomitant conversion of α-ketoglutarate (α-KG) to glutamate. The reaction involves the conversion of the cofactor pyridoxal-5′-phosphate to pyridoxamine-5′-phosphate. Coupling of this reaction to the conversion of SSDH to succinic acid allows for conversion to be monitored by NADPH production.

Related to Figures S1 and S2.

to characterize life cycle stage-specific expression of *Tg*O/GABA-AT. Genetic knockouts for Type II parasites and an unusual Brazilian parasite (EGS) were performed utilizing genetics and CRISPR/Cas9 techniques. Parasites of different genotypes were utilized to characterize phenotypes that this enzyme produces during critical life cycle stages.

Expression in the sporozoite has been reported to be ~245 times higher than in tachyzoites and bradyzoites[43,44]; additional insight into this pathway was therefore sought. First, we utilized CRISPR/Cas9 to knockout *Tg*O/GABA-AT in a parasite, EGS, that could be indefinitely cultured as a bradyzoite and thereafter infect cats to produce oocysts following genetic manipulation. The intent of this experiment was to determine whether this enzyme was absolutely essential for the formation of oocysts and not just contributing to their formation. When we found *Tg*O/GABA-AT was not essential, we asked whether the function of OAT's products, or molecules that influenced their function,

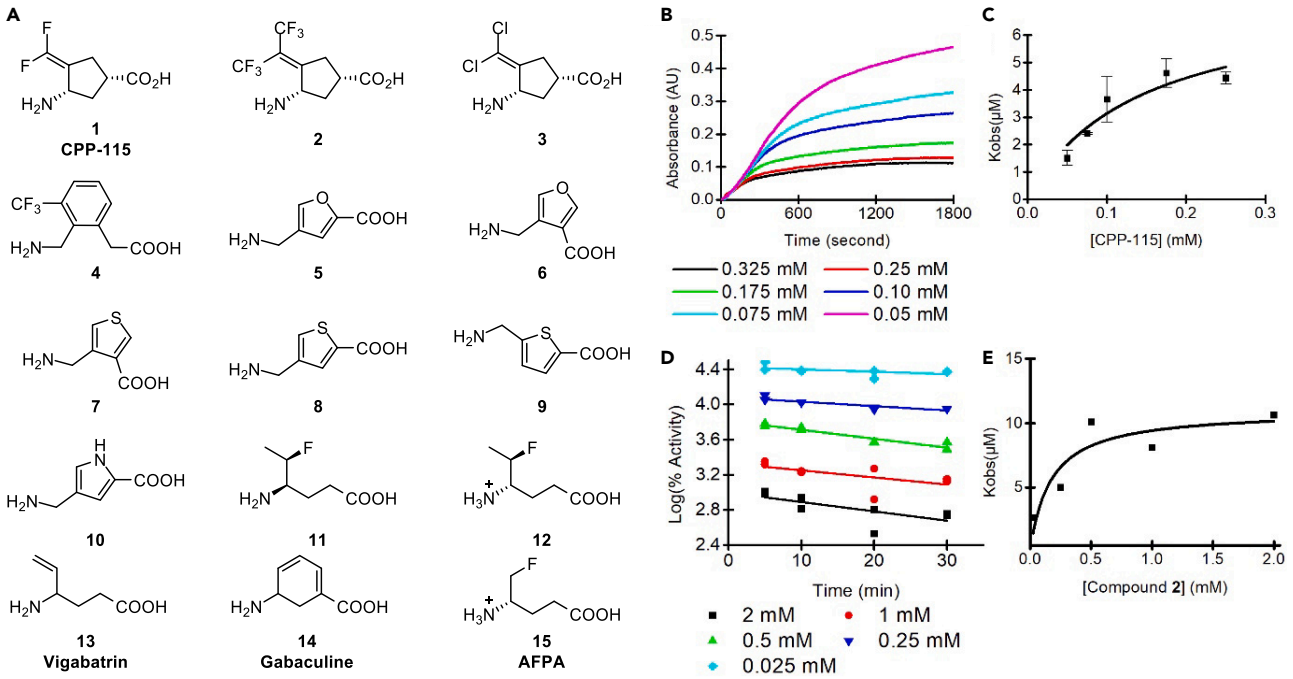

Figure 2. Inhibitors and inactivators of *Tg*O/GABA-AT and kinetics

(A) Selected inhibitors screened against *Tg*O/GABA-AT.

(B) Kinetic data for assay of **1** with GABA as substrate.

(C) Replot of k_{obs}, calculated from (B), and inhibitor concentration via curve fitting method.

(D) Time dependent assay of **2** with ornithine as the substrate.

(E) Replot of k_{obs}, calculated from (D), and inhibitor concentration via time dependent assay method. For accompanying Figures S3C and S3F, this has error bars which represent mean ± SEM, n = 2.

Related to Table S1 and Figure S3.

might be essential for oocyst formation. To explore this hypothesis, we determined the genome sequence of a mutagenized parasite, T-263, incapable of forming oocysts in cats, revealing nonsynonymous mutations in 18 protein-coding genes that have increased expression in merozoites and/or sporozoites (oocysts). Quite remarkably, one of these mutated genes encodes a sodium: GABA symporter. *Tg*O/GABA-AT may function to convert ornithine to L-glutamate (Figure 1B), which can be converted to GABA by L-glutamate decarboxylase. *Tg*O/GABA-AT also may function to convert GABA to succinic semialdehyde (Figure 1C), which is oxidized to succinate, and enters the TCA cycle via the GABA shunt. By either function, GABA would be central to these integral metabolic pathways in the parasite. GABA concentration has been found to modulate capacitation of gametes (sperm) in other species.[45] Since sequence data were available and a phenotype of lack of maturation beyond microgamete and macrogamete stages was noted, genes that could be related to capacitation at the merozoite stages or acrosome formation also were of interest.

RESULTS

Interrelatedness of OATs shown in multi-sequence alignment

The multiple sequence alignment of six OAT proteins from Apicomplexan, human, and cat species (Figure S1) shows a high degree of conservation. Very high conservation is seen among *T. gondii*'s close relatives, *Hammondia hammondi* and *Neospora caninum*, with 96% and 89% sequence identity, respectively. As expected, there is markedly less conservation between *T. gondii* and the more distant cat and human homologues with approximately 49% sequence identity. Interestingly, cysteines Cys179 and Cys187 of *Tg*O/GABA-AT are also conserved within species of the phylum Apicomplexa (Figure S1, in green), which has been demonstrated, via insertional mutagenesis, to bind thioredoxin increasing enzymatic activity in *P. falciparum*.[46] Moreover, these Cys residues are positioned such that they could, in an oxidative environment, form a disulfide linkage. The role of this linkage is unknown; however, thioredoxin appears to play a role in binding to and positioning the substrate-binding site. It has been shown that the *Eimeria* enoyl reductase (ENR) also contains a similar feature not seen in any bacterial homologue.[47] Of note, we found that human and cat OATs do not contain these two cysteine residues. To further investigate the frequency of the two cysteine residues in the OAT family, a more extensive sequence alignment was conducted on 499 protein sequences with between 24 and 97% sequence identity (data not shown). Only six showed the presence of two cysteines in equivalent positions, highlighting this to be a rare feature of the OAT family.

Population diversity of *Tg*OAT

Analysis of OAT genetic variability in 53 *T gondii* isolates by parsimony analysis revealed six distinct clusters of strains based on haplotype, as shown in Figure S2, consistent with major clades previously established on the basis of multilocus and genome-wide SNP analysis.[48]

Notable distinct isolate clusters in the OAT consensus tree include haplogroups 1, 3, 4, 11, and 14. Haplogroups 2 and 12, related clonal groups common in North America, comprise a single major branch. Some Guiana isolates appear to be hypervirulent for some humans. The Guiana isolates have diverse individual patterns for their OAT sequences.

*Tg*O/GABA-AT activity

For this assay, we monitor both the rate of consumption and amount of consumption. Since we are monitoring consumption over time it is therefore a rate. The assay conditions employed in the measurement of GABA-AT activity were shown to be effective at measuring the rate of consumption of GABA at 37°C (See Figure S3). This means that the activity of GABA-AT was measured as the rate of oxidation of the formed product, succinic semialdehyde, with excess succinic semialdehyde dehydrogenase. This corresponds to the rate of consumption of substrate GABA. A reaction rate can be measured by the rate of the formation of the product or the rate of the disappearance of the starting material. In the assay that we chose, we measured the reaction rate by the rate of the disappearance of the starting material.

We have previously employed two coupled-enzyme assays for the continuous measurement of the consumption of *L*-ornithine by *Tg*O/GABA-AT (Figure 1B; [29]) and GABA by GABA-AT (Figure 1C). The ornithine assay monitors the conversion of *L*-ornithine to *L*-glutamate-5-semialdehyde, which spontaneously cyclizes to form Δ^1-pyrroline-5-carboxylate (P5C), by coupling it to the NADH-dependent reduction of P5C to *L*-proline by pyrroline-5-carboxylate reductase 1 (PYCR1). The disappearance of NADH at 340 nm is monitored with excess NADH, PYCR1, and α-ketoglutarate. For the GABA assay, the conversion of GABA to succinic semialdehyde (SSA) and concomitant conversion of α-ketoglutarate to glutamate is coupled to the $NADP^+$-dependent oxidation of SSA to succinic acid by succinic semialdehyde dehydrogenase (SSDH), and the appearance of NADPH is monitored at 340 nm.

The first step was to validate both enzyme assays for the compatibility with *Tg*O/GABA-AT. The assay conditions employed in the measurement of GABA-AT activity were shown to be effective at measuring the rate of consumption of GABA at 37°C (See Figure S3). Likewise, the assay conditions for measurement of OAT activity were effective at measuring ornithine consumption. An experiment to determine applicable conditions for the bioassay of *Tg*O/GABA-AT was executed at various concentrations of *Tg*O/GABA-AT, employing both GABA and ornithine as substrates (Figures S3A and S3D, respectively). Optimal concentrations of enzyme for GABA- and ornithine-based assays were determined to be 15 μg/mL and 100 μg/mL, respectively. To determine the K_m of GABA and ornithine against *Tg*O/GABA-AT, an assay at various concentrations of GABA (Figure S3B) and ornithine (Figure S3E) was performed. A K_m value of 3.77 ± 0.68 mM was obtained with GABA as substrate, whereas a value of 31.0 ± 4.0 mM was obtained with ornithine as the substrate ((*18*) published K_m values of 1.32 ± 0.02 mM and 6.9 ± 0.3 mM for GABA and ornithine, respectively, although they obtained these values using different methods). The K_m for GABA was found to be 3.8 mM and that for ornithine was 31.0 mM. Because of the poorer substrate binding of ornithine, in order to see a reasonable rate of reaction, a larger concentration of enzyme was required.

Effect of inhibitors on *Tg*O/GABA-AT enzyme activity

Compounds screened against *Tg*O/GABA-AT are shown in Figure 2A. For reversible inhibitors, concentration dependence was observed and K_i, the inhibition constant, was determined by previously developed methods.[49] For compounds showing time dependence and saturation kinetics, K_I and k_{inact}, the binding constant and rate constant of inactivation, respectively, were calculated (*vide infra*). The k_{inact}/K_I value affords a measure of the efficiency of the inhibitor. Two methods for the calculation of K_I and k_{inact} were employed. We recently employed a curve fitting method for the measurement of K_I and k_{inact} for potent inhibitors of *porcine*GABA-AT (*p*GABA-AT,[50]). This method effectively estimates kinetic constants for highly potent inhibitors but struggles with weaker inhibitors. Thus, for weaker inhibitors, we employed a time-dependent assay and a Kitz and Wilson replot method, which we have used with GABA inhibitors in the past.[49] For ornithine, we used the latter method, consistent with our previous work with *h*OAT.[33] All calculations are described in the Methods section.

Known *p*GABA-AT and *h*OAT inhibitors were screened against *Tg*O/GABA-AT with ornithine as a substrate. The results are presented in Table S1. Of these compounds, **1**, **2**, **3**, and **14** are potent, irreversible inhibitors of *Tg*O/GABA-AT. The activity of compounds **1**, **2**, and **3** were of particular interest (Table 1), given their similarity in structure. These compounds were also screened against *Tg*O/GABA-AT with GABA as the substrate (Table 1). CPP-115 (**1**) showed saturation kinetics (Figure 2B), and kinetic constants (with GABA as the substrate) were calculated via the curve fitting method (Figure 2C). Compound **2** was potent against *h*OAT and *Tg*O/GABA-AT, yet a weak inhibitor of *p*GABA-AT, and **3**, which was of most interest to this study, is solely selective for *Tg*O/GABA-AT. Kinetic constants for **2** and **3** were calculated via the time-dependent replot method (Figures 2D and 2E).

The enzyme assays with inactivator were performed with enzyme from Type II strain parasites in parallel with the study of the original knockout Type II Prugneaud strain that was characterized (*vide infra*).

Overall structure of *Tg*O/GABA-AT and PLP binding site

The crystal structures obtained of *Tg*O/GABA-AT show that the asymmetric unit contains a homodimer as reported previously.[41] Each monomer consists of three domains: the large PLP-binding domain (Figure 3A, in green) and two small domains in the N- (in gold) and C-terminus (in orange). The N-terminal domain adopts a small β-sheet with three antiparallel β-strands surrounded by three α-helices. The large PLP-binding

Table 1. Selected kinetic constants for inactivation of *TgO/GABA-AT*, *porcine* GABA-AT, and *human* OAT

Inactivator	*Tg*O/GABA-AT GABA as substrate	*Tg*O/GABA-AT Ornithine as substrate	GABA-AT GABA as substrate[a]	hOAT Ornithine as substrate[b]
1	K_I = 0.04 mM k_{inact} = 0.48 min^{-1} k_{inact}/K_I = 12 $min^{-1}mM^{-1}$	K_I = 0.09 mM k_{inact} = 0.02 min^{-1} k_{inact}/K_I = 0.022 $min^{-1}mM^{-1}$	K_I = 0.031 mM k_{inact} = 0.18 min^{-1} k_{inact}/K_I = 5.7 $min^{-1}mM^{-1}$	K_I = 0.0021 mM k_{inact} = 0.097 min^{-1} k_{inact}/K_I = 23.8 $min^{-1}mM^{-1}$
2	K_I = 1.5 mM k_{inact} = 0.05 min^{-1} k_{inact}/K_I = 0.033 $min^{-1}mM^{-1}$	K_I = 0.85 mM k_{inact} = 0.011 min^{-1} k_{inact}/K_I = 0.013 $min^{-1}mM^{-1}$	K_i = 4.2 mM	K_I = 0.0064 mM k_{inact} = 0.018 min^{-1} k_{inact}/K_I = 0.04 $min^{-1}mM^{-1}$
3	K_I = 19.25 mM k_{inact} = 0.10 min^{-1} k_{inact}/K_I = 0.005 $min^{-1}mM^{-1}$	K_I = 4.67 mM k_{inact} = 0.035 min^{-1} k_{inact}/K_I = 0.007 $min^{-1}mM^{-1}$	K_i > 10 mM	K_i > 10 mM

[a]adapted from Lu et al. (2006).
[b]adapted from Zigmond et al. (2016). See supplemental information for complete Table S1.

domain adopts a central eight-stranded β-sheet surrounded by ten α-helices including four short helical segments. The β-strands within the central β-sheet are parallel except for strand βj, which runs in opposite direction to all other strands inside the β-sheet. The C-terminal domain comprises four stranded antiparallel β-sheets surrounded by three α-helices (Figure 3A). Both monomers of the *Tg*O/GABA-AT dimer have a similar fold. The dimer interface of the *Tg*O/GABA-AT is formed by PLP-binding and the N-terminal domains between αI, αII, βA, αIV, βa, αV, βb, αVI, αVII, and αVIII (Figures 3A and 3B). In addition to 63 hydrogen bonds and three salt bridges, a disulfide bond between two adjacent Cys96 residues on opposite monomers outside of the active site region contributes to dimer formation.

There are two PLP-binding sites per *Tg*O/GABA-AT dimer, 15 Å apart from each other. Inside the cavity of the structure of *Tg*O/GABA-AT, and in the presence of the PLP-Lys286 aldimine (PDB: 4ZLV), PLP binds in a similar binding mode observed in the structures of *h*OAT, *Pf*OAT, and *E. coli*GABA-AT. 36–38[40,46] Residues from both monomers of the *Tg*O/GABA-AT dimer form the PLP-binding site (Figure 3C). In the cavity, PLP is surrounded by residues V79, T135, G136, A137, Y171, W172, G173, E224, D257, I259, Q260, S315 (opposite subunit), and T316 (opposite subunit). All these residues are highly conserved in the *Tg*O/GABA-AT and *Pf*OAT structures (Figure S4). Exceptions were found with residues V75, A137, and Y171, which in *h*OAT are substituted by phenylalanine, tyrosine, and valine, respectively.[36] By dialysis of *Tg*O/-GABA-AT a structure without PLP liganded can be obtained (not shown). In the unliganded *Tg*O/GABA-AT structure (PDB: 5EAV) a single inorganic phosphate anion (from buffer) occupies the position of the phosphate group of PLP in both protein monomers. Analysis of the *Tg*O/GABA-AT structures in the presence and absence of PLP shows that there are no notable differences in the positions of side chain residues surrounding the PLP-binding sites.

Structure of 15-inactivated*Tg*O/GABA-AT

The proposed mechanism of compound **15**-mediated inactivation of *Tg*O/GABA-AT is shown in Figure 4A. Following initial Schiff base formation with PLP (**16**), deprotonation and elimination of F^- gives intermediate **17**. Attack by Lys286 releases an enamine, which attacks the Lys-PLP imine to give adduct **18**. The structures of **15**-inactivated *Tg*O/GABA-AT were determined in two ways: incubation of enzyme with **15** and PLP for 4 h followed by co-crystallization shows the electron density at the protein active site with intermediate **17** bound in both monomers (Figure 4B, PDB: 5E3K); incubation of enzyme and PLP with **15** overnight (14–15 h) followed by co-crystallization shows **17** bound in one monomer and **18** (X = NH_2^+ or O) in the other monomer (Figure 4C, PDB: 5E5I). This is the first time that an enamine precursor intermediate (**17** in this case) has been observed by crystallography; typically, only the final enamine addition product (in this case, **18** or maybe **S1**,Figure S5A) is observed. To dismiss a possible alternative interpretation of the **17** structure (Figure S5Bi), namely, that our **17** structure is instead **S1**, the electron density was modeled as **S1**, where X = O (Figure S5Bii) or NH, NH_2^+ (Figure S5Biii); the structure analysis did not support any of these alternative structures, only **17** (Figure S5B). Taken together, these crystallographic results solidify the enamine inactivation mechanism and, because of the observation of **17**, suggests that, at least in this case, the slow step in the inactivation is attack of Lys286 on **17** to give the enamine and lysine-bound PLP. In forming **18**, the PLP undergoes ~8° rotation around the C5A-O4P bond, delivering C4A closer to the primary amine of K286, while the CA-CB-CG group of **15** undergoes a conformational change and rotates ~30° around the CD-CG bond (Figure S5C). The overall position of the PLP portion of **17** and **18** in the active site of these structures remains unchanged.

In all monomers, the compound bound to the PLP occupies the *Tg*O/GABA-AT substrate-binding pocket that is formed by residues L76, G78, V79, N48, Y49, L106, R107, A108, Y171, R174, E229, K401, R409 and by H313, G314, S315, and T316 from the opposite monomer. In the pocket, the inactivator's carboxyl group hydrogen bonds with the OH group of Y49 and the N atom in the main chain of S315 from the opposite monomer (Figure 4D). Additionally, the carboxylate of 15 in *Tg*O/GABA-AT is hydrogen bonded through a network of water molecules with the NH_2 and OH groups of R174 and Y171, respectively, the backbone amide of S315, nitrogen of R107, and the phosphate group of the

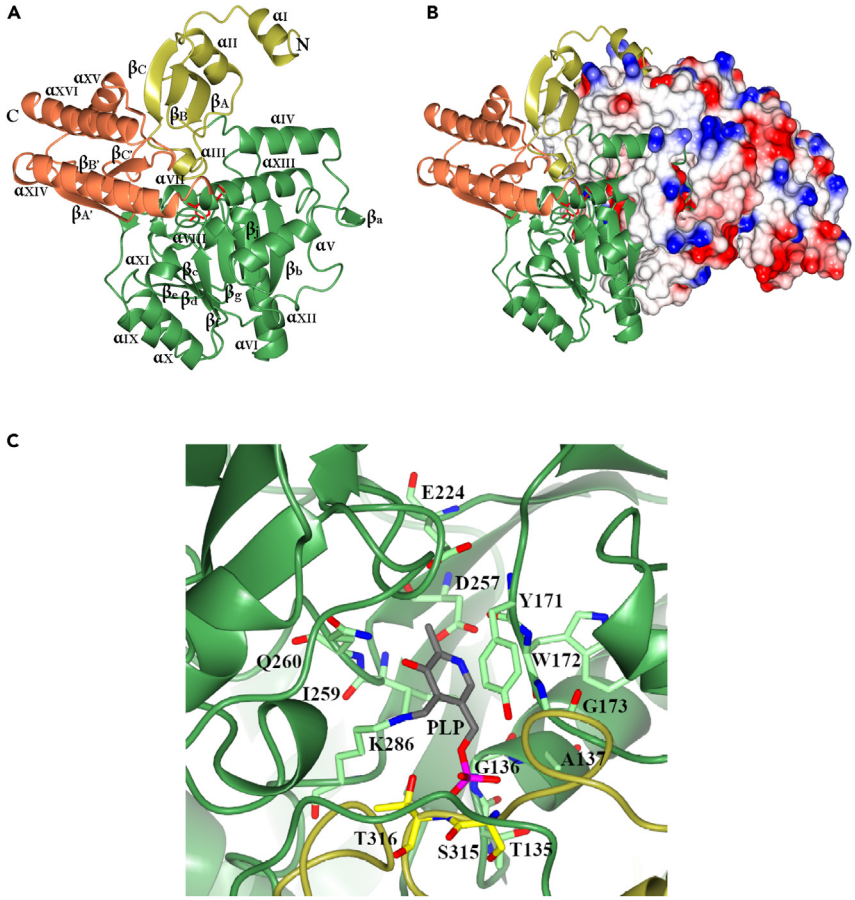

Figure 3. *Tg*O/GABA-AT overall structure fold and PLP-binding site

(A) Ribbon diagram of the *Tg*O/GABA-AT monomer. The N-terminal domain, large PLP-binding domain and C-terminal domain are colored in gold, green and orange, respectively.

(B) *Tg*O/GABA-AT dimer. The electrostatic surface is displayed for one monomer and colored by surface potential charge scaled from negative in red (-0.5 V) to positive in blue (+0.5 V). The PLP molecule is shown as a cylinder model in red on both figure panels.

(C) PLP-K286 aldimine binding site. In the figure, residues from monomers A and B are colored in light green and yellow, respectively. Oxygen atoms are colored in red, carbons in light green (in yellow for monomer B), and nitrogens in blue.

Related to Table S2 and Figure S4.

cofactor (Figure 4D). A conformational change is apparent in the loop (50–54 residues) surrounding the substrate-binding site between the compound-bound and compound-free states when the *Tg*O/GABA-AT structures are compared.

Structure of gabaculine-inactivated *Tg*O/GABA-AT

To identify the bound structure of gabaculine (**14**), a nonselective, yet potent aminotransferase inhibitor, in TgO/GABA-AT (S2, Figure S6), we performed co-crystallization experiments with 5 mM gabaculine and 2 mM PLP and obtained the *Tg*O/GABA-AT crystal structure with the aromatized inactivator bound to pyridoxamine (Figure 5; inactivation mechanism leading to S2 is shown in Figure S6). The carboxylate group of gabaculine interacts with the OH group of Y49 and the N atom in the main chain of S315. The position of the gabaculine in the TgO/GABA-AT active site is similar to its position observed in the structure of *h*OAT.[36] It has been shown that the interaction between the aromatic ring of the gabaculine adduct and Y85 and F177 residues in hOAT modulates the binding affinity and keeps the product in a specific pose within the active site of *h*OAT.[35] This leads to the same inactivation mechanism for gabaculine with *Tg*O-GABA-AT as was proposed for *h*OAT.[36]

Absence of effect of *Tg*O/GABA-AT small molecule inactivators on tachyzoite replication *in vitro*

None of the inactivators tested against Type I *T. gondii* tachyzoites had a statistically significant effect *in vitro*, even when the compounds were tested in the millimolar range. Additionally, some compounds (including Compounds **1** and **2**) were found to be toxic to host cells as demonstrated by a WST assay. In separate experiments, gabaculine was found to inhibit *T. gondii* tachyzoites at relatively high concentrations (>1 μM) (data not shown).

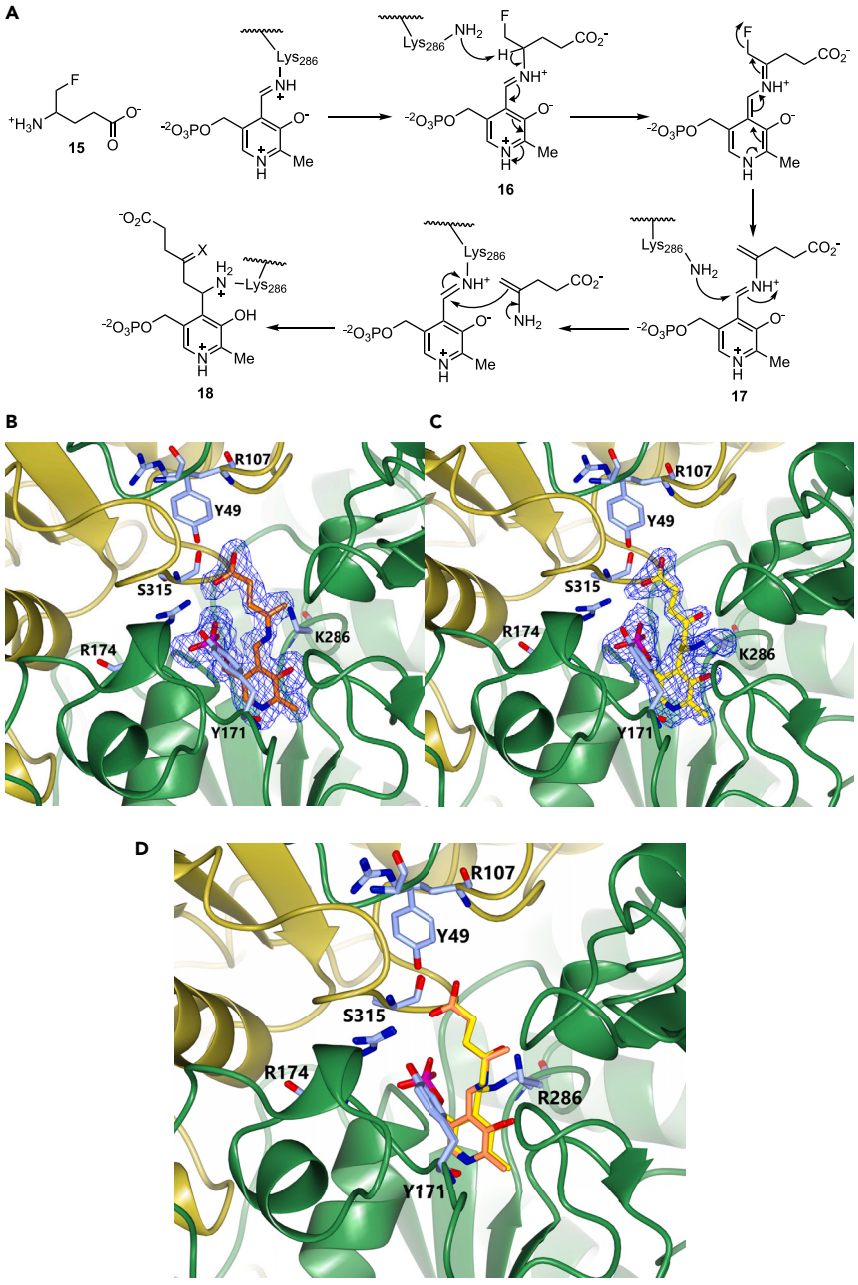

Figure 4. *TgO*/GABA-AT complexed with 15 at different points in the reaction mechanism

(A) Proposed mechanism of inactivation of *Tg*O/GABA-AT by **15**; X in **18** could be NH_2^+ or O (after hydrolysis).

(B and C) (B) *Tg*O/GABA-AT structure in complex with intermediate **17** (cylinder model in orange) and (C) covalent adduct **18** (cylinder model in yellow). The electron density F_o-F_c omit maps for the compound in its intermediate (**17**) and covalently bound (**18**) states are shown at the 3σ contour level in blue.

(D) Superimposition of intermediate **17** and covalent adduct **18** binding sites. In the figures, oxygen atoms are colored in red, nitrogen atoms in blue, carbon atoms in ice blue/orange/yellow (for residues/**17**/**18**), and sulfur atom in pink.

Related to Table S2 and Figure S5.

Absence of effect of *TgO*/GABA-AT inactivators on *P. falciparum in vitro*

Compounds **1**, **2**, and **3** were tested in the malaria SYBR Green fluorescence assay for drug potency against a drug sensitive *P. falciparum* parasite, D6 (Sierra Leone). All of the drugs tested showed IC_{50} values >10,000 ng/mL, indicating no detectable activity against *P. falciparum* (data not shown).

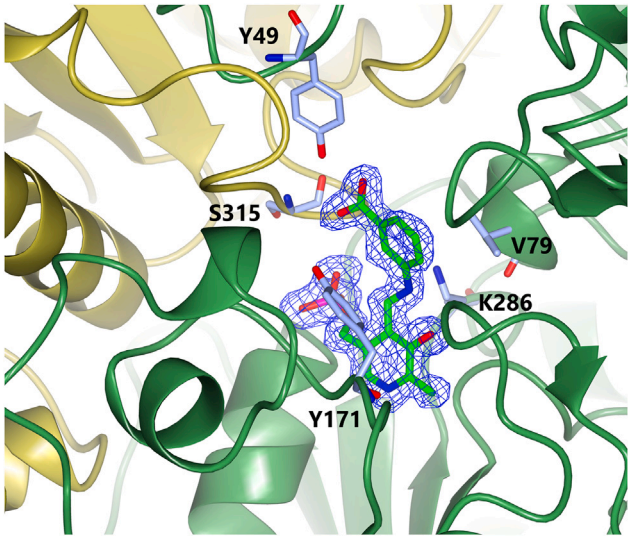

Figure 5. *Tg*O/GABA-AT in complex with gabaculine

*Tg*OAT/GABA-AT structure in complex with gabaculine (cylinders model in bright green). The electron density F_o-F_c omit map for the final adduct is shown at the 3σ contour level in blue. Oxygen atoms are colored in red, carbon atoms in ice blue/green (for residues/compound), nitrogen atoms in blue, and sulfur atom in pink. Related to Figure S6.

In vitro and *in vivo* phenotypes of type II parasites with deleted *Tg*O/GABA-AT suggest functions

To investigate the role of *Tg*O/GABA-AT in acute and chronic phases of infection, the gene coding region of *Tg*O/GABA-AT was targeted and knocked out in the type II PruΔ*ku80* background using a well-established strategy for targeting and genotype validation[51,52] (Figure 6A). The *in vitro* replication rate (Figure 6B) and plaque sizes (Figure 6C) of Type II parental PruΔ*ku80* and Δ*oat* parasites were essentially identical. To examine the chronic phase of infection *in vivo*, C57BL/6 mice were infected intraperitoneally with 200 tachyzoites of parental PruΔ*ku80* or Δ*oat* parasites and brain cyst burdens were measured 3 weeks (Figure 6D) and 5 weeks (Figure 6F) later. Surprisingly, mice infected with Δ*oat* parasites harbored a greater number of brain cysts than mice infected with the parental PruΔ*ku80* parasites. Moreover, we also noticed that a greater percentage of mice (~40%) infected with just 200 Δ*oat* tachyzoites succumbed to infection. In contrast, fewer than 10% of mice infected with 200 tachyzoites of the parental PruΔ*ku80* succumbed to acute infection (Figure 6E). To verify whether Δ*oat* parasites have increased acute virulence, mice were challenged with 2 X 10^5 tachyzoites of parental PruΔ*ku80* or Δ*oat* parasites and survival was monitored. Mice infected with Δ*oat* parasites succumbed faster than mice infected with the parental PruΔ*ku80* strain (Figure 6G). Collectively, these results show that Type II Δ*oat* parasites exhibit no deficiency in their ability to replicate, but rather have increased virulence, during the acute tachyzoite phase of infection or in their ability to establish chronic infection of mice characterized by brain cysts harboring the bradyzoite stages. This is consistent with the findings of Macrae et al.[42] that GABA can enter the TCA cycle through the GABA shunt increasing motility and infectivity.

Protein, expression, and immunofluorescence assays demonstrate merozoite and/or sporozoite *Tg*O/GABA-AT

Expression of *Tg*O/GABA-AT at different *T. gondii* stages was investigated by western blot using total protein extracts obtained from ME49 tachyzoites, bradyzoites, and sporozoites. To study this expression, a bacterially expressed recombinant protein was produced and used to make a mouse polyclonal antibody. Recombinant *Tg*O/GABA-AT protein was prepared and purified as in our enzyme assays and in our solution of crystal structures.[41]

As shown in Figure 6H, anti-*Tg*O/GABA-AT antibodies detected a band at approximately 48 kDa exclusively in the sporozoite lysate, in perfect agreement with the predicted molecular mass of the enzyme. The observed sporozoite-specific expression was consistent with the results of several proteomic studies conducted on tachyzoites and sporozoites[43,44] and was further supported by transcriptomic data available in ToxoDB, showing a marked upregulation of *Tg*O/GABA-AT transcription in sporozoites compared to tachyzoites and bradyzoites. Immunofluorescence analysis of freshly excysted ME49 sporozoites with anti-OAT antibodies showed immunostaining in cytoplasm and that co-localized with mitotracker using a method similar to that used in tachyzoites by Bzik et al.[53] With deconvolution the pattern in sporozoites *Tg*O/GABA-AT is in the cytoplasm and in mitochondria (Figures 6H, 6I, and 6J). Confocal images with an optical thickness of 0.12 microns were taken by a Zeiss LSM 980 microscope using a planapo objective 60x oil A.N. 1,42. It was not possible to visualize *Tg*O/GABA-AT in fixed tissue sections with either antibody so the cat intestinal stages were not visualized with our method. Tachyzoites did not show immunostaining with anti-*Tg*O/GABA-AT wheras there was immunostaining of the sporozoites at the same time (Figure 6I).

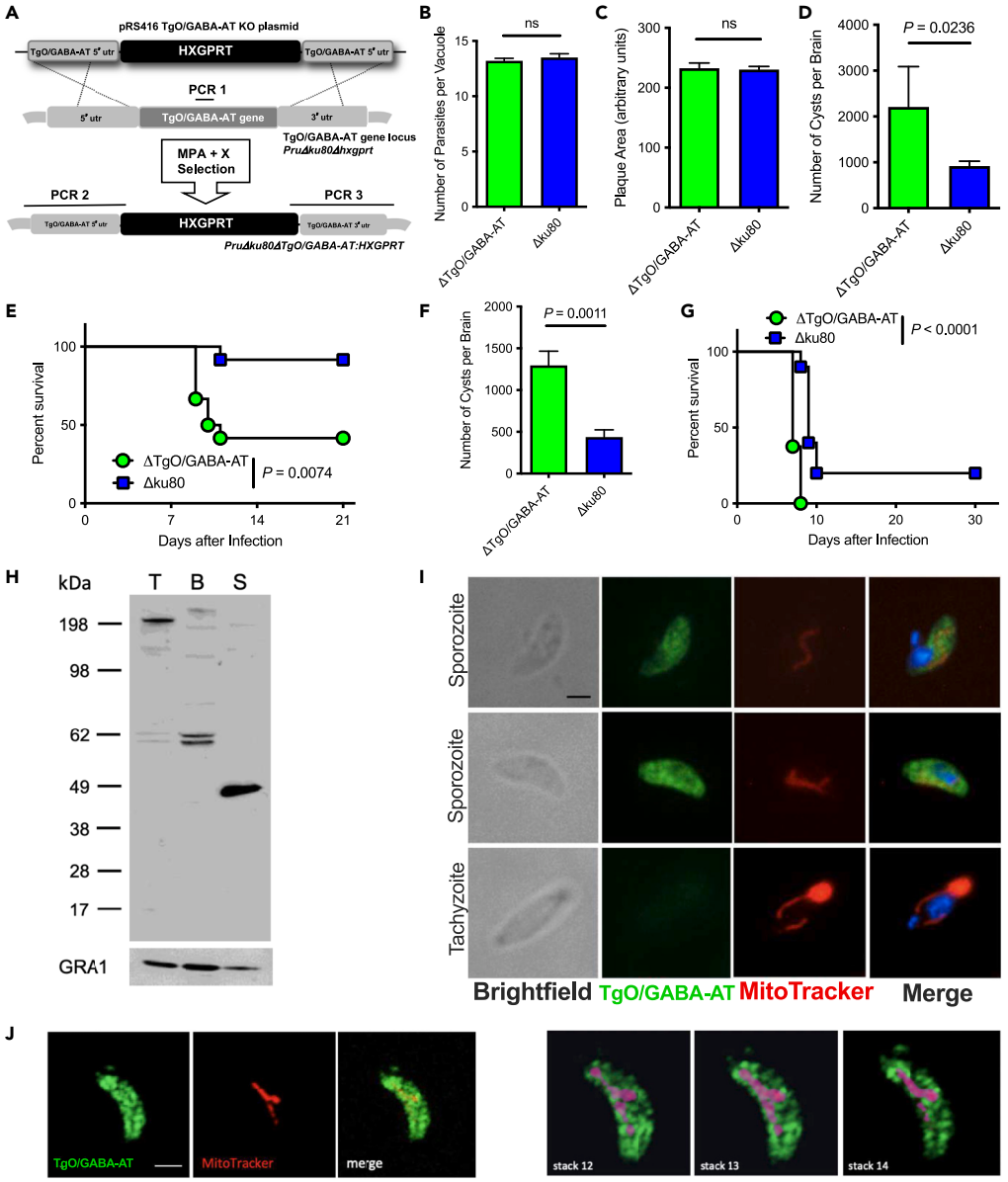

Figure 6. *In vitro* and *In vivo* phenotypes of Type II parasites deleted for *Tg*O/GABA-AT

(A) Schematic showing the strategy for targeted deletion of the *Tg*O/GABA-AT gene and validation of Δoat knockout.

(B) Growth rate of Type II Δoat knockout strain compared to parental Δku80.

(C) 12-day-old plaques of Δoat and Δku80 strains were measured for plaque size area.

(D) C57BL/6 mice were infected with 200 tachyzoites and brain cyst burdens were measured 21 days post-infection.

(E) Representative experiment showing survival of C57BL/6 mice infected with 200 tachyzoites of Δoat or parental Δku80.

(F) C57BL/6 mice were infected with 200 tachyzoites and brain cyst burdens were measured 35 days post-infection, Mean ± s.d.

(G) Representative experiment showing survival of C57BL/6 mice infected with 2×10^5 tachyzoites of Δoat or parental Δku80. ns was not significant; $p < 0.05$ was significant.

(H) Western blot analysis with antibodies generated using recombinant *Tg*OAT/GABA-AT indicate evidence of protein expression in sporozoites (S), but not in tachyzoites (T) or bradyzoites (B). The expected band is observed around 48 kDa.

(I and J) (I) Immunofluorescence analysis of ME49 sporozoites (upper and middle panel) and tachyzoites (bottom panel) with anti-*Tg*OAT mouse polyclonal antibodies (green). The parasite mitochondrion labeled with MitoTracker Red CMXRos is visible in red. Scale bar, 2 μM. Tachyzoites did not show immunostaining with anti- *Tg*O/GABA-AT whereas there was immunostaining of the sporozoites at the same time (I). Dual staining with MitoTracker was included and deconvoluted (J). The tertiary color, red-violet, blended with its opposite, the tertiary color yellow-green, creates maroon showing co-localization with mitochondria as well as *Tg*O/GABA-AT in the cytoplasm. *Tg*O/GABA-AT is shown in the cytoplasm and in mitochondria in I. J). Confocal

Figure 6. *Continued*
images with an optical thickness of 0.12 microns were taken by a Zeiss LSM 980 microscope using a planapo objective 60x oil A.N. 1,42. It was not possible to visualize *Tg*O/GABA-AT in fixed tissue sections with either antibodies so the cat intestinal stages were not visualized with our method. Scale bar corresponds to 2 microns.
Related to Table S3.

Knockout of *Tg*O/GABA-AT in EGS in murine and cat experiments

Creation of knockout of TgO/GABA-AT in the EGS strain of T. gondii allows characterization of TgO/GABA-AT in mice and cats

This knockout was created in EGS strain parasites because of the ease of *in vitro* culture with retention of the bradyzoite phenotype of oocyst production even after multiple passages *in vitro*. This is likely due to the disordered C terminus of the Apetela2 protein, Apetela 2 IV-4, a protein that blocks parasite transition through a checkpoint that licenses tachyzoites to form.[54] This keeps these EGS parasites as the required bradyzoite needed to form oocysts.

Our cultured EGS is capable of formation of oocysts in the cat even after prolonged times in tissue culture and many *in vitro* passages.[55] The oocyst formation trait is often lost with time and passages by other strains. EGS belongs to the same haplogroup as other Brazilian parasites. EGS was initially isolated in the 1990s and was also characterized by Vomero,[56] Santos, and Weiss[57] in separate publications in addition to our own work together earlier.[55] The control was *EGS-spGFP*. This EGS parasite was used to create CRISPR/Cas9 mutants for this experiment because oocysts capable of infecting mice form from bradyzoites. A schematic diagram of the CRISPR/Cas9 cassette, experimental design, and summary of results for each step of these studies are shown in Figure 7. Knockout of *Tg*O/GABA-AT was confirmed via PCR.

Infection of mice with *Tg*O/GABA-AT EGS knockout parasite was virulent and produced brain cysts

Mice inoculated with this *Tg*O/GABA-AT EGS knockout strain became noticeably ill secondary to toxoplasmosis. The signs of infection in the mice that received either single organisms of EGS from culture or the sub-inoculated sporozoites from oocysts excreted by the cat (please see below under "Infections of cats with EGS *TgO/GABA-AT* parasites") were ruffled fur and peritonitis. DNA from these isolated parasites was sequenced documenting *Tg*O/GABA-AT knockout was present. Further, brain cysts were noted after euthanasia, confirming that *Tg*O/GABA-AT is not essential for cyst formation or virulence. Parasites recovered from these mice had their genomic DNA sequenced, which confirmed that the knockout was still present.

Infection of cats with EGS *Tg*O/GABA-AT knock out parasites produced viable infectious oocysts

Concerning the initial inoculum of brain containing cysts that were fed to the cats, all 5 of 5 mice that received infected brains at the same time the cats were fed were infected (Figure 7). The cats infected with the control EGS strain parental brain and *Tg*O/GABA-AT mutant parasites developed serum antibody to *T. gondii*, tested using MAT.

When these cats produced oocysts, sporozoites that were excysted from these oocysts were sequenced. This sequencing of the parasite from the oocysts verified the knockout of the *Tg*O/GABA-AT gene in the EGS strain parasite. These oocysts were infectious to additional mice. Viability of oocysts was confirmed with excystation and sub-inoculation into 2 Balb/c mice that were found to be infected (Figure 7).

Based on many experiments and publications, quantification of oocyst shedding is variable, unreliable, and would have been considered an unacceptable use of additional cats in research in the US at this time.[58]

Further details and results of these studies with EGS-*Tg*O/GABA-AT KO show viable oocysts can form

Further specific details of the EGS-*Tg*O/GABA-AT KO given to cats are in Figure 7 and are as follows: *T. gondii* infected mouse brains from 10 mice infected with (EGS-*Tg*O/GABA-AT KO—cat 04) and EGS-spGFP (cat 05) were homogenized by syringe and fed to two female, 141 and 144-day-old, coccidia-free cats from the USDA's cat colony by placing them at the back of the tongue. All feces for each cat were collected daily after feeding infected mouse brains, and examined for *T. gondii* oocysts. Screening and harvesting of *T. gondii* oocysts were done between 3 and 21 days after infection by following procedures as described previously.[59–61] This is a usual prepatent period following feeding of bradyzoites stage.[61] Cats were euthanized on day 21 post infection and blood was collected to do modified agglutination tests (MAT) to test for immunological reactivity to *T. gondii* antigens. Oocysts were collected by floatation methods using sucrose solution with a specific gravity of 1.15 or higher. Concentrated oocyst pellets were suspended in an aqueous solution containing 2% H_2SO_4, and aerated on the shaker for 7 days at room temperature (20–22°C) to allow for oocyst sporulation. Cat 04 excreted *T. gondii* oocysts 13–15 days post inoculation. Cat 05 did not excrete oocysts. At least some oocysts were seen in the feces of the cat fed with this knockout strain, although the numbers of oocysts shed were not quantified because of logistical difficulties,[58] the intrinsic variability in such experiments (J.P. Dubey, personal unpublished observations) and we were also looking for an all or none response (JP Dubey, personal observations). These experiments do not exclude or include a role of *Tg*O/GABA-AT in oocyst formation but there is not a complete absence of oocysts phenotype. Specific detailed description of this experiment is in Figure 7. Our knockout of *Tg*O/GABA-AT in the Type II strain led to increased cyst formation (Figure 6). It did not completely abrogate capacity of knockout parasites to form infectious, pathogenic, sporulated oocysts (Figure 7).

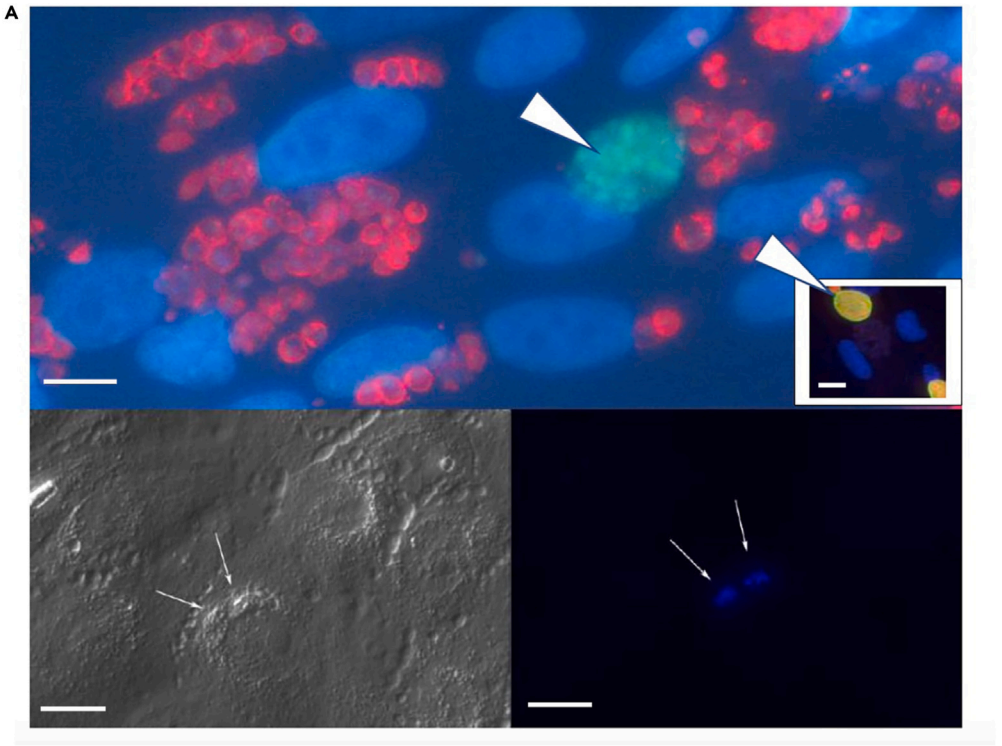

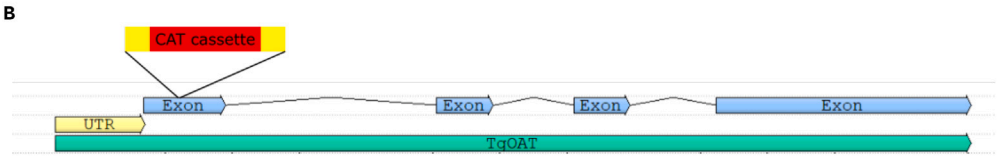

C

Parameter measured	Species	Result
Sequence modified in knockout	cat and mouse	Infected mice and cats with encysted bradyzoites in parallel. Infection confirmed
Oocyst shedding by cat	cat	Oocysts in flotation preparation from cats that received knockout; MAT in control
Ex-cysted sporozoites inoculated	mouse	Recipient mice had ruffled fur and peritonitis with *Toxoplasma* visualized
Knockout confirmed. DNA, mice *Toxoplasma* in recipient mice	mouse	Knockout confirmed in DNA from sub-inoculation of sporozoites into mice

Figure 7. CRISPR Knockout of *TgO*/GABA-AT in EGS strain of *Toxoplasma*

(A) Dual fluorescent EGS strain (SAG1-mCherry, LDH2- sfGFP) in tissue culture HFF, green cyst [blue arrow] red tachyzoites, from Weiss laboratory by Tatiana Paredes Santos and Yan Fen Ma. Bottom panels in A are triple color fluorescent EGS parasite (SAG1-mCherry, LDH2- sfGFP, and MSF-BFP) in cat intestinal cells *in vitro* demonstrating expression of MSF-BFP *in vitro* (from Weiss and Kim. Third Edition of *Toxoplasma gondii-The Model Apicomplexan*. This bottom panel is captioned in the book figure legend "FIGURE 18.10 *Toxoplasma gondii* sexual stage development *in vitro*). (A) Photomicrograph of cat intestinal cells in sexual stage differentiation media (containing bovine serum with 200 μM linoleic acid). Cells were infected with bradyzoites isolated from mouse brain derived EGS strain (Paredes-Santos et al., 2015). *T. gondii* tissue cysts digested with pepsin and acid. Cells were imaged at 403 magnification five days after infection using an EVOS cell imaging station. (Knoll L, manuscript in preparation). (B) Corresponding fluorescence image demonstrating expression of MSF-BFP in EGS strain *T. gondii* (arrows). This EGS strain expresses three distinct stage specific differentiation markers: SAG1-mCherry, LDH2- sfGFP, and MSF-BFP (Weiss L., unpublished data). Source: Courtesy L. Knoll and Bruno Martorelli Di Genova. Reproduced with permission."); Inset in A bottom right hand part of panel dolichos staining of cyst wall [white arrow] from McPhillie, McLeod et al., with permission. Scale bar corresponds to 10 μm. (B) Design and creation of knockout. (C) Results of experiments summarized. This knockout parasite when fed to cats as a bradyzoite still formed at least some oocysts.

Recognition of relationship of *Tg*O/GABA-AT and its substrate GABA to potential roles of candidate T-263 Mutated genes in capacitation and conception

Recognition of this relationship arose from noting regulation of *Tg*O/GABA-AT by MORC[62] combined with culture and sequencing of Frenkel Live Vaccine strain T-263 and analysis of T-263 mutations[43–46,63–71] which occurred in genes responsible for capacitation and conception (Tables 2, 3, and 4, and in color Tables S4–S6; Figures 8, 9, 10, 11, and 12).[72–183]

MORC complex containing AP2V-2 regulates *Tg*O/GABA-AT expression that is increased in merozoites

As noted above *Tg*O/GABA-AT expression and protein levels are increased in sporozoites. Further, the MORC complex regulates expression of *Tg*O/GABA-AT[62] (Figure S7). AP2V-2 is part of the MORC complex and also is regulated by MORC. Please also see below under AP2V-2 and Figure S8.[62] These and several other observations led to our interest in whether a chemically mutagenized clone of *T. gondii*, T-263, might provide insights into roles of GABA, *Tg*O/GABA-AT, or related genes in the formation of the feline intestinal stages of *Toxoplasma* and capacitation: Specifically, T-263 had been found to be incapable of forming oocysts; there is increased expression of *Tg*O/GABA-AT not only in sporozoites but also in feline intestinal enteroepithelial merozoites. Others have observed that GABA, the substrate of *Tg*O/GABA-AT, can lead to phosphorylation of tyrosine of proteins involved in capacitation in other species studied.

Although the capacitation process in *T. gondii* is unstudied, in other species capacitation is initiated by pH changes, HCO_3^-, ROS, and GABA. Then, a PKA leads to phosphorylation of tyrosine in proteins critical to this capacitation process. PKA induces capacitation through this signal transduction pathway involving Ca^{2+}, cAMP and tyrosine phosphorylation. GABA also enters the GABA shunt increasing energy production and increases motility in tachyzoites.[42]

Characterization and analysis of T-263[63–71] and its parental C56 C strain parasites reveals genes known in other species to affect capacitation and fertility[72–172] including those related to *Tg*O/GABA-AT, and GABA.

T-263 retained its original phenotype at the time of sequencing and other new analyses herein

Studies of a chemically (nitrosoguanidine) mutagenized parasite, called T-263, had been conducted[63–68] decades ago. These studies demonstrated that this T-263 mutant was defective in oocyst formation and prevented subsequent oocyst shedding when immunized cats were exposed to otherwise infectious oocysts.[63–71]

This parasite clone and parental strain were retrieved from JP Dubey's collection of parasites. Culture of this Frenkel Live Cat Vaccine strain called T-263 and its parent non-mutagenized C56 parasite allowed expansion of the parasite clones used for other new more current studies herein. The T-263 clone was expanded in human foreskin fibroblast (HFF) cells to collect tachyzoites. Parasite genomic DNA was used for genotyping by multilocus PCR-RFLP markers and confirmed that T-263 belongs to type III lineage as C56.[171] These studies demonstrate that the T-263 parasite that we sequence and use in subsequent experiments herein retains its original defective in oocyst formation phenotype. This phenotype included inability to form fused micro and macrogametes (Figures 8 and 9 and in[63]) even after decades of storage and coincident with use in our sequencing studies described below (Tables 2, 3, and 4 [and in color Tables S4–S6 and S7]).[72–172]

In a single pilot study in a cat intestinal organoid model,[72] the reduction in a replicating form associated with differentiation to zygotes and subsequent oocyst formation was impaired in the mutant T-263, but not its parental C strain control studied simultaneously (data not shown but provided to Editors and Reviewers for verification). This parasite that retained its original phenotype was used for sequencing below. It might therefore be suitable to use in future studies to replicate this phenotype in organoid culture[71] and with CRISPR rescue of its mutations to determine which, if any alone or together, rescue its phenotype in organoid culture or the recently developed barcoded cat pass through model (Silva, Grigg Toxo 2022 Abstract, Riverside, California).

Sequencing of T-263 and its parental C56 strain parasite reveals mutations capable of influencing oocyst formation that are related to *Tg*O/GABA-AT

We sequenced the genome and performed SNP analysis of the T-263 strain and its wild type parental strain C56 to identify parasite genes essential for oocyst formation and infectivity and determine if they were related to *Tg*O/GABA-AT. Relationship to *Tg*O/GABA-AT includes the following: through a direct mutation; mutation in genes responsible for regulation of expression of *Tg*O/GABA-AT; mutations in genes that otherwise modulate amounts of its substrate GABA; or mutations in genes involved in the transport of its substrate GABA influencing energy metabolism and critical merozoite capacitation and conception functions. This analysis identified a number of genes with functions related to *Tg*O/GABA-AT and its substrate GABA (Tables 2, 3, and 4, Box S1 [and in color Tables S4–S6 and S7]: Summary of relationships of *Tg*O/GABA-AT, GABA and mutations in T-263;Figures 8, 9, 10, 11, 12, 13, 14, 15, and 16).

Stage associated expression of mutated genes reveals potential importance of capacitation in merozoites in T-263 phenotype

Mutations in T-263 were sorted based on previous data regarding expression patterns across life cycle stages of *T. gondii* (Tables 2, 3,[36–43,62,72–172] and in color Tables S4–S6 and S7). Genes shown in bolded or in red (in color Tables S4 and S5 correspond to Tables 2 and 3) are noted to be transcriptionally expressed (modulated) in merozoites and or sporozoites of the parasitic life cycle (bold in sporozoites, and red in merozoites, in color Tables S4 and S5 corresponding to Tables 2 and 3).[43–46] Although we find that the T-263 mutant has 116 mutations in merozoite or sporozoite expressed genes (Table 3 [and in color Table S5]), we find that there are no mutations in genes

Table 2. Candidate mutations in T-263 clone compared with Me49 and parental CTG strains

Part A													Part B										
	ME49	CTG	T-263				Data from: Fritz HM et al., 2012. (PMID:22347997)					Data from Hehl et al., 2015		ME49	CTG	T-263				DATA FROM: Fritz HM et al., 2012. (PMID:22347997)					Data from Hehl et al., 2015
							RMA value (Log2)					Percentile								RMA value (Log2)					Percentile
CHROM	ALLELE	ALLELE	ALLELE	MUTATION	GENE_ ID	PRODUCT NAME	d0[1]	d4[1]	d10[1]	Tz[2]	Bz[3]	Merozoite[4]	CHROM	ALLELE	ALLELE	ALLELE	MUTATION	GENE_ ID	PRODUCT NAME	d0[1]	d4[1]	d10[1]	Tz[2]	Bz[3]	Merozoite[4]
Apicopl.	C	C	T	1389G>A	TGME49_ 328900	hypothetical protein	–	–	–	–	–	–	chrVIII	C	C	T	Ser654Phe	TGME49_ 272040	WD domain, G-beta repeat-containing protein	3.49	3.02	2.99	3.29	3.20	–
Apicopl.	A	A	G	Leu215Pro	TGME49_ 329200	hypothetical protein	–	–	–	–	–	–	chrVIII	G	G	T	Ala655Ser	TGME49_ 272040	WD domain, G-beta repeat-containing protein	3.49	3.02	2.99	3.29	3.20	–
chrIa	A	A	T	Met14Leu	TGME49_ 294890	hypothetical protein	–	–	–	–	–	–	chrVIII	G	G	T	Ala815Glu	TGME49_ 271370	hypothetical protein	3.66	3.20	2.96	3.19	4.00	–
chrIb	**T**	**T**	**G**	**Leu460Arg**	**TGME49_ 208420**	**Sodium: neurotransmitter symporter family protein**	**5.79**	**4.85**	**4.76**	**5.10**	**5.70**	**69.8**	chrVIII	A	A	G	Ser191Pro	TGME49_ 271370	hypothetical protein	3.66	3.20	2.96	3.19	4.00	–
chrIb	**T**	**T**	**A**	**Thr107Ser**	**TGME49_ 209985**	**cAMP-dependent protein kinase**	**3.86**	**10.24**	**9.44**	**4.44**	**10.53**	**99.3**	chrVIII	T	T	A	Gln298Leu	TGME49_ 270950	hypothetical protein	7.65	11.81	12.33	3.80	3.93	–
chrIb	C	C	G	His473Asp	TGME49_ 209755	hypothetical protein	2.63	2.76	2.42	2.90	3.76	–	chrVIII	T	T	C	Val3029Ala	TGME49_ 270720	hypothetical protein	–	–	–	–	–	–
chrIb	C	C	G	His521Asp	TGME49_ 209755	hypothetical protein	2.63	2.76	2.42	2.90	3.76	–	chrVIII	C	C	T	Pro3030Leu	TGME49_ 270720	hypothetical protein	–	–	–	–	–	–
chrIb	G	G	A	Ala343Val	TGME49_ 210095	hypothetical protein	3.30	5.18	5.29	3.60	4.07	–	chrVIII	T	T	G	Ser3031Ala	TGME49_ 270720	hypothetical protein	–	–	–	–	–	–
chrII	**T**	**T**	**C**	**Glu1177Gly**	**TGME49_ 221675**	**hypothetical protein**	**3.30**	3.29	**2.97**	**4.00**	**4.08**	**47.6**	chrVIII	T	T	C	phe1522Ser	TGME49_ 270595	UBA/TS-N domain-containing protein	–	–	–	–	–	–
chrII	G	G	A	Ser1773Phe	TGME49_ 222330	hypothetical protein	3.28	3.21	3.04	3.61	3.41	–	chrVIII	G	G	C	Pro1664Ala	TGME49_ 270090	hypothetical protein	3.16	3.22	2.87	3.46	3.64	–
chrII	**C**	**C**	**A**	**Ala1725Ser**	**TGME49_ 297960**	**rhoptry neck protein RON6**	**3.49**	**5.62**	**5.75**	**7.98**	**5.36**	**84.1**	**chrVIII**	**G**	**G**	**A**	**Leu1684Phe**	**TGME49_ 269290**	**hypothetical protein**	**3.19**	**3.25**	**4.16**	**4.39**	**4.37**	**30.4**
chrIII	T	T	C	Thr545Ala	TGME49_ 252065	KRUF family protein	4.83	4.82	4.91	4.35	8.85	–	**chrVIII**	**C**	**C**	**T**	**Ser393Asn**	**TGME49 _268260**	**hypothetical protein**	**4.30**	**5.76**	**5.52**	**4.51**	**4.16**	**40.8**
chrIII	G	G	A	Pro544Ser	TGME49_ 252065	KRUF family protein	4.83	4.82	4.91	4.35	8.85	–	**chrIX**	**T**	**T**	**G**	**Ser38Ala**	**TGME49 _267590**	**Ribophorin II family protein**	-	-	-	-	-	**48.6**
chrIII	**G**	**G**	**A**	**Pro875Ser**	**TGME49_ 252380**	**hypothetical protein**	**3.68**	**3.70**	**3.27**	**3.67**	**4.14**	**39.6**	chrIX	A	A	G	Gln249Arg	TGME49_ 267020	PF13414 TPR_ 11: TPR repeat	3.01	2.81	4.04	3.30	3.19	–

(*Continued on next page*)

Table 2. *Continued*

Part A													Part B										
	ME49	CTG	T-263				Data from: Fritz HM et al., 2012. (PMID:22347997)					Data from Hehl et al., 2015		ME49	CTG	T-263				DATA FROM: Fritz HM et al., 2012. (PMID:22347997)					Data from Hehl et al., 2015
							RMA value (Log2)					Percentile								RMA value (Log2)					Percentile
CHROM	ALLELE	ALLELE	ALLELE	MUTATION	GENE_ ID	PRODUCT NAME	d0[1]	d4[1]	d10[1]	Tz[2]	Bz[3]	Merozoite[4]	CHROM	ALLELE	ALLELE	ALLELE	MUTATION	GENE_ ID	PRODUCT NAME	d0[1]	d4[1]	d10[1]	Tz[2]	Bz[3]	Merozoite[4]
chrIII	A	A	C	Ser116Ala	TGME49_ 252465	radical SAM domain-containing protein	4.45	5.81	4.80	4.91	4.96	25.3	chrIX	G	G	C	Gly250Ala	TGME49_ 267020	PF13414 TPR_ 11: TPR repeat	3.01	2.81	4.04	3.30	3.19	–
chrIII	C	C	G	Pro487Ala	TGME49_ 252870	hypothetical protein	3.91	3.54	2.89	3.51	4.03	–	chrIX	A	A	G	Ser849Pro	TGME49_ 266390	DNA mismatch repair protein, C-terminal domain-containing protein	3.29	3.39	3.02	3.12	4.05	–
chrIV	C	C	T	Gly80Asp	TGME49_ 320230	SAG-related sequence SRS15C	2.77	2.95	3.24	2.81	2.99	96.8	chrIX	C	C	A	Ala283Ser	TGME49_ 266390	DNA mismatch repair protein, C-terminal domain-containing protein	3.29	3.39	3.02	3.12	4.05	–
chrIV	C	C	T	Thr342Ile	TGME49_ 319380	hypothetical protein	3.99	2.88	2.68	3.22	3.49	–	chrIX	T	T	G	Asp36Ala	TGME49_ 266380	PF04614 Pex19: Pex19 protein family	6.57	8.10	7.78	4.03	4.28	–
chrIV	G	G	A	Pro931Ser	TGME49_ 318130	Toxoplasma gondii family E protein	3.18	3.87	3.38	3.80	3.64	63.5	chrIX	C	C	T	Pro146Ser	TGME49_ 266330	Toxoplasma gondii family A protein	3.25	3.12	3.01	3.02	3.20	–
chrIV	A	A	G	Cys2453Arg	TGME49_ 211270	sushi domain (scr repeat) domain-containing protein	6.51	4.86	4.87	4.50	4.36	47.5	chrIX	T	T	C	Arg508Gly	TGME49_ 266150	hypothetical protein	2.88	2.84	2.67	2.73	3.28	–
chrIV	C	C	A	Asp1225Glu	TGME49_ 211010	hypothetical protein	5.75	4.54	5.63	4.70	4.70	42.1	chrIX	A	A	G	Glu7644Gly	TGME49_ 266010	phosphatidylinositol 3- and 4-kinase	3.47	3.32	3.12	3.34	3.40	–
chrIV	C	C	T	Ala455Val	TGME49_ 301480	hypothetical protein	2.93	2.83	2.81	3.09	3.18	86.2	chrIX	C	C	G	Gln957Glu	TGME49_ 265840	hypothetical protein	3.70	3.76	3.99	3.27	3.47	37
chrIV	G	G	C	Glu457Gln	TGME49_ 301480	hypothetical protein	2.93	2.83	2.81	3.09	3.18	86.2	chrIX	G	G	T	Pro624Thr	TGME49_ 265500	chloride transporter, chloride channel (ClC) family protein	3.75	3.46	3.29	3.65	3.56	34.2

(*Continued on next page*)

Table 2. *Continued*

Part A													Part B											
	ME49	CTG	T-263				Data from: Fritz HM et al., 2012. (PMID:22347997)					Data from Hehl et al., 2015		ME49	CTG	T-263				DATA FROM: Fritz HM et al., 2012. (PMID:22347997)					Data from Hehl et al., 2015
							RMA value (Log2)					Percentile								RMA value (Log2)					Percentile
CHROM	ALLELE	ALLELE	ALLELE	MUTATION	GENE_ ID	PRODUCT NAME	d0[1]	d4[1]	d10[1]	Tz[2]	Bz[3]	Merozoite[4]	CHROM	ALLELE	ALLELE	ALLELE	MUTATION	GENE_ ID	PRODUCT NAME	d0[1]	d4[1]	d10[1]	Tz[2]	Bz[3]	Merozoite[4]
chrIV	A	A	T	Asn863Ile	TGME49_ 301480	hypothetical protein	2.93	2.83	2.81	3.09	3.18	86.2	chrIX	G	G	A	Pro623Ser	TGME49_ 265500	chloride transporter, chloride channel (ClC) family protein	3.75	3.46	3.29	3.65	3.56	34.2
chrV	G	G	A	Ala282Val	TGME49_ 220640	hypothetical protein	5.17	7.52	8.33	7.70	7.72	–	chrIX	T	T	C	Gln473Arg	TGME49_ 265010	glutamate 5-kinase domain-containing protein	6.17	3.40	3.28	3.20	3.26	32.5
chrV	A	A	G	Arg3757Gly	TGME49_ 212810	hypothetical protein	3.07	2.65	2.81	2.86	3.69	–	chrIX	T	T	C	Ile472Met	TGME49_ 265010	glutamate 5-kinase domain-containing protein	6.17	3.40	3.28	3.20	3.26	32.5
chrV	G	G	A	Gly521Glu	TGME49_ 212860	hypothetical protein	8.71	8.04	7.56	5.78	6.21	68.4	chrIX	A	A	G	Ile472Thr	TGME49_ 265010	glutamate 5-kinase domain-containing protein	6.17	3.40	3.28	3.20	3.26	32.5
chrV	G	G	A	Ala140Thr	TGME49_ 213050	hypothetical protein	3.38	3.80	3.79	4.21	3.28	–	chrIX	T	T	C	Leu1164Pro	TGME49_ 264430	PF02664 LuxS: S-ribosylhomocysteinase LuxS	3.71	3.78	4.97	3.69	4.12	30.7
chrV	G	G	A	Gly575Arg	TGME49_ 213790	hypothetical protein	4.62	3.98	4.10	5.30	4.79	31	chrIX	A	A	G	Glu99Gly	TGME49_ 264420	lipoprotein, putative	2.70	5.89	5.06	3.71	3.90	44.9
chrV	T	T	A	Glu402Val	TGME49_ 286910	hypothetical protein	3.04	2.63	2.60	2.66	2.65	–	chrIX	C	C	A	Ala1779Glu	TGME49_ 264420	lipoprotein, putative	2.70	5.89	5.06	3.71	3.90	44.9
chrV	T	T	C	Arg3175Gly	TGME49_ 286270	PF10243 MIP-T3: microtubule-binding protein MIP-T3	3.02	3.23	3.06	2.91	3.59	–	chrIX	C	C	T	Arg591His	TGME49_ 290270	SPRY domain-containing protein	2.90	2.84	2.57	2.69	2.91	47.2
chrV	G	G	C	His534Gln	TGME49_ 286180	tRNA ligases class I (M) protein	5.79	3.56	4.29	4.08	3.93	–	chrIX	T	T	A	Val181Glu	TGME49_ 290645	hypothetical protein	–	–	–	–	–	–
chrV	GAC	GAC	AGA	Asp657Arg	TGME49_ 285895	AP2 domain transcription factor AP2V-2	5.54	4.27	3.27	3.08	3.15	–	chrIX	T	T	C	His68Arg	TGME49_ 292190	PF04900 Fcf1: rRNA processing protein, FCF1 family	-	-	-	-	-	45.2

(*Continued on next page*)

Table 2. *Continued*

Part A													Part B											
	ME49	CTG	T-263				Data from: Fritz HM et al., 2012. (PMID:22347997)					Data from Hehl et al., 2015		ME49	CTG	T-263				DATA FROM: Fritz HM et al., 2012. (PMID:22347997)					Data from Hehl et al., 2015
							RMA value (Log2)					Percentile								RMA value (Log2)					Percentile
CHROM	ALLELE	ALLELE	ALLELE	MUTATION	GENE_ ID	PRODUCT NAME	d0[1]	d4[1]	d10[1]	Tz[2]	Bz[3]	Merozoite[4]	CHROM	ALLELE	ALLELE	ALLELE	MUTATION	GENE_ ID	PRODUCT NAME	d0[1]	d4[1]	d10[1]	Tz[2]	Bz[3]	Merozoite[4]
chrV	T	T	C	Ile156Thr	TGME49_ 285540	DNA-directed DNA polymerase	3.45	3.26	3.00	3.22	3.61	30.1	chrIX	A	A	T	Glu861Asp	TGME49_ 292390	KRUF family protein	3.03	2.95	2.60	3.08	3.72	
chrV	G	G	A	Pro2014Leu	TGME49_ 285445	CULLIN_2 domain-containing protein	3.27	3.18	2.86	2.80	3.14	31.9	chrIX	G	G	C	Gly236Arg	TGME49_ 210600	KRUF family protein	3.06	2.92	2.76	3.02	3.46	–
chrV	G	G	A	Gly4627Glu	TGME49_ 285140	hypothetical protein	3.26	3.52	3.85	3.17	3.37	–	chrIX	A	A	T	Glu179Val	TGME49_ 210235	EF-hand domain-containing protein	-	-	-	-	-	26.4
chrV	G	G	T	Ala235Ser	TGME49_ 284050	DEAD/DEAH box helicase domain-containing protein	3.44	3.24	3.23	3.32	3.72	36.4	chrIX	T	T	C	phe1630Ser	TGME49_ 305630	PF12937 F-box-like: F-box-like	–	–	–	–	–	–
chrV	G	G	A	Ser1549Phe	TGME49_ 284040	hypothetical protein	3.73	3.35	3.19	3.52	3.74	–	chrIX	C	C	T	Ser1631Phe	TGME49_ 305630	PF12937 F-box-like: F-box-like	–	–	–	–	–	–
chrVI	C	C	A	Ala2090Ser	TGME49_ 244120	PF07496 zf-CW: CW-type Zinc Finger	3.98	3.66	3.61	4.03	3.93	27.5	chrX	G	G	T	Leu544Phe	TGME49_ 228350	elongation factor Tu GTP binding domain-containing protein	–	–	–	–	–	–
chrVI	A	A	G	His406Arg	TGME49_ 244450	protein phosphatase 2C domain-containing protein	2.99	2.84	2.78	3.08	3.16	89.7	chrX	C	C	G	Pro610Arg	TGME49_ 228340	hypothetical protein	5.02	4.19	4.34	4.01	4.22	25.6
chrVI	T	T	C	Leu1298Ser	TGME49_ 244630	PF12937 F-box-like: F-box-like	2.92	2.53	2.47	2.92	3.07	–	chrX	C	C	A	Ala711Ser	TGME49_ 226072	Ser/Thr phosphatase family protein	4.86	4.68	5.33	4.85	4.93	35.1
chrVIIa	C	C	T	Gly5168Glu	TGME49_ 280660	HECT-domain (ubiquitin-transferase) domaincontaining protein	3.45	3.30	3.21	3.41	3.45	–	chrX	T	T	C	Thr1156Ala	TGME49_ 225980	hypothetical protein	6.50	6.12	6.00	5.29	5.78	28.2
chrVIIa	A	A	C	Gln2235Pro	TGME49_ 206510	toxolysin TLN4	4.44	8.23	7.25	6.07	5.14	81.9	chrX	G	G	A	Leu140Phe	TGME49_ 224920	hypothetical protein	4.85	4.74	4.05	4.62	4.76	26.7
chrVIIa	C	C	T	Pro2254Leu	TGME49_ 206510	toxolysin TLN4	4.44	8.23	7.25	6.07	5.14	81.9	chrX	A	A	C	Ser192Ala	TGME49_ 224750	SAG-related sequence SRS40F	4.90	3.08	3.00	2.86	2.84	94.6
chrVIIa	A	A	G	Cys3422Arg	TGME49_ 206430	formin FRM1	3.61	3.92	3.84	5.23	5.64	27.8	chrX	G	G	C	Ala1864Pro	TGME49_ 234270	hypothetical protein	5.40	6.69	5.93	7.53	6.34	54.4
chrVIIa	A	A	C	1674T>G	TGME49_ 205680	hypothetical protein	4.55	5.65	5.95	7.26	7.35	93.1	chrX	T	T	G	Met1100Leu	TGME49_ 234300	hypothetical protein	3.91	4.58	3.86	2.85	3.19	–

(*Continued on next page*)

Table 2. *Continued*

Part A													Part B											
	ME49	CTG	T-263				Data from: Fritz HM et al., 2012. (PMID:22347997)					Data from Hehl et al., 2015		ME49	CTG	T-263				DATA FROM: Fritz HM et al., 2012. (PMID:22347997)					Data from Hehl et al., 2015
							RMA value (Log2)					Percentile								RMA value (Log2)					Percentile
CHROM	ALLELE	ALLELE	ALLELE	MUTATION	GENE_ ID	PRODUCT NAME	d0[1]	d4[1]	d10[1]	Tz[2]	Bz[3]	Merozoite[4]	CHROM	ALLELE	ALLELE	ALLELE	MUTATION	GENE_ ID	PRODUCT NAME	d0[1]	d4[1]	d10[1]	Tz[2]	Bz[3]	Merozoite[4]
chrVIIa	T	T	G	Asp93Glu	TGME49_ 205500	PF04615 Utp14: Utp14 protein	3.46	3.42	3.40	6.19	4.62	62.5	chrX	G	G	T	Ala3308Ser	TGME49_ 234900	PHD-finger domain-containing protein	5.24	4.46	4.65	4.71	5.27	48.7
chrVIIa	C	C	T	Pro3022Leu	TGME49_ 204560	type I fatty acid synthase, putative	5.25	3.31	3.26	3.48	3.14	25.1	chrX	T	T	C	Leu242Pro	TGME49_ 234990	hypothetical protein	3.68	3.31	3.06	3.61	3.82	32.5
chrVIIa	G	G	C	Cys595Ser	TGME49_ 204050	subtilisin SUB1	3.29	4.23	5.02	6.18	4.28	–	chrX	T	T	A	244T>A	TGME49_ 235370	kinase domain-containing protein	3.74	3.66	3.06	3.21	3.16	91.6
chrVIIa	C	C	T	Leu1118Phe	TGME49_ 203950	Myb family DNA-binding domain-containing protein	5.02	4.20	4.21	3.70	3.71	35.2	chrX	A	A	C	Met194Leu	TGME49_ 236050	fructose-bisphosphate aldolase, putative	4.66	5.76	5.68	4.28	4.61	85.7
chrVIIa	A	A	T	Val313Asp	TGME49_ 203320	zinc finger in N-recognin protein	6.72	7.59	7.54	5.83	5.17	–	chrX	G	G	T	Leu196Phe	TGME49_ 236050	fructose-bisphosphate aldolase, putative	4.66	5.76	5.68	4.28	4.61	85.7
chrVIIa	T	T	A	Ile133Lys	TGME49_ 202850	ATP-binding domain-containing protein	3.31	3.27	3.08	3.64	4.80	–	chrX	T	T	G	Ser200Ala	TGME49_ 236050	fructose-bisphosphate aldolase, putative	4.66	5.76	5.68	4.28	4.61	85.7
chrVIIa	G	G	A	Pro1515Ser	TGME49_ 202490	AP2 domain transcription factor AP2VIIa-7	5.47	4.03	4.05	4.28	4.37	28	chrX	G	G	A	Ala325Val	TGME49_ 236400	hypothetical protein	5.33	4.45	4.85	4.65	5.19	77.3
chrVIIa	T	T	C	Val429Ala	TGME49_ 202370	T-complex protein 1, epsilon subunit (TCP-1epsilon), putative	4.87	3.44	3.58	4.62	4.23	93.6	chrX	A	A	C	Ser1007Ala	TGME49_ 215640	zinc finger, C3HC4 type (RING finger) domaincontaining protein	4.52	3.60	3.64	4.46	3.93	33.9
chrVIIa	G	G	T	Pro936Thr	TGME49_ 201180	hypothetical protein	3.93	3.64	4.08	4.52	5.29	96	chrX	T	T	C	Leu1084Ser	TGME49_ 215690	hypothetical protein	3.05	3.08	2.90	3.05	2.96	–
chrVIIa	A	A	G	Asn521Asp	TGME49_ 282140	cwf21 protein	9.35	6.10	5.94	3.98	4.39	52.9	chrX	G	G	T	Leu1084Phe	TGME49_ 215690	hypothetical protein	3.05	3.08	2.90	3.05	2.96	–
chrVIIa	A	A	G	His522Arg	TGME49_ 282140	cwf21 protein	9.35	6.10	5.94	3.98	4.39	52.9	chrX	C	C	T	Pro945Ser	TGME49_ 207040	hypothetical protein	3.08	3.95	3.46	2.81	2.86	–
chrVIIb	T	T	C	phe1119Ser	TGME49_ 263980	pentatricopeptide repeat domain-containing protein	4.60	5.19	4.74	4.29	4.71	30.6	chrX	G	G	A	Thr276Ile	TGME49_ 207110	hypothetical protein	–	–	–	–	–	–

(*Continued on next page*)

Table 2. *Continued*

Part A							Data from: Fritz HM et al., 2012. (PMID:22347997)					Data from Hehl et al., 2015	Part B							DATA FROM: Fritz HM et al., 2012. (PMID:22347997)					Data from Hehl et al., 2015
	ME49	CTG	T-263				RMA value (Log2)					Percentile		ME49	CTG	T-263				RMA value (Log2)					Percentile
CHROM	ALLELE	ALLELE	ALLELE	MUTATION	GENE_ ID	PRODUCT NAME	d0[1]	d4[1]	d10[1]	Tz[2]	Bz[3]	Merozoite[4]	CHROM	ALLELE	ALLELE	ALLELE	MUTATION	GENE_ ID	PRODUCT NAME	d0[1]	d4[1]	d10[1]	Tz[2]	Bz[3]	Merozoite[4]
chrVIIb	**T**	**T**	**C**	**Ser1132Pro**	**TGME49_ 263980**	**pentatricopeptide repeat domain-containing protein**	**4.60**	**5.19**	**4.74**	**4.29**	**4.71**	**30.6**	**chrX**	**C**	**C**	**T**	**Ser77Asn**	**TGME49_ 207150**	**SAG-related sequence SRS49C**	**3.93**	**2.98**	**2.65**	**5.51**	**8.15**	**88.7**
chrVIIb	**A**	**A**	**G**	**Glu105Gly**	**TGME49_ 263670**	**ribosomal RNA large subunit methyltransferase FTSJ1, putative**	**3.30**	**2.93**	**2.79**	**3.20**	**3.60**	**29.9**	**chrXI**	**A**	**A**	**C**	**Ile208Ser**	**TGME49_ 311720**	**chaperonin protein BiP**	**7.21**	**4.14**	**6.88**	**10.38**	**9.16**	**99**
chrVIIb	**G**	**G**	**C**	**Ser195Thr**	**TGME49_ 263610**	**hypothetical protein**	-	-	-	-	-	**26.2**	chrXI	C	C	T	Ser1748Asn	TGME49_ 313210	hypothetical protein	2.68	2.70	2.48	2.84	3.07	–
chrVIIb	G	G	C	Val5446Leu	TGME49_ 262825	peptidase family c50 protein	3.44	3.30	2.73	3.55	3.07	–	**chrXI**	**A**	**A**	**T**	**Leu35Phe**	**TGME49_ 216140**	**tetratricopeptide repeat-containing protein**	**5.40**	**3.24**	**4.10**	**5.70**	**9.78**	**32.4**
chrVIIb	**A**	**A**	**C**	**Glu453Ala**	**TGME49_ 262530**	**leucine rich repeat-containing protein**	**5.32**	**4.74**	**4.42**	**3.87**	**3.51**	**54.4**	chrXII	C	C	T	Leu44Phe	TGME49_ 300160	hypothetical protein	3.32	3.03	3.00	3.17	2.96	–
chrVIIb	G	G	A	Met220Ile	TGME49_ 262470	C protein immunoglobulin-A-binding beta antigen, putative	12.95	10.54	11.27	3.66	3.57	–	**chrXII**	**T**	**T**	**A**	**Asp2433Glu**	**TGME49_ 219738**	**hypothetical protein**	**3.10**	**3.26**	**3.01**	**3.12**	**3.48**	**31.4**
chrVIIb	A	A	C	Glu191Asp	TGME49_ 259900	hypothetical protein	3.32	13.56	12.89	2.87	2.83	–	**chrXII**	**C**	**C**	**T**	**Gly3025Asp**	**TGME49_ 219660**	**hypothetical protein**	**3.68**	**3.41**	**3.01**	**3.38**	**3.54**	**62.6**
chrVIIb	**A**	**A**	**G**	**Glu106Gly**	**TGME49_ 258850**	**hypothetical protein**	**3.27**	**2.96**	**3.50**	**3.59**	**3.66**	**66.4**	**chrXII**	**C**	**C**	**T**	**Gly171Ser**	**TGME49_ 250880**	**kinase, pfkB family protein**	**5.93**	**4.46**	**5.17**	**7.62**	**6.39**	**85.5**
chrVIIb	A	A	G	Ser652Pro	TGME49_ 255860	hypothetical protein	3.56	3.68	3.74	3.60	3.74	–	chrXII	G	G	A	Ser463Phe	TGME49_ 278020	hypothetical protein	3.58	2.89	3.04	3.07	3.25	–
chrVIII	**A**	**A**	**G**	**Val148Ala**	**TGME49_ 231880**	**hypothetical protein**	**2.90**	**2.84**	**2.50**	**2.94**	**3.25**	**95.5**	chrXII	C	C	G	Gly450Ala	TGME49_ 278020	hypothetical protein	3.58	2.89	3.04	3.07	3.25	–
chrVIII	T	T	A	Ile28Phe	TGME49_ 231996	hypothetical protein	–	–	–	–	–	–	chrXII	T	T	C	Ser840Pro	TGME49_ 277895	ubiquitin carboxyl-terminal hydrolase	3.85	3.89	3.91	3.73	3.97	–

Candidate mutations identified in the T-263 clone of *T.gondii* compared with the ME49 strain and parental CTG clone. These are the same data as in the companion Table S4, and Supplemental excel Table S7, which have color coding where red font and yellow columns are visible. In the companion Tables S4 and S7, yellow columns denote gene expression values across different parasite stages as reported by Fritz et al. (PMID:22347997) and Hehl et al. (PMID:25757795). 1, Oocysts sporulated after 0 (d0), 4 (d4) or 10 (d10) days; 2, *in-vitro*-derived tachyzoites (2 days post-infection); 3, in-vivo-derived bradyzoites (21 days post-infection). For Fritz et al. dataset, numbers represent mean normalized, log-transformed expression values and calculated fold-change in expression levels for each pairwise comparison. Numbers in the Hehl et al. dataset represent percentile gene expression values above 25% only considering sense transcripts in the merozoite stage. Red font in the companion Tables S4 and S7 denotes genes expressed in the merozoite stage, while bold font indicates genes expressed during the oocyst/sporozoite stages. Table S7 is the Excel chart that shows the same one hundred sixteen mutations in T-263.

Table 3. Candidate mutations identified in the T263 strain of *T. gondii* and not present in the genome sequence of other wild-type *T. gondii* strains available at NCBI-SRA database

	ME49	CTG	T-263				Fritz et al., 2012									
MORHC	ELELLA	ELELLA	ELELLA	NOITATUM	GENE_ID	PRODUCT NAME	d0[1]	d4[1]	d10[1]	Tz[2]	Bz[3]	d4 vs. d0	d10 vs. d0	d10 vs. d4	d10 vs. tachy	d10 vs. brady
chrIa	A	A	T	Met14Leu	TGME49_294890	hypothetical protein	–	–	–	–	–	–	–	–	–	–
chrIb	T	T	G	Leu460Arg	TGME49_208420	Sodium:neurotransmitter symporter	5.13	4.46	4.27	4.69	4.99	0.738	0.689	–	–	0.739
chrIb	T	T	A	Thr107Ser	TGME49_209985	cAMP-dependent protein kinase	–	–	–	–	–	–	–	–	–	–
chrIV	A	A	G	Cys2453Arg	TGME49_211270	sushi domain (scr repeat) domain-c	–	–	–	–	–	–	–	–	–	–
chrV	G	G	A	Ala140Thr	TGME49_213050	hypothetical protein	–	–	–	–	–	–	–	–	–	–
chrV	T	T	C	Ile156Thr	TGME49_285540	DNA-directed DNA polymerase	–	–	–	–	–	–	–	–	–	–
chrV	G	G	A	Pro2014Leu	TGME49_285445	hypothetical protein	–	–	–	–	–	–	–	–	–	–
chrVIIa	C	C	T	Gly5168Glu	TGME49_280660	HECT-domain (ubiquitin-transferas	4.84	4.58	4.26	4.66	4.32	–	0.795	–	–	–
chrVIIa	A	A	G	Cys3422Arg	TGME49_206430	formin FRM1	4.01	4.12	3.89	4.97	5.17	–	–	–	0.66489	0.596
chrVIIa	A	A	C	1674T>G	TGME49_205680	hypothetical protein	–	–	–	–	–	–	–	–	–	–
chrVIIa	C	C	T	Leu1118Phe	TGME49_203950	Myb family DNA-binding domain-co	–	–	–	–	–	–	–	–	–	–
chrVIIa	T	T	A	Ile133Lys	TGME49_202850	ATP-binding domain-containing pr	4.10	3.73	3.32	4.05	4.49	–	–	–	–	0.71
chrVIIa	T	T	C	Val429Ala	TGME49_202370	T-complex protein 1, epsilon subuni	–	–	–	–	–	–	–	–	–	–
chrVIIb	A	A	G	Glu106Gly	TGME49_258850	hypothetical protein	–	–	–	–	–	–	–	–	–	–
chrVIII	A	A	G	Val148Ala	TGME49_231880	hypothetical protein	–	–	–	–	–	–	–	–	–	–

(*Continued on next page*)

Table 3. *Continued*

	ME49	CTG	T-263				Fritz et al., 2012									
MORHC	ELELLA	ELELLA	ELELLA	NOITATUM	GENE_ID	PRODUCT NAME	d0[1]	d4[1]	d10[1]	Tz[2]	Bz[3]	d4 vs. d0	d10 vs. d0	d10 vs. d4	d10 vs. tachy	d10 vs. brady
chrVIII	T	T	A	Ile28Phe	TGME49_231996	hypothetical protein	–	–	–	–	–	–	–	–	–	–
chrVIII	T	T	A	Gln298Leu	TGME49_270950	hypothetical protein	6.53	8.86	8.67	3.84	4.47	8.626	7.123	–	31.25	25.275
chrVIII	G	G	A	Leu1684Phe	TGME49_269290	hypothetical protein	–	–	–	–	–	–	–	–	–	–
chrVIII	C	C	T	Ser393Asn	TGME49_268260	hypothetical protein	4.42	5.21	4.75	4.54	4.35	1.444	–	–	–	–
chrIX	T	T	G	Ser38Ala	TGME49_267590	hypothetical protein	–	–	–	–	–	–	–	–	–	–
chrIX	T	T	G	Asp36Ala	TGME49_266380	PF04614 Pex19: Pex19 protein fam	5.23	6.14	5.72	3.90	4.52	–	–	–	2.34192	1.903
chrIX	A	A	T	Glu179Val	TGME49_210235	hypothetical protein	–	–	–	–	–	–	–	–	–	–
chrX	G	G	A	Leu140Phe	TGME49_224920	hypothetical protein	4.32	4.10	3.78	4.49	4.62	–	–	–	0.79554	0.756
chrX	T	T	A	244T>A	TGME49_235370	hypothetical protein	–	–	–	–	–	–	–	–	–	–
chrXI	A	A	C	Ile208Ser	TGME49_311720	chaperonin protein BiP	7.02	4.10	5.92	7.43	6.64	0.164	0.414	2.53165	0.2849	–
chrXI	C	C	T	Ser1748Asn	TGME49_313210	hypothetical protein	–	–	–	–	–	–	–	–	–	–
chrXI	A	A	T	Leu35Phe	TGME49_216140	tetratricopeptide repeat-containing	5.52	3.27	3.96	4.91	7.10	0.416	0.495	–	0.69589	0.145
chrXII	C	C	T	Gly171Ser	TGME49_250880	kinase, pfkB family protein	5.25	4.08	4.36	5.86	5.54	0.603	0.664	–	0.44984	0.558

Candidate mutations identified in the T263 strain of *T. gondii* and not present in the genome sequence of other wild-type *T. gondii* strains available at NCBI-SRA database. This version of this table is without color coding as described for the companion Table S5 and also in the accompanying Supplemental excel Table S7. In Table S5 Yellow columns denote gene expression values across different parasite stages as reported by Fritz et al. 2012 and Hehl et al. 2015. 1, Oocysts sporulated after 0 (d0), 4 (d4) or 10 (d10) days; 2, *in vitro*-derived tachyzoites (2 days post-infection); 3, *in vivo*-derived bradyzoites (21 days post-infection). For Fritz et al. dataset, numbers represent mean normalized, log-transformed expression values and calculated fold-change in expression levels for each pairwise comparison. Numbers in the Hehl et al. 2015 and Ramakrishnan, C et al. 2019 datasets represent merozoite percentile gene expression values above 25% only considering sense transcripts. Red font in Tables S5 and S7 denotes genes expressed during the merozoite stage, while bold font indicates genes expressed during the oocyst/sporozoite stages. The mutation is a T- > A at nucleotide position 244 within the 5′ UTR of TGME49_235370, and the change does **not** generate an early start codon. Therefore, it is unlikely of having any impact on the function/expression of the encoded protein. Please also see accompanying Excel Table S7.

Table 4. Genes with mutations, annotation in GeneBank or ToxoDB or with PFAM search that identifies gene in another species where this is a recognized function in capacitation, fertilization, gamete fusion or pre-fusion development*

ToxoDB ID -Gene name or PFAM	Mechanism (References*[45, 72–173])
TGME49_208420- Na/GABA symporter	Ionicity, maturation, fertilization, motility, Na:GABA shunt, energy. Change in bicarbonate, pH, ionicity triggers development process. (*GABA modulates all steps of capacitation)[45,73–75,84] **AlphaFold2 predicts mutation could affect function**
TGME49_209985-PKA^{+} (cAMP-dependent protein kinase A) (Noted because mutation annotated as a single copy in ToxoDB- not certain mutated) (Rhoptry +other?)	Cell signaling, capacitation, adenyl cyclase, male and female gamete, motility, cell volume, osmolality. Mutation noted in Toxo DB even considered as a single copy gene. Now know there are 14 copies with mutation uncertain-possible gene-relay[76,77])
TGME49_211270-Sushi domain-containing protein	Capacitation all steps; tissue distribution[161]; NO activates cyclic GMP, Ca^{++} efflux[73]
TGME49_203950-Myb DNA-binding domain-containing protein	Anthar stamen in plant differentiation male gamete[79]
TgO/GABA-AT and relationship to substrate **GABA** (central in capacitation process but not a mutation in a gene)· E.g., Genes that affect GABA like symporter ot Tg0/GABA AT	Concentration modulates all steps of capacitation. Note *Tg*O/GABA-AT in GABA synthesis[45,80–87] Note MORCC complex regulates expression of TgO/GABA-AT in merozoites
TGME49_285540-DNA-directed DNA polymerase	Reactive oxygen[88,179] **AlphaFold2 predicts mutation coul affect function.**
TGME49_206430--formin	Actin, mobility[78,89,90]
TGME49_273760–Hsp70 chaperone	don't undergo meiosis, infertile[8,89,90]
TgME49_216140-tetratricopeptide repeat-containing protein	Actin polymerization motility[91]
TGME49_287510-Aromatic amino acid hydrolase AAH1	AAH1[92–94]
TGME49_212740–Aromatic amino acid hydrolase AAH2	Infectivity Durability; not mutation[92–94]
TGME49_250880–Kinase, pfkB family protein	Fusion; Like 1,2 carbohydrate kinase, sperm motility[72,95–98,101,102,104,105]
TGME49_235370 Protein kinase domain-containing protein	**AlphaFold2 predicts mutation could affect function** Protein kinase domain
TGME **TGME4 TGME49_285445** CULLIN_2 domain-containing protein	Cullin[118]
TGM **TGME49_267590** oligosaccharyltransferase subunit Ribophorin II	Ribophorin II
TGME **TGME49_210235** EF-hand domain-containing protein	EFhand domain[119–122]

Genes expressed in merozoites among 116 mutations noted, with mutations in genes with loss of function with mechanism identified by name. These genes have relationships to other genes known to affect capacitation, fusion of gametes in other species that might provide examples of roles for homologues in *Toxoplasma*. A literature search of Google Scholar, PubMed, and cross references generated the reference list that follows. This provided a road map to relevant genes/proteins and regulatory mechanisms involved in genetics and mechanisms of failure of fusion of male and female gametes and infertility with key words "infertility," "triggering," "capacitating," "building an acrosome," "sperm motility", Genes in this table were generated from the following ref.[43,72–173] In this version bold with gray shading indicates AlphaFold2 suggests possible loss of function. In the accompanying Table S6 these are indicated with green font.

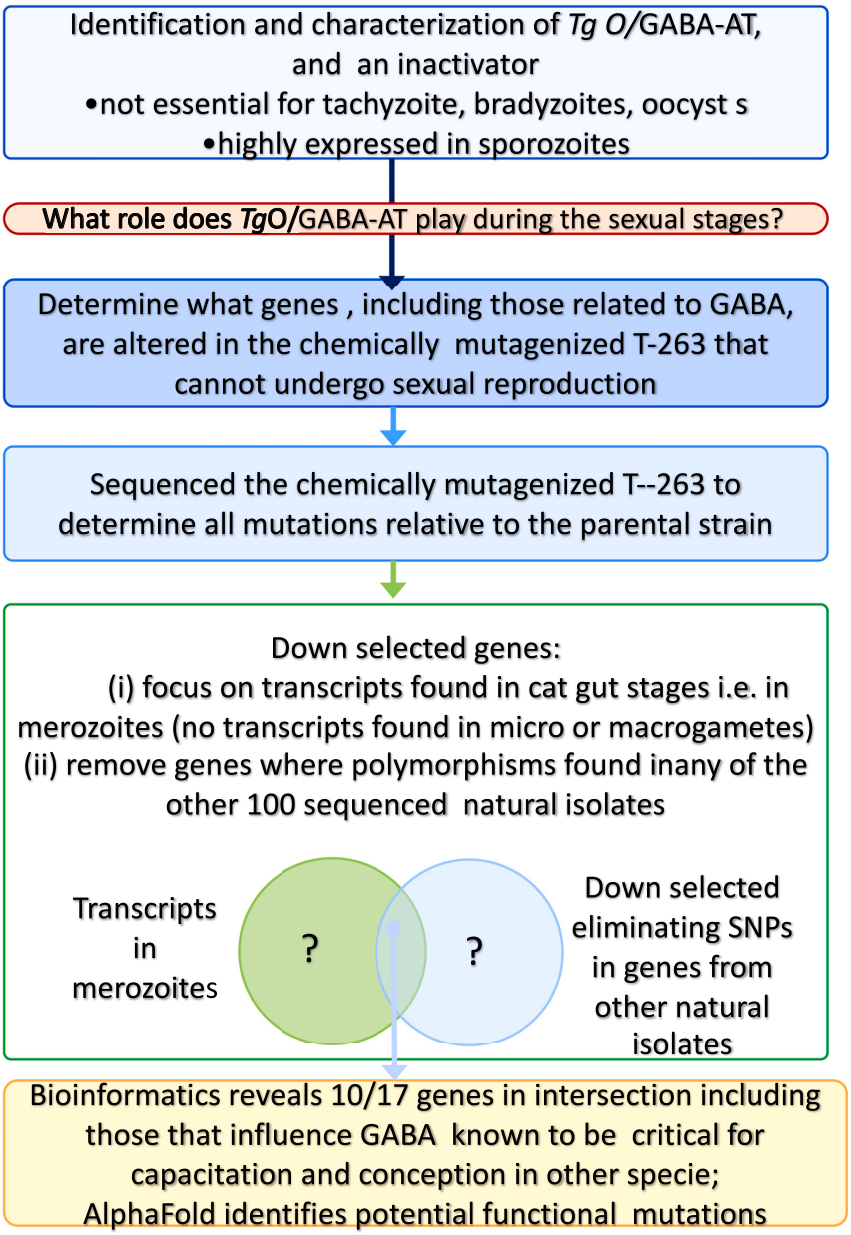

Figure 8. Experiments and logic of studies that led us from *Tg*O/GABA-AT, GABA, Sporozoites, Merozoites, and MORC regulation of *Tg*O/GABA-AT to T-263, analysis of its mutations in feline intestinal stages, and specific mutated genes

Herein we found evidence for the enzymes of *Tg*O/GABA-AT which are not essential for tachyzoites, bradyzoites or oocyst formation, although 245-fold over expressed in sporozoites and over-expressed in merozoites. We noted that knock out of *Tg*O/GABA-AT led to increased brain cysts and decreased survival and would increase the amount of its substrate GABA. We note that *Tg*O/GABA-AT is regulated by the MORC complex (Supplemental MORC Influences genes Figures S7 and S8 with tables, adapted from Farhat Hakimi with permission) which includes AP2V-2. This made further study of the formation of a *Toxoplasma gondii* zygote of interest. This led us to look for the mutations in T-263 which cannot make oocysts, has gametes but does not progress beyond the stage where male and female gametes form but cannot fuse to make a zygote. We obtained stored T-263 and its parental strain, confirmed that when we grew this mutagenized parasite and its parental C strain parasite that the mutant recapitulated its earlier phenotype in cats (Figure 9) and an organoid model whereas the parental did not (data not shown but provided to Editor and Reviewers). When this mutagenized parasite was sequenced, and stage associated expression of the mutated genes was analyzed, no mutations were found in the genes expressed in gametes. This led us to look for overlap between genes essential for other species for capacitation and conception and those overexpressed in merozoites. We considered whether SNPs that were mutated in T-263 were found in any of 100 sequenced isolates of *T. gondii* found in nature from throughout the world. It seemed highly unlikely that a

Figure 8. *Continued*

parasite could be transmitted in nature if it could not progress through the cat stages. Such an SNP that stopped conception would be incompatible with a parasite's perpetuation and survival in nature. This assumption allowed us to down select our candidates to the genes shown in Tables 2, 3, and 4 supplemental MORC expression Tables from Farhat, Hakimi *et al.*, Figures S7 and S8 and identify genes that were further characterized by AlphaFold and to query whether mutations might alter functions[42,72–183] of the genes (Figures 9, 10, 11, 12, 13, 14, 15, and 16).

expressed in micro or macro gametes in T-263. Since we find that a defect in the mutagenized T-263 strain still yields morphologically identifiable micro and macrogametes in the cat intestine (Figure 9A), we deduce that the crucial defect must occur in genes involved in the capacitation process of the merozoite creating macro and/or microgametes that cannot fuse. Although additional mutations in genes expressed in sporozoites could contribute to an additional defect in oocyst formation, the defect in fusion would obviate significance of the mutations in sporozoites because sporozoites could not form unless there was parthenogenesis as suggested might be possible by Ferguson.[173]

In our analysis of the sequence of T-263 that identified a total of 116 genes carrying potential change-of-function (CoF) exonic mutations in T-263 that were not present in C56 (Table 2, [and in color Table S4]), one hundred thirteen protein coding genes harbor nonsynonymous mutations. Two hypothetical genes and a protein carrying a kinase domain had mutations at either donor splice sites or a new in-frame start codon.

One gene encoding a potential PKA/G (TGME49_209985) was initially thought to have a mutation based on the reference ME49 genome sequence available at ToxoDB (Figure 9B). However, further analysis of a PacBio assembly of *T. gondii* strain RH-88 showed that TGME49_209985 belongs to a highly conserved multicopy gene array (Genebank: CM023082.1 positions 198570–349402) and therefore we could not verify its mutation. Still, the gene and its potential mutation were left in the list of candidate genes due to its potential involvement in gamete formation (see below).

Mutations in T-263 expressed in merozoites and sporozoites not found in natural isolates allowed for down selection of candidate genes for initial study by using CRISPR CAS 9 to rescue mutations

The inductive processes to down select candidate genes for further study are shown in Figure 8: One hundred isolates of *T. gondii* that were sequenced at The J. Craig Venter Institute (JCVI) had meta-data (Lorenzi unpublished) that allowed us to query whether mutations found in T-263 also were identified in any parasite natural isolates. We hypothesized that critical mutations that blocked fusion of male and female gametes might be selected against in natural infections, although it is also possible that transmission from carnivore to carnivore could still occur with such a mutation in certain ecologic niches. For example, the AP2 V-2 and the SRS15C mutations were of interest although they occurred in at least some natural isolates (Tables 3 and 4 [Tables S5 and S6 in color]).

To further analyze the mutations that might be critical for the absence of fusion of the male and female gamete, we down-selected mutations in genes expressed in the merozoite stage (pre fusion and before formation of micro and macrogamete that might affect gamete formation) that were not found in natural isolates in the JCVI collection of sequences of all natural isolates (Figures 9, 10, 11, and 12). We identified 21 such genes (Tables 3 and 4 [Tables S5 and S6 in color]).

Genes critical in capacitation and fertilization which are mutated in T-263, with mutations not found in 100 natural isolates sequenced

Bioinformatics, analysis of genes with mutations in T-263 PFAM analysis, and literature searches for genes related to GABA, failure of gametes to make zygotes, or infertility reported in other species revealed genes critical for capacitation and conception in other species. This was done to further identify candidate genes mutated in T-263 that could contribute to or be solely responsible for the failure of zygote formation phenotype and whether they might be related to *Tg*O/GABA-AT. We focused on genes that had no mutations in any of 100 isolates we sequenced at JCVI. Once we had sequences for our mutated, down selected genes, we performed PFAM analyses on those 21 genes. We then looked for homologues for these genes in Pubmed and Google Scholar that when mutated caused infertility in any species.[73–173] Those genes with mutations that did not occur in any of the natural isolates are considered candidates for causing similar defects in fitness in T-263 suitable for further study in the future. Examples include the cyclic AMP dependent protein kinase and the sodium GABA symporter critical for entry of GABA into the GABA shunt, to the TCA cycle. These genes also had homologues that when mutated caused infertility in other species.

Specific candidate genes associated with fertility/infertility and/or capacitation in other species are among our genes mutated in T-263

Cyclic AMP dependent protein kinase-encoding gene is a candidate mutated in T-263 with mutation not found in other natural isolates that can affect conception in other species.

Sequence of T-263 mutagenized *Toxoplasma* provides further insight into related molecular mechanisms critical in creation of *T. gondii* zygotes. During our analysis of T-263 described above, a putative cyclic AMP-dependent protein kinase-encoding gene (Figure 9; Tables 2 and 3 [Tables S4 and S5, and Excel Table S7 in color]) (TGME49_209985) that is overexpressed in merozoites was evident in our initial analyses when we were using ToxodB to identify the nonsynonymous mutations. Structure of this cyclic AMP dependent kinase is modeled with AlphaFold2 (Figures 9 and 12). However, later, this nonsynonymous mutation could not be confirmed because it was in a highly

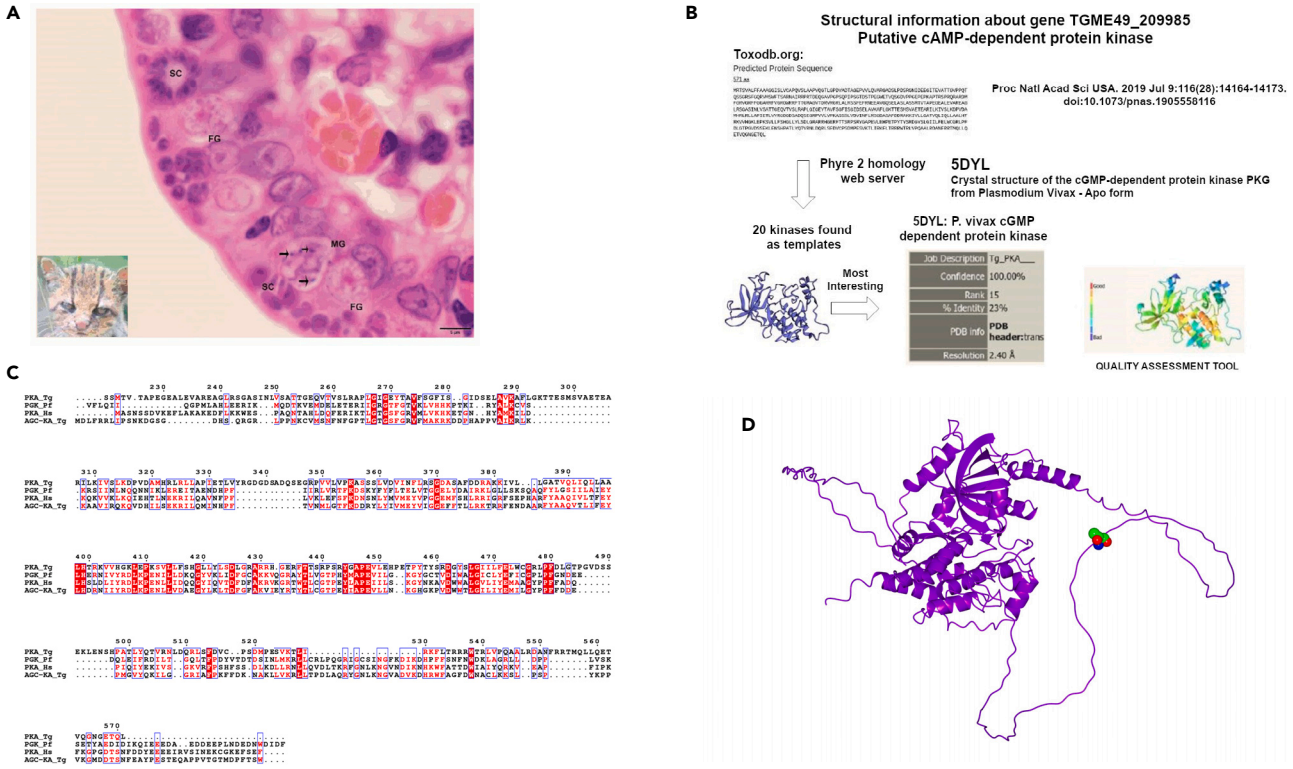

Figure 9. Capacitation of merozoites to microgametes and macrogametes, and cyclic-AMP dependent PKAs essential in all organisms

(A) Failure of development of stages beyond morphologically normal microgametes and macrogametes. Histological section of ileum of cat showing schizonts (sc), male gamonts (mg with mature male gametes, arrows), and female gamonts (fg) in surface enterocytes, five days post-inoculation with T- 263 strain tissue cysts. Hematoxylin and eosin stain. Almost all enterocytes are infected and the *T. gondii* stages are located above the host cell nucleus. Because we could not find genes expressed in microgametes or macrogametes with mutations in T-263 we deduced that mutations must be in the stage just before and therefore we considered merozoite genes that could be responsible. There were candidate genes for capacitation expressed in merozoites that included a Sodium: GABA symporter and a putative PKA.

(B) Merozoite PKA sequence. Pathways to capacitation are known in other species.[72–172] In these other species ranging from chlamydomonas to mammals, with variations, these pathways include processes initiated by pH, $HCO3^-$, affecting cyclic-AMP dependent PKA and proteins phosphorylated on tyrosine. GABA modulates these as shown in Figure 16. Identification of a merozoite plasmodial PKG with 23% homology with the *Toxoplasma* PKA. Areas of homology between PKA and Plasmodia PKG and PKAs involved in capacitation in other species are shown in multisequence alignments. (C) Multisequence alignment with a focus on capacitation PKA sequences in other species. We found some similarities but no strong gene orthologues or homologues of *Tg* merozoite putative PKA were identified.

(D) Cyclic AMP kinase structure from AlphaFold2. Figure S12 corresponds to this.

conserved repetitive region. This repetitive nature of TGME49_209985 was revealed by using third generation sequencing technologies (PacBio/MinION). While potentially very interesting biologically, we are unable to confirm the presence or absence of a mutation, so the gene may not be critical for the oocyst deficient T-263 phenotype. Nonetheless, since such PKAs are essential for zygote formation across all species studied, in the pre-gamete stages (similar to merozoites), we asked whether this PKA we noted could be relevant to that preparation process.

Thus, we compared the PKA we identified to other species PKAs. We note as shown in Figure 9, that our PKA has some modest sequence similarities to PKA s in other species that are critical for formation of functional male gametes[76,87,124,173] (Figure 9; Table S4), and a PKG (ASSN# genebank: AF465544.1) in plasmodia merozoites.[83,] In other species, this process is called "capacitation"(Figure 9) and a PKA in the pre gamete stage is critical for capacitation. A similar PKA has been found in every species studied (Figure 9). Although our PKA is a multicopy gene, the similarities to the malaria PKG led us to notice its unusual relay mode of regulation of multicopy units (Figure 9). It seems possible that a single mutation could regulate a critical initiating or perpetuating step in a relay process, even if in only one copy of a multicopy gene. As with mutations in other genes, the nonsynonymous mutation noted in the ToxodB annotation does not occur as a natural variant in any isolate *in T.gondii* in nature. The putative cyclic AMP dependent PKA seems likely to play a significant role in the conception process whether or not it is mutated in this ~14 copy gene. These gene mutations are candidates that could contribute to, and thereby explain the observed loss of function phenotype where male and female gametes do not fuse and thereby fail to make oocysts and result in elimination of oocyst shedding in initial T-263 peroral infection, and prevention of subsequent shedding by challenging with oocysts.

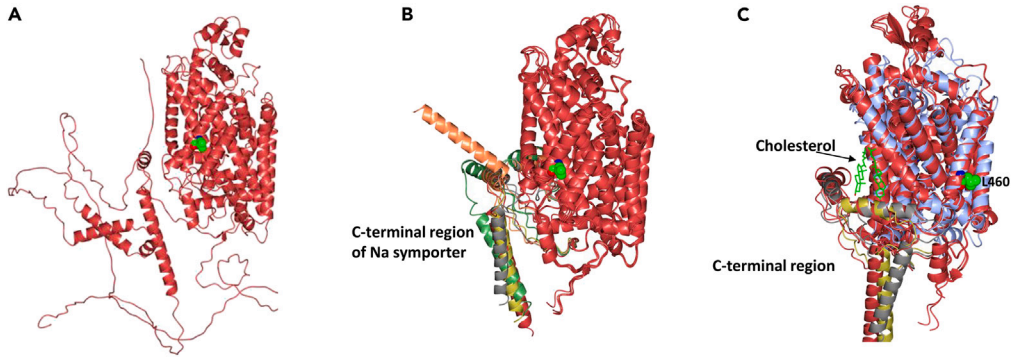

Figure 10. Sodium GABA symporter AlphaFold2 analysis

(A) Predicted structure of *Tg* sodium GABA symporter. The position of L460 residue is shown as sphere model in green/red/blue for carbons/oxygen/nitrogen.

(B) Structure superposition of the wild type and mutated variant of Tg sodium GABA symporter AlphaFold2 models. Helices that undergo conformational differences in predicted mutated models are colored in lawn green (model 1), gray (model 2), gold (model 3) and coral (model 4).

(C) Superposition of *Tg* sodium GABA symporter (pile crimson) and dopamine transporter (ice blue) bound to cholesterol molecules (green cylinder model). Helices involved in conformational change due to mutation in Tg sodium GABA symporter are shown in gray (model 1) or gold (model 3). Figure S11 corresponds to this.

Sodium GABA symporter gene with functions related to TgO/GABA-AT is mutated in T-263 and mutations in other species are associated with infertility

Although *Tg*O/GABA-AT does not have mutations in T-263, genes responsible for transcription of *Tg*O/GABA-AT, related to *Tg*O/GABA-AT expression in merozoites, and levels of GABA in parasites have mutations in T-263. These are described and presented in Figures 10, 11, and 12, and Tables 3 and 4 [Tables S5 and S6], and herein. This sodium GABA symporter gene that is also mutated in T-263 also has a modest increase in transcription with knockdown of MORC in Prugneaud strain parasites[62] (Figure S7[42]). Because *Tg*O/GABA-AT converts GABA to succinate it thereby lowers the amount of GABA, as described above (Figure 1). Thus, when *Tg*O/GABA-AT is knocked out this conversion will not occur, increasing the amount of GABA. *Tg* GABA enters the GABA shunt if/when it is transported into mitochondria by the sodium GABA symporter.[42] Our analysis of the *Tg*O/GABA-AT sequence shows that there is no mitochondrial targeting sequence in the sequence of *Tg*O/GABA-AT. However, but the pattern of immunostaining of *Tg*O/GABA-AT and mitotracker[53] co-localized with mitochondria and occurred in the cytoplasm of sporozoites (Figures 6I and 6J). Also, and we find a mutation in the symporter for the GABA that is the substrate for *Tg*O/GABA-AT (Tables 2 and 3 [Tables S4 and S5 in color]). This mutation in the sodium GABA symporter was corrected by CRISPR (Figure 11) creating a parasite which can be used in future studies. This would be to assess whether there is a loss or gain of function effect from the mutation using the kitten intestinal organoid *in vitro* and/or cat pooled barcoded knockout *in vivo* models (Silva, Grigg et al., Toxo 2022, Abstract. Riverside, California).

Precursor GABA would accumulate with knockdown of *Tg*O/GABA-AT in Pru as it is the substrate of *Tg*O/GABA-AT. In earlier studies,[42]MacCrae, Streipen et al. found that in extracellular parasites the GABA shunt then produces additional energy through the TCA cycle that enhances and increases extracellular parasite motility. Parasite (tachyzoite) invasion of host cells involves such motility. With increased motility and hence invasion, the number of parasites initiating cyst formation increases, leading to more established cysts. This is the phenotype we find with the *Tg*O/GABA-AT Prugniaud strain knockout parasite, shown above in Figure 6. Sporozoite and merozoite invasion also likely involves motility in a similar manner to tachyzoites. Microgamete contact with the macrogamete also likely involves motility of this flagellated form. Extracellular microgametes outnumber macrogametes 15 to 35:1 which favors contact of microgametes with macrogametes as these flagellated microgametes move to encounter and fertilize the female gametes before gamete fusion in the cat intestine (Figure 9A). Energy facilitating motility is important in this process, making translocation of GABA into the mitochondria requiring the sodium GABA symporter central to that process. The sodium GABA symporter is overexpressed and regulated by diminution in MORC in the merozoite, the stage that precedes formation of microgametes and we find this symporter is mutated in T-263 (Tables 2, 3, and 4; Tables S4–S6 and S7 in color).

Structure modeling of sodium GABA symporter with AlphaFold2 demonstrates mutation in T-263 surrounds the cholesterol binding cavity that is likely to have functional significance

To investigate how T-263 gene mutations could contribute to deficiencies in oocyst formation we asked AlphaFold2 to predict the structure of the *Tg* sodium GABA symporter by comparing the wild type T-263 mutant sequence with the identified point mutation L460R (Figure 10). Both wild type and mutant of *Tg* sodium GABA symporter were well modeled by AlphaFold2 with high pLDDT confidence values above 70 (Figure 10A). The overall fold of predicted *Tg* sodium GABA symporter structure is shown on Figure 10. *Tg* sodium GABA symporter exhibits helical structure fold with 14 predicted transmembrane helices. Based on structure alignment using VAST search,[174] dopamine transporter from Drosophila[175] is the closest structural homolog to *Tg* sodium GABA symporter (RMSD 3 Å over 750 Cα atoms,

A Method to Rescue mutations in GABA-Na symporter of T263 strain

1. **Disrupt HXGPRT locus from T263 strain.** Design a Cas9 gRNA HXGPRT_1768_revcom **sequence(**GTCAATGTAGGGCTTGCAGT|GGG) targeting HXGPRT, Construct Cas9 plasmid with pCas9-null-Bael and transfect T263 strain of *T. gondii* then select with 6TX.

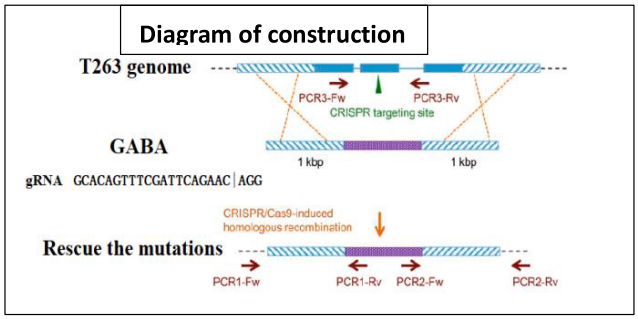

2. **Construct Cas9 targeting GABA-Na symporter mutation region.**
   1) Design the gRNA target GABA mutation region in T263
   gRNA1 GCACAGTTTCGATTCAGAAC|AGG
   gRNA2 CTGTTTCTGTGCAAGCGTAC|TGG
   gRNA3 CCCCACAGCAGACGACGAAG|CGG
   2) Construct Cas9 plasmid: Use pCas9-HXGPRT-Bael plasmid to construct GABA- Cas9 plasmid.
3. **Construct a Donor vector**

The fragment contains 1kb flanking region each of the 500bp replacement fragment using NEB DNA assembly mix. Both 5' and 3' 1kb flanking region should have homologous recombination sequences. Obtain the correct sequence fragments from the wild type C56 by PCR, and construct it into the donor vector.

4. **Co-transfect** both a-GABA-Cas9-HXGPRT and the donor DNA with correct sequence into T263 (HXGPRT knock out) and select with MP/X medium transiently. Anything that grows in monolayer is placed into 96-well without MP/X drug.
5. **PCR the target sequence and perform survey assay for screening.**

B CRISPR rescue of Gaba-Na Symporter

1. **HXGPRT locus from T263 strain Disrupted.**

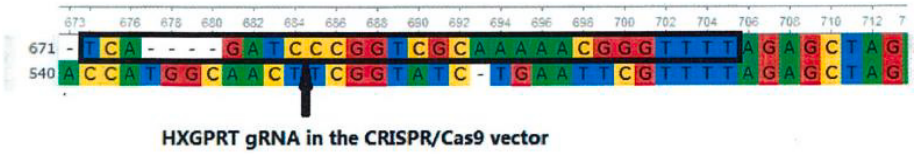

2. **Cas9 vector targeting GABA-Na symporter mutation region Constructed.**

Sequences showed the Cas9 vector targeting GABA was constructed with gRNA1 GCACAGTTTCGATTCAGAAC|AGG.

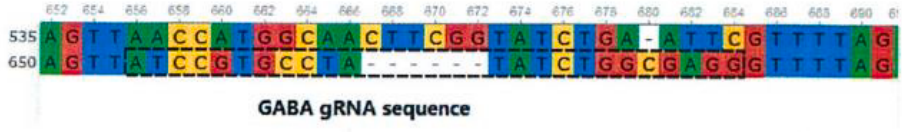

3. **Donor vector Constructed** Construct GABA gene into the donor vector pcDNA3.1 and co-transfect both a-GABA-Cas9-HXGPRT and the donor DNA with correct sequence into T263 (HXGPRT knock out) and select with MP/X medium transiently. Anything that grows in monolayer placed into 96-well without MP/X drug.
4. **By dilution/ selection and screening positive clone found.**

Figure 11. Approach for method to rescue mutant T-263 sodium GABA symporter

(A) Design for CRISPR/Cas9 rescue of the mutation in the sodium:GABA symporter.

(B) Non synonymous SNP was rescued in T-263 using CRISPR/Cas9 providing parasite that can be tested in future studies with either or both the Knoll organoid or Grigg barcode CRISPR/Cas9 cat pass through models when they become available. Figure S11 is related to this.

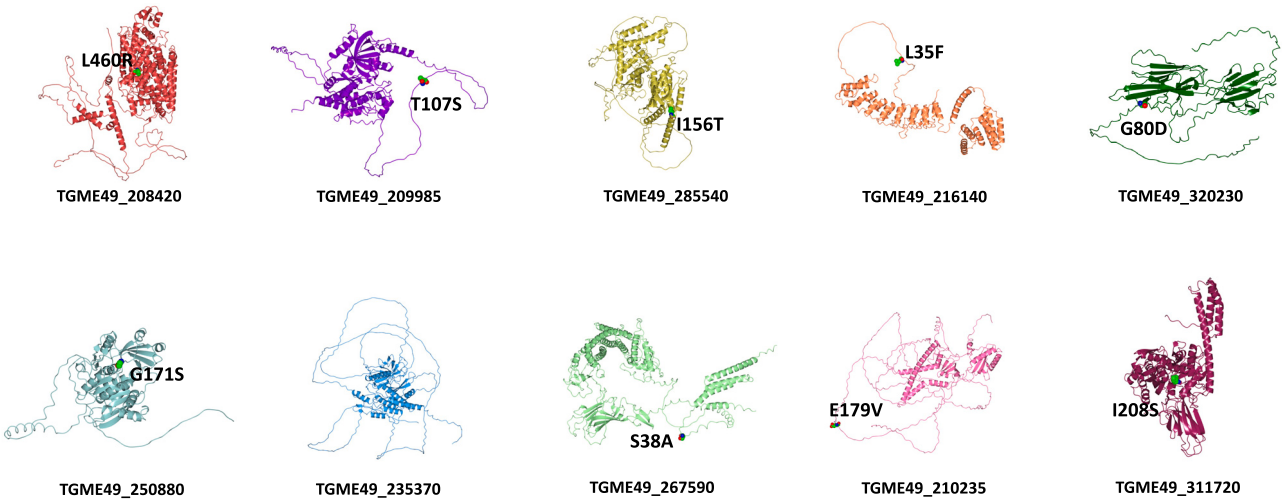

Figure 12. AlphaFold2 predicted structures of proteins containing mutation with recognized function in capacitation, fertilization, gamete fusion or pre-fusion development

Supplement shows each of these ten structures enlarged (Figure S11–S20).

Figure 10B). Structural alignment also suggests that *Tg* sodium GABA symporter most likely displays similar drug and ion-binding sites to dopamine transporter.[175]

The predicted model of the mutated *Tg* sodium GABA symporter (mutation L460R located on the TM4 helix) shows structural differences in two regions (Figures 10C and 10D). First region contains the extended loop with short α-helix between TM11 and TM12. The second region contains two C-terminal helices. Interestingly, these regions of the *Tg* sodium GABA symporter surround a cholesterol-binding cavity observed in the structure of the dopamine transporter (Figure 10D). Cholesterol plays a key role in regulating function of known neurotransmitter sodium symporters.[176,177] In the dopamine transporter, cholesterol stabilizes the outward-open conformation that increases binding of cocaine.[175,178] Therefore, if *Tg* sodium GABA symporter binds a cholesterol molecule in a similar cavity like the dopamine transporter, then conformational differences induced by mutation L460R may disturb symporter function and subsequent transport of GABA into the GABA shunt. We have rescued the sodium GABA symporter mutation in the C56 T-263 mutant tachyzoite as described below as in Figure 11. It is possible with the HDAC 3 inhibitor or in a knockout of MORC to turn off tachyzoite genes. Thus, this approach including AlphaFold2 can be used for other proteins as herein (Figures 9, 10, 11, 12, and 13; Tables 3 and 4 [Tables S5 and S6, in color]). This approach also provides the foundation for future studies to test this rescued parasite versus the parasite with the unrescued mutated gene to determine whether the mutation is the mutation in T-263 that is critical for or contributes to the T-263 zygote oocyst defective phenotype.

Candidate genes found in some natural isolates

AP2V-2 that is part of MORC complex that regulates expression of TgO/GABA-AT is mutated but the mutation is found in some natural isolates

Tg AP2-V-2 is of interest, as the MORC complex that coordinately regulates gene expression as the pre-gamete merozoite develops during capacitation, has *Tg*O/GABA-AT as one of its many coordinately regulated genes (Figure S7, adapted from Table S4 in[62] with permission). This MORC regulatory complex includes several Apetela 2 proteins, including AP2 V-2, and an HDAC.[42] Merozoites thereby undergo capacitation prior to fusion of the micro and macrogametes.

Pertinent to our and others' findings related to the MORC regulated genes presented above under *Tg*O/GABA-AT, we found that there are three tandem mutated bases in the merozoite expressed AP2 V-2 gene (Table 2, [Table S4]). A barcoded CRISPR knockout of the AP2 V-2 gene parasite has been created and is currently being studied by Grigg et al. Downregulation of the MORC complex including AP2 V-2 recently described[62] to license expression of merozoite genes would license coordinated transcription of our merozoite genes, including *Tg*O/GABA-AT. The mutated AP2 V-2 also regulates other of our genes expressed in merozoites that have mutations. Structure modeling of AP2-V2 with AlphaFold2 failed to predict structure due to low AP2-V2 sequence homology specifically at the N-terminal part of the protein containing mutation. This mutation in AP2V-2 also is found in some natural isolates.

Mutations in SRS 15C is related to a gene where knockout blocks oocyst shedding but the mutation is found in some natural isolates

Motility is critical to invasion and likely to fertilization. SRS family proteins are critical in invasion. SRS 15C, expressed in merozoites, is also mutated in T-263 with three tandem mutations. A protein in the SRS family related to SRS 15C knocked out in CRISPR/Cas9 barcode pass through experiments of Silva, Grigg et al. (2022) also has a loss of function oocyst forming phenotype demonstrating the feasibility of defining

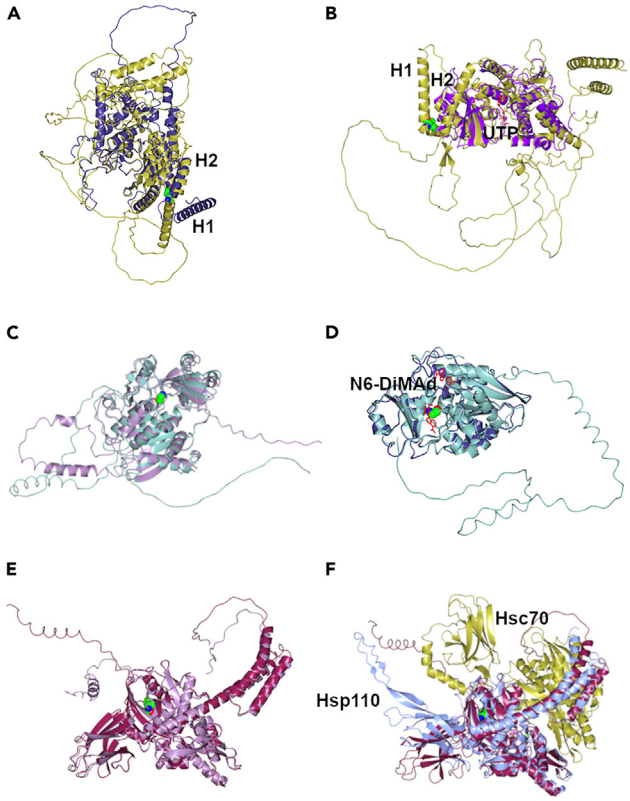

Figure 13. Mutation where Alphafold2 prediction suggests may affect function

(A) Superposition of wild type (yellow) and mutated (dark purple) structures of DNA-directed DNA polymerase TGME49_285540 predicted by Alphafold2.

(B) Superposition of wild type DNA-directed DNA polymerase TGME49_285540 (yellow) and homologous structure of Uridylyl transferase URT1 (purple) complexed with uridine 5′-triphosphate (UTP) shown in red (PDB : 6L8K).

(C) Superposition of wild type (sea green) and mutated (lilac) structure models of Kinase, pfkB family protein TGME49_250880 predicted by Alphafold2.

(D) Superposition of wild type Kinase, pfkB family protein TGME49_250880 (sea green) and homologous structure (dark purple) of adenosine kinase complexed with N6-dimethyladenosine (N6-DiMAd) shown in red (PDB : 2A9Y).

(E) Superposition of wild type (dark purple) and mutated (lilac) structures of Chaperonin protein BIP TGME49_311720.

(F) Superposition of wild type Chaperonin protein BIP TGME49_311720 (dark purple) and homologous structure of Hsp110 complexed with Hsc70 and ADP as shown in ice blue and yellow (PDB: 3C7N). The position of mutated residues in predicted structures is shown as sphere model in green/red/blue for carbons/oxygen/nitrogen. Nucleotides (UTP, N6-DiMAd and ADP on Figures 13B, 13D, and 13F are shown as cylinder model in red). Figures S12, S14, S16, and S20 also show these.

critical mutation(s) alone or in combination with this method (Silva, Grigg et al., Toxo 2022, Abstract. Riverside, California). Further, this gene with a loss of function phenotype in this cat model (Toxo2022) has a *plasmodia* homologue that renders the plasmodium micro gamete incapable of fusion, which resembles the T-263 phenotype[63] (Figures 12 and 14).

We run AlphaFold2 to predict the model for SRS 15C (purple) and for its mutant G80D (gray) (Figures 12 and 14). Structural modeling of SRS 15C with AlphaFold2 indicates that the tandem mutations in this gene in T-263 do not alter the predicted protein structure. Modeling shows that this mutation is located on the surface of SRS 15C, which might be important for SRS's function. Many surface residues that critical for protein function among SAG-related proteins are conserved. Therefore, more analysis is needed to elucidate functional importance of the SRS 15C G80D mutant. Further study of parasites with knockout and introduction of the T-263 mutation/allelic variation is in progress/planned (Silva, Grigg et al., Toxo 2022, Abstract. Riverside, California and Grigg, McLeod, in progress, planned for future, 2023).

Summary of relationships that link MORC regulated TgO/GABA-AT, MORC, AP2V-2, sodium GABA symporter, GABA and capacitation of merozoites to make fusogenic capable gametes and a zygote

These relationships are summarized as shown in the Box in the Supplement. They show the interconnection of MORC regulation of *Tg*O/GABA-AT, the MORC with HDAC 3, AP2V-2, the sodium GABA symporter, GABA and their putative function in capacitation of merozoites to make fusogenic capable gametes and a zygote.

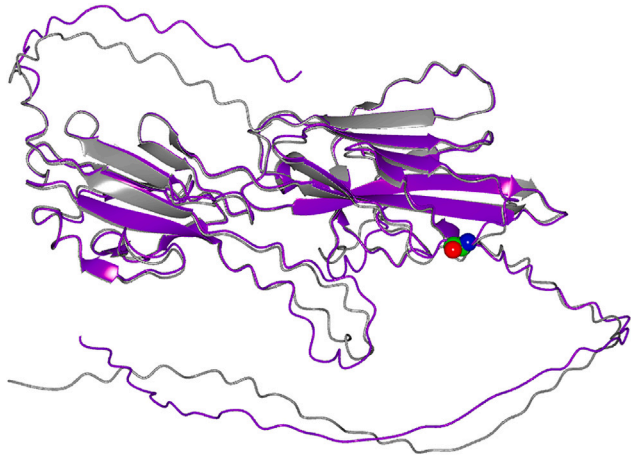

Figure 14. Superposition of SRS 15C wild type (purple) and containing mutation G80D (gray) structures predicted with AlphaFold2
Figures S12, S13, and S16, also show these.

Other candidate genes associated with fertility/infertility and capacitation were also among the mutated genes in T-263 where there was no similar mutation in natural isolates

As we eliminated from the final list any gene carrying a mutation shared with any of the ~100 wild type parasites that had been sequenced at The J. Craig Venter Institute (Hernan Lorenzi, unpublished data), we found that a sodium-GABA symporter (TGME49_208420) was among the proteins encoded by mutated genes with increased expression in sporozoites and merozoites. This is related to GABA as a substrate for *Tg*O/GABA-AT (Figure 1). Genes encoding for a phosphofructokinase B adenosine kinase related gene (TGME49_250880) and an ATP-binding protein (TGME49_202850) were also mutated and found overexpressed. Mutations in either the sodium-GABA symporter or the PKA/G encoding genes have been associated with infertility in other species and are therefore consistent with the phenotype seen in T-263. We did not find any exonic mutation in genes that were highly expressed in microgametes or macrogametes, but 74 potential CoF mutations fell within genes that are expressed in the merozoite stage (Table 2 and highlighted in red in Table 2 companion Tables S4 and S7), including a hypothetical protein coding gene (TGME49_231880) that is overexpressed in merozoites compared to tachyzoites identified by Hehl et al.[169] Other identified mutated genes expressed in merozoites encode for a tetratricopeptide repeat containing protein (TGME49_216140), formin FRM1 (TGME49_206430), chaperonin protein BiP (TGME49_311720), Sushi domain-containing protein (TGME49_211270), DNA-directed DNA polymerase (TGME49_285540), Myb family DNA-binding domain-containing protein (TGME49_203950), T-complex protein 1 epsilon subunit (TGME49_202370), and a number of hypothetical proteins. Some of these genes are fundamentally important in biological processes that affect fertilization in multiple other species, e.g., formin FRM1, BiP or Myb family encoding genes (Table 3 [Table S5]). We ran AlphaFold2 to investigate if mutations in these protein structures are potentially capable of influencing function (Table 4 [Table S6]); Figures 9, 10, 12, and 13; Figures S11–S20. AlphaFold2 predicted structural models of candidate proteins from *T. gondii* with mutations with recognized functions in capacitation, fertilization, gamete fusion, or pre-fusion development (Figures 9C, 10, 12, and 13) and Figure S11–S20).

AlphaFold2 failed to accurately predict structures of several proteins including TGME49_206430 (formin FRM1), TGME49_211270 (sushi domain-containing protein), and TGME49_203950 (Myb family DNA-binding domain-containing protein) due to large MW of proteins and low sequence homology. Among predicted AlphaFold2 models, most of the mutations are in disordered regions of the protein structure (TGME49_216140, TGME49_267590, and TGME49_210235) similar to the PKA protein. Therefore, it is hard to predict how they might affect function of target protein (Figure 12). We have found that mutations in three targets TGME49_285540 (DNA-directed DNA polymerase), TGME49_250880 (pfkB kinase) and TGME49_311720 (chaperonin protein BiP) might be functionally important.

In the structure of polymerase, which might be RNA polymerase based on predicted structural model, mutation I156T is located between N-terminal helices H1 and H2. AlphaFold2 prediction indicates that mutation might induce conformational change of these helices. Comparison of the structure with its closest homolog (URT1)[180] based on VAST search shows that these helices might affect nucleotide binding-site of the polymerase (Figure 13).

In the second target, mutation is located in the adenosine binding pocket of the kinase and might directly affect binding of the adenosine. Structure of TGME49_250880 is well-studied adenosine kinase from *Toxoplasma*.[119] We found that this mutation does not alter conformational changes in the protein structure based on AlphaFold2 prediction. Similarly, we have found that mutation in the third target TGME49_311720 (chaperonin) does not trigger conformational changes in chaperonin protein BiP. However, mutation might affect binding activity of chaperonin with its possible binding partner while forming protein complex. Superposition of chaperonin model with its closest homologous structure of Hsp110 shows position of mutated residue in close proximity to Hsp110/Hsc70 binding interface (Figure 13). Additional analysis is needed to elucidate functional importance of these mutations.

It is feasible that one of these or more than one together could be responsible for the T-263 phenotype. A genetic cross between T-263 and a barcoded wild type parasite followed by genome sequencing or the barcode CRISP cat pass through method with MORC likely will in the

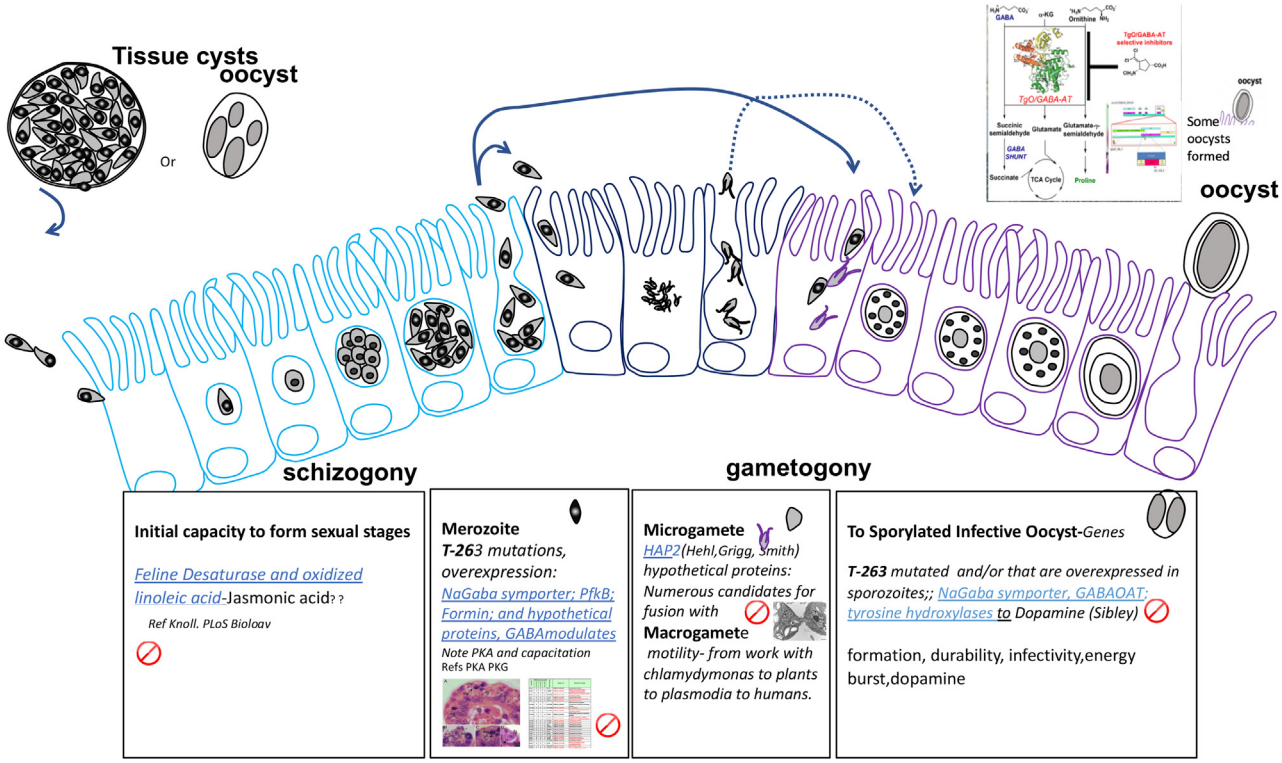

Figure 15. Diagram showing morphologic development and conception of *Toxoplasma* in the cat intestine and ways in which certain mutations might be relevant to those processes

Related to Tables 2, 3, 4, S4–S6, and S7.

future allow us to identify the critical gene(s). Figures 10, 11, 12, and 13 and Table 4 [in color in Table S6] show the likely effects of the mutations as predicted using AlphaFold2 as shown above.

Foundational methodologic approach uses mutation and knock out of candidate genes and correction of mutations using CRISPR/Cas9

This is foundational to identify critical genes responsible for lack of fusion phenotype in T-263.CRISPR/Cas9 rescue of the sodium GABA symporter gene with no mutation, like the one in T-263 in wild type parasites, was prepared to determine whether it loses the defect in producing oocysts. It is feasible that this approach to CRISPR could rescue more mutations (Figures 10 and 11). Gene knockout of other putative responsible or key genes such as the PKA/G gene array is another approach to link genotype and phenotype. These methods should provide empirical proof of critical gene(s) responsible for the T-263 phenotype. It is likely that these genes will be among those conserved in this "capacitation" process in other species. Thus, these next step experiments can be placed in the context of the results of our list of genes that were identified in a literature search with the keywords "fertility, zygote, or infertility" (Tables 4 and S6). These future studies are likely to reveal the essential gene(s).

To further define these defects the *in vitro* cat intestinal organoid and *in vivo* in cat pass through phenotypes will be useful. We have developed the first step analyses by using a CRISPR/Cas9 rescue of mutations, amenable to analysis of T-263 mutants *in vitro*,[179] and barcoded pass through system in cats (Silva, Grigg et al., Toxo 2022, Abstract. Riverside, California). This seems like T-263 may function as a "Rosetta stone that will help us to identify the critical mutation(s) that lead to its phenotype of failure to move beyond the morphologic male and female gamete to form a zygote in the cat intestine.[73–173] Data and analyses from other investigators[72] complement this as they demonstrate that creation of the zygote, and subsequent steps in producing later stages[125] involves multiple genes, common broadly across other species[66] (Tables 2 and 4 [Tables S4 and S6]; Figures 9, 10, 11, 12, and 13; Figure S11–S20).

Further analysis using data and analyses from other investigators[65] demonstrated that it is likely that creation of the zygote, and subsequent steps in producing later stages[66] involves multiple steps, present broadly across species,[62,76] a number of these are critical to fertility and capacitation and thereby may contribute to the formation of infectious sporozoites (Tables 2, 3, and 4 [; Tables S4–S6]; Figure 12).

DISCUSSION

Herein, we studied a previously uncharacterized *Toxoplasma* enzyme, *Tg*O/GABA-AT. This was done to comprehensively characterize the genetics, enzymology, inhibition/inactivation, and biology of this enzyme, and the pathway in which it functions. We hypothesized that

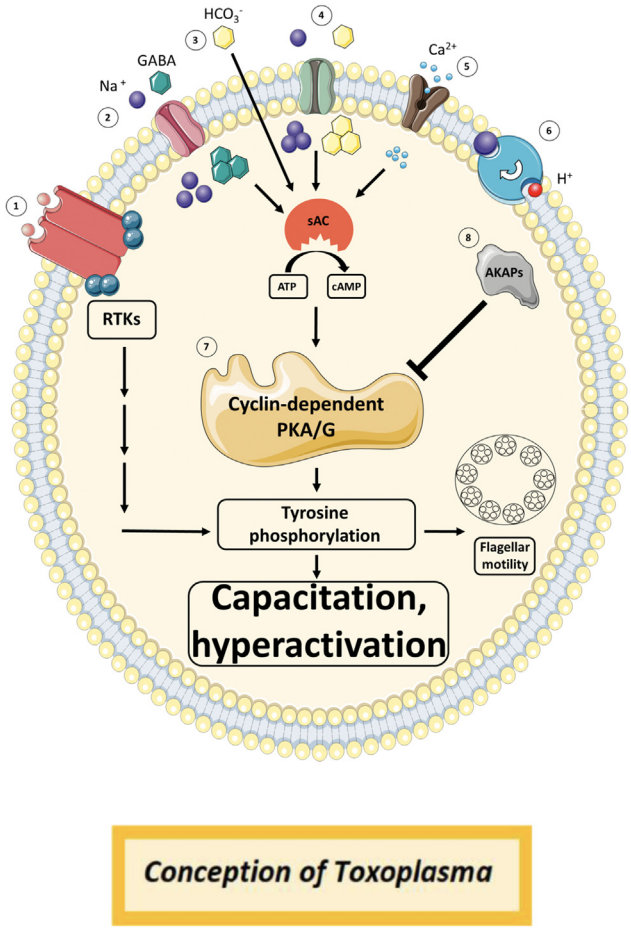

Figure 16. Summary model using our synthesis from experiments, bioinformatics, literature search and systems analysis from our rosetta stone-like T-263 to understand aspects of conception in *Toxoplasma*

Capacitation occurs in merozoite, GABA modulates capacitation, motility, change in ionicity, pH, cyclic-AMP dependent adenyl cyclase, PKA, motility, and lipids in membranes. These are all putative ways conception and fertilization are affected-in other species and are evident in merozoite transcription and/or T-263 mutations. The abbreviations and symbols depicting this process are: (1) Receptor tyrosine kinase (RTK) with phosphorylation sites marked in turquoise; (2) Sodium: GABA symporter with sodium (dark blue circles) and GABA (green hexagons) both transported intracellularly. GABA is implicated in upregulation of soluble adenylyl cyclase (sAC) activity catalyzing conversion of ATP to cAMP as well as modulating each step in the capacitation process; (3) Bicarbonate (yellow hexagon) can transit the plasma membrane, but is also moved into the cell via channel proteins (5) that move it with sodium ions (dark blue circles); (4) Calcium channels move calcium ions (light blue circles) into the cell, which in turn increase sAC activity; (6) Sodium-hydrogen exchangers (NHE) move sodium out of the cell and import hydrogen ions, increasing intracellular pH as another level of regulation; (7) Cyclin-AMP dependent protein kinase A (gold) is a central node of regulation of capacitation, hyperactivation and PKAs have been demonstrated to play a critical, essential role in this process, mediated via tyrosine phosphorylation. PKA also plays a role in cellular/flagellar motility. PKA is regulated by A-kinase anchoring proteins (AKAPs, gray) (8). Other processes cyclic AMP and its targets regulate include: 1) membrane lipid remodeling; 2) hyperpolarization of the sperm plasma membrane; 3) increase in intracellular pH; 4) increase in intracellular Ca2+; and 5) increase in protein tyrosine phosphorylation. The PKA/PKG pathway also was informed by the work of others whose work showed that "for mammals, when GABA was added to incubation medium percentage of capacitated spermatozoa increased with increasing concentrations of GABA. GABA also significantly increased intracellular $Ca^{++}$and cAMP. GABA A-R antagonists, abrogated these effects. Thus, these investigators concluded that "GABA seemed to induce sperm capacitation through a signal transduction pathway involving Ca^{++}, cAMP and tyrosine phosphorylation."[45,84] Related to Tables 2, 3, 4, S4–S6, and S7, Figures 6, 8, 9, 10, 11, 12, 13, and S7–S20.

this might provide a new approach for drug discovery and to identify small molecule inhibitors/inactivators effective against the Apicomplexan parasites *T. gondii* and *P. falciparum*. Improved treatments are needed because these parasites cause significant morbidity and mortality, there are limitations of available treatments, and *T. gondii* is the most prevalent parasitic infection, with approximately two billion people infected worldwide. *T. gondii* is present throughout the environment, since cats are a critical vector for its dissemination. An acutely infected cat excretes up to 500 million oocysts; one oocyst is enough to establish a successful infection in the intermediate host, and they can persist in water or moist soil for up to a year.

On the basis of a report regarding *Tg*O/GABA-AT,[18] there is an additional dimension to our analysis, as we have considered how *Tg*OAT might function differently in circumstances of different abundance of substrates, accessibility of nutrients, or other stress conditions. This report suggests that, while *Tg*OAT demonstrates the capacity to act on ornithine and acetylornithine, its greatest activity is actually on GABA as a substrate, suggesting that the enzyme called *Tg*O-AT may metabolize GABA as well. *Tg*O/GABA-AT is a key part of amino acid biosynthesis, the urea cycle, and potentially the shuttling of carbon from GABA, via the GABA shunt, into the TCA cycle for addressing the energetic needs of the parasite. Additionally, GABA plays a role in the regulation of tyrosine hydroxylase activity, which is implicated in oocyst formation.[94] Therefore, it was considered to be a potential antimicrobial target in any life cycle stage where it was essential. These considerations led to our characterization of this enzyme for Apicomplexans.

Phylogeny of TgO/GABA-AT

Phylogenetic analysis revealed a highly conserved enzyme across parasite strains, leading to our supposition that OAT might be used for arginine, proline, glutamate, and GABA synthesis in *T. gondii*, as well as the clearance of nitrogenous wastes by the urea cycle. Multi-sequence alignment revealed substantial variation between species and the presence of two cysteines (Cys179 and Cys187) within Apicomplexan phylum members, which are Ile185 and Ser193 in human, and may provide an additional level of regulation absent in any other OAT homologue, including the human and cat isoforms of OAT. This site has demonstrated capacity for thioredoxin-binding in *P. falciparum* OAT.[46] If there is a life cycle stage where this is essential, this difference might be useful for targeting antimicrobial agents, because it ought not interfere with the mammalian enzyme, perhaps providing selectivity for the parasite *Tg*O/GABA-AT. Although there are some residue differences, it should be noted that the substrate binding sites are highly conserved across the apicomplexan and human O/GABA-AT families, such that any rational drug design program would have to be tailored toward these subtle differences. Alternatively, the unique nature of the putative regulatory Cys residues, and the role they play in changing the nature of the substrate-binding pocket due to their close proximity, may provide a new angle for inhibitor design, such as the design of inactivators containing Cys-specific warheads.

*Tg*O/GABA-AT has a structure similar to those of known OAT and GABA-AT enzymes

The *Tg*O/GABA-AT structure resembles a similar structural fold with other enzymes from subgroup II of the aminotransferase protein family.[180,181] The list of known OAT enzymes with determined structures that have a similar structural fold includes the *h*OAT,[36,38] the OAT from *P. falciparum*,[40,46] the OAT from *P. yoelii* and GABA-AT from *E. coli*.[182] In addition, there are structures of uncharacterized OAT enzymes in the Protein Data Bank,[183] the OAT from *Bacillus anthracis* (PDB:3RUY), the OAT from *Elizabethkingia anophelis* (PDB:5VIU), and GABA-AT from *Mycobacterium smegmatis*.[184] A structure comparison between *Tg*O/GABA-AT, *h*OAT, *Pf*OAT, *Py*OAT and *E. coli*GABA-AT shows that the differences among identified structures are found mainly in the region that comprises residues from the C-terminal domain (Figure S1). Among them, the *h*OAT structure shares the closest secondary structural fold with similar PLP and substrate-binding site to *Tg*O/GABA-AT.[41] The details of *Tg*O/GABA-AT structure and comparison analysis to its structural homologs provided a starting point for the identification of selective *Tg*O/GABA-AT inhibitors.[41]

Inhibitors and inactivators of *TgO*/GABA-AT *in vitro*

Recombinant protein was used to screen for inhibitors and inactiators of *Tg*O/GABA-AT from a part of our library of *p*GABA-AT inhibitors and inactivators (to identify lead compounds for the development of new anti-toxoplasmosis and anti-malarial drugs. Compounds were chosen in the screened library because of their diversity in structures, including conformationally-rigid, aromatic, and flexible structures, in an attempt to identify different binding modes of the compounds to the active site of *Tg*O/GABA-AT. Four compounds (**1**, **2**, **3**, and gabaculine) that have high activity in inactivating *Tg*O/GABA-AT were identified and are considered mechanism-based enzyme inactivators (MBEIs). MBEIs are unreactive compounds that are converted through the target enzyme's catalytic mechanism to form intermediates that either bind tightly to the enzyme or form covalent bonds.[185] Because these molecules are not initially reactive, indiscriminate reactions with off-target proteins should be greatly reduced, and, therefore, greater selectivity and potency can be achieved.[186] To place the observation that *Tg*O/GABA-AT acts on both ornithine and GABA as substrates in the context of our inhibitor data, as presented in Table 1 and Figure 2, the enhanced specificity of *Tg*O/GABA-AT for GABA and the enlarged active site that is more capable of accommodating larger molecules, we have found that large cyclic GABA-analogue inhibitors more potently modulate the enzyme's activity; compound **3** is highly selective for *Tg*O/GABA-AT. Although compounds **1**, **2**, and gabaculine are potent inhibitors of *Tg*O/GABA-AT, they also inhibit both *p*GABA-AT and *h*OAT. Of most interest is compound **3**, which selectively inactivates *Tg*O/GABA-AT. Studies are ongoing to determine the reasons for this selectivity and the mechanism of inactivation.

*Tg*O/GABA-AT crystal structure with selected inactivators

Recombinant protein also was used to solve the crystal structure of *Tg*O/GABA-AT in the presence of selected inactivators of GABA-AT. The crystal structure of gabaculine (**14**)-inactivated *Tg*O/GABA-AT (Figure 5) confirmed a similar structure and inactivation mechanism determined with pGABA-AT[187,188] and hOAT.[36] A comparison of the crystal structure of *Tg*O/GABA-AT in complex with gabaculine and structures of human OAT complexed with 5-fluoromethylornithine[38] and pGABA-AT with (2S,4S)-4-aminotetrahydrothiophene-2-carboxylic acid[189] revealed a number of differences in their substrate-binding pockets (Figure S9). These differences may explain the enzyme's specificity toward different substrates and inhibitors. One major difference is the presence of Val79 in the substrate-binding site of *Tg*O/GABA-AT, which is

substituted by Ile79 and Tyr85 in GABA-AT and hOAT, respectively. In GABA-AT, Ile79 is thought to narrow the pocket, allowing for binding solely of GABA. In hOAT, Tyr85 helps to stabilize the α-nitrogen of L-ornithine but does not prohibit GABA from binding. Markova et al. showed that mutation of this tyrosine to an isoleucine results in more productive binding of GABA.[35] They surmised from their data that Ile85 serves to orient GABA in such a way that γ-proton abstraction after aldimine formation is enhanced. Val79 could be accomplishing the same task in *Tg*O/GABA-AT.[18] A second major difference is the presence of a phenylalanine residue in both GABA-AT (Phe189) and hOAT (Phe177), whereas *Tg*O/GABA-AT contains a tyrosine (Tyr171). However, the role of these residues in substrate binding remains unclear. A third major difference observed in comparative structures occurs on the carboxylate binding side of the substrate-binding pocket (Figure S9). In GABA-AT, this region is occupied by Phe351, which serves to restrict the active site size, allowing only for binding to GABA. In hOAT, this region is occupied by Tyr55, which is rotated at about a 90° angle relative to that of Phe351 in GABA-AT. Tyr55 is located on the other subunit of the protein on a loop that extends into the substrate-binding site and serves to allow binding to the α-nitrogen of L-ornithine in hOAT but not in GABA-AT. This same tyrosine (Tyr49) is found in *Tg*O/GABA-AT. Finally, the fourth difference is the presence of Gly320 in hOAT that occupies the location of Phe351 in GABA-AT (Figure S9). This change results in the active site of hOAT being larger and more flexible than that of GABA-AT.[35] Thus, we believe that large inhibitors such as 2 and 3 can bind to hOAT and not to GABA-AT. *Tg*O/GABA-AT has these same residues at the substrate-binding site (Gly314 and Tyr49, located on the other subunit of the protein) and produces the same activity with similar inhibitors.

Cys179 and Cys187 in the *TgO*/GABA-AT structure do not form a disulfide bond

In *P. falciparum* OAT, Cys154 and Cys163 have been demonstrated to bind an activator, thioredoxin, which reduces protein disulfides via a disulfide-exchange mechanism.[46] The two residues, Cys154 and Cys163, in *P. falciparum* OAT correspond to Cys179 and Cys187 in *Tg*O/GABA-AT, but there is no homologous sequence in *H. sapiens* OAT. On the basis of the crystal structure of *Tg*O/GABA-AT (Figure S10), the formation of a disulfide bond between Cys179 and Cys187 in *T. gondii* is unlikely because of the large distance between them (4.4 Å), and the formation of a disulfide bond is only likely when the distance is less than 2.5 Å.

Is *TgO*/GABA-AT a GABA-AT?

It is important to recognize that these biochemical data with *Tg*O/GABA-AT, upon which much of the previous assertions and suppositions are based, does not confirm that there is a biological *in vivo* role for the observed GABA-AT activity. The capacity for nonspecific binding leading to catalysis of reactions using both substrates does not mean that *Tg*OAT functions biologically as a GABA-AT. Additionally, if *Tg*OAT is, in fact, a GABA-AT, it is structurally distinct from mammalian GABA-AT, given that some inactivators of *Tg*O/GABA-AT, e.g., compounds **2** and **3**, do not inactivate mammalian GABA-AT. This *Tg*OAT or GABA-AT activity would be outside of the activity of the sporozoite in oocysts but not the merozoite, because the oocysts are walled-off in their own, separate, sequestered niche.

Effect of *TgO*/GABA-AT inactivators in cells

What remains is a modest phenotype *in vivo* and increased expression in merozoites and sporozoites. The aforementioned *Tg*O/GABA-AT inactivators demonstrated to effectively modulate *Tg*O/GABA-AT activity via *in vitro* enzymatic assays, were tested against Type I tachyzoites *in vitro* as well as against P. falciparum. Since we later learned that the enzyme is not expressed in tachyzoites we found as would be expected with hind-sight that these studies revealed no significant effect on *T. gondii* replication, with some host-cell toxicity. Similarly, a live-cell parasite assay for *P.falciparum* revealed the compounds had no antimalarial activity at concentrations up to 10,000 ng/mL. Thus, inhibition of this enzyme is not likely to significantly modify outcomes resulting from active tachyzoite or dormant bradyzoite infection in humans.

GABA shunt in *TgO*/GABA-AT

Moreover, the biochemical data showing that *Tg*O/GABA-AT has increased specificity for GABA relative to ornithine corresponds well to a previous study, which demonstrated, metabolically, that *Toxoplasma* has a functional GABA shunt in a nutrient-poor environment.[42] In MacCrae's supplemental data, shown in their Table S1, they identified the four predicted *Toxoplasma* genes involved in this GABA shunt. The GABA shunt eliminates two steps in the TCA cycle via the sequential action of glutamate decarboxylase (TGME49_280700), which first converts glutamate to GABA in the parasite cytosol, followed by the import of GABA into the mitochondria by the putative transporter (TGME49_208420) predicted to be a sodium:neurotransmitter symporter. This gene, TGME49_208420, is the very gene predicted to be important and noted to have a nonsynonymous SNP in the Frenkel vaccine strain. This could be of significance, assuming, of course, this mutation actually makes an amino acid change or truncation of the GABA transporter for a predicted null phenotype. The AlphaFold2 analysis suggests this mutation could have functional significance (Figure 10). Additionally, MacRae et al.[42] predicted *Tg*OAT (TGME49_269110) was the most likely candidate for the GABA-AT that converts GABA to succinate semialdehyde, and TGME49_057480 as the NADP-dependent succinate semialdehyde dehydrogenase that converts succinate semialdehyde to succinate, which then reenters the TCA cycle.

Effect of elimination of GABA in *TgO*/GABA-AT and GABA accumulation in *TgO*/GABA-AT knockout

Furthermore, the MacRae paper[42] showed that deleting the parasite gene for glutamate decarboxylase completely eliminated the production of GABA. This GABA deficient mutant had no replication defect *in vitro*, but *in vivo* in mice they showed a very modest reduction in

tissue burden of tachyzoites by day 5–7 post-infection, as well as a very modest reduced virulence in mice. Thus, absence of parasite GABA production slightly reduced acute virulence. MacRae et al. 2012 knocked out the type I RH Glutamate decarboxylase gene that converts glutamate to GABA and is essential for the formation of GABA. In contrast, we knocked out the type II (PRU) *Tg*O/GABA-AT gene that consumes GABA by converting GABA into succinate semialdehyde in the TCA cycle. Consequently, these mutants are not directly comparable.

Interestingly our *in vitro* and *in vivo* results with deletion of *Tg*OAT as a GABA-AT found slightly different results. Utilizing a knockout of the Type II parasite, to determine biologic phenotype, we found a mildly increased virulence phenotype *in vivo*, with slightly diminished survival of infected mice and increases in cyst number. This was not reflected *in vitro*. Explaining the underlying mechanism of these findings requires an appreciation for the downstream impact of inhibiting this pathway. Knocking out the parasite's GABA-AT would most likely create an increased metabolic pool of GABA, since glutamate will be converted to GABA by glutamate decarboxylase, but there would be no GABA-AT to convert GABA to succinate semialdehyde. Thus, our finding in Type II parasites that deletion of *Tg*O/GABA-AT did not affect *in vitro* replication of tachyzoites, but slightly increased acute virulence, is consistent with the idea of perturbation of this metabolic pathway, leading to the accumulation of GABA.

Importance of GABA

If *Tg*OAT were to function as a GABA-AT, there is certainly precedence for the importance of this pathway, and its transporter identified as mutated in merozoites and sporozoites in the T-263 vaccine strain. GABA is critically important to defend against a variety of environmental stresses in plants and plant pathogens. GABA is also a key signaling molecule, allowing plants to sense how much carbon and nitrogen are available, facilitating the balancing of carbon, nitrogen, and energy needs through the TCA cycle and other metabolic pathways. This role in plants was only recognized recently, but GABA seems to play an important role in response to environmental stress. In *Fusarium*, a deletion of the fungal GABA-AT induced accumulation of GABA, which adversely affected mitochondrial respiration, the redox state of the cell, and compromised fungal virulence *in vivo* in wheat plants.[190] Additionally, GABA has been shown to play a critically important role in angiosperm sexual reproduction.[191] While sexual reproduction in plants might seem unrelated to reproduction in a eukaryotic parasite like *Toxoplasma*, several key metabolic pathways are shared between these organisms suggesting common ancestry.[192–195]

Effect of deletion of *TgO*/GABA-AT in *T. gondii* on cat oocyst shedding

This finding, in conjunction with the observations of the 245-fold increase in expression in sporozoites and the increased expression in merozoites, leads to our hypothesis that inhibition of the cat form might be useful in blocking transmission or shedding upon challenge with the parasite. The transcriptional and proteomic data, as well as immunofluorescence assays, suggested that the cat forms might require *Tg*O/GABA-AT. Therefore, the active site and binding pocket of OAT was mutated using a CRISPR/Cas9 system in the EGS cyst-forming *T. gondii* strain. Abrogation of *Tg*O/GABA-AT was confirmed via PCR. Feeding of these CRISPR/Cas9 knockout parasites to cats revealed continued shedding of oocysts in the feces, although this was not quantitated nor was durability of the oocysts determined so it is not clear whether a reduction in oocyst shedding occurred. These oocysts were tested, and it was confirmed that they still had the construct in place preventing expression of *Tg*O/GABA-AT. We can conclude therefore that *Tg*O/GABA-AT is not essential for shedding of oocysts, although we cannot rule out some contribution of the enzyme to oocyst formation or durability, given the role of numerous metabolic pathways to this process.

Is there an alternative *TgO*/GABA-AT gene in the *T. gondii* mutant strain T-263, that is unable to produce oocysts in cats?

Given the importance of the process of oocyst formation to transmission and infection, we further characterized a mutagenized strain of *T. gondii*. This mutant, named T-263, created and characterized by Frenkel, Pfefferkorn et al.,[63–71] is known to be unable to produce oocysts when fed to cats and to block shedding of oocysts with challenge following immunization. We hypothesized that we might encounter a non-synonymous SNP or other mutation in this T-263 parasite that was related to the OAT pathway, given the high level of OAT expression in the sexual stages of the parasite, or perhaps even OAT itself. Alternatively, a mutation could alter splicing or regulatory region in the DNA. As our studies herein were ongoing, we (JPD) found that the phenotype of T-263 was an arrest in oocyst development beyond the stage of morphologically normal-appearing male and female gametes[63] and Figures 8 and 9. Thus, mutations in this pathway might logically cause this phenotype. Any gene potentially involved in the enhanced production of energy (i.e., via the GABA shunt) or in enhancing substrate formation for such an enzyme, especially for an extracellular organism like the male microgamete, could be the responsible gene. A kinase like cyclic AMP dependent protein kinase (PKA) that is critical for development of the male gametes of other species[77] is also likely to be important in this process in the merozoite state even if it is not one of the mutated genes in T-263. A PKA overexpressed in merozoites could be critical for gamete functions. Therefore, T-263 was grown in tissue culture from a stored stock (Jitender P Dubey parasite collection on the C Strain background [JPD,CLS][63–71,196] and sequenced herein to begin to determine the genetic underpinning of this defect in zygote production phenotype and how it might relate to *Tg*O/GABA-AT and GABA. This led to identification of nonsynonymous SNPs. These were studied to identify those genes which might have evidence of upregulation in merozoites, macrogametes, microgametes, or sporozoites. This latter criterion suggested the potential importance to critical aspects of the sexual life cycle stages and, therefore, relevance to earlier stages of functional gamete/zygote formation (merozoites, microgametes) or later stages of oocyst (sporozoite or the other sexual stages) formation. We found no genes with mutations that were over expressed in microgamete or macrogametes. In merozoites, a gene that was of unknown function and a gene that has been identified as a cyclic-AMP dependent protein kinase (PKA) were found to be overexpressed in the merozoite. This

seemed to be a gene of high importance as it is a gene critical for formation and capacitation of the functional male gamete (Figures 8 and 9). Although the *Toxoplasma* database reported this initially as a single copy gene, it appears that there may be as many as 14 copies of this gene. Thus, a single mutation in this gene, unless it was a critical regulatory SNP or enhancer response element, would make it less likely to be critical. As the merozoite was the only stage in which this 14-copy gene was overexpressed, the multiple copies could not be the only reason that it was noted to be overexpressed only in this life cycle stage.

Phenotype relevance of multicopy protein kinase A genes

Other PKAs have been noted to be important in a *T. gondii* stage switch.[158,197,198] Interestingly this cyclic-AMP protein dependent kinase has 23% homology with a PKG in *Plasmodia* which has a unique relay mechanism allowing it to respond rapidly to environmental conditions[83] (Figure 9). However, the biological function of this gene in other organisms would exactly account for the phenotype of arrest of the cat stage parasite at the stage where gametes are formed before zygotes are formed, but then do not progress beyond that stage. Thus, the gene with relatedness to a malaria PKG (see Figure 9) might contribute to the phenotype observed, although it is not consistent with being the critical gene in the mutant T-263. The work herein highlights the likely critical importance of this multicopy gene for *the T. gondii* merozoite and the conception of *T. gondii*. There are also multiple hypothetical genes overexpressed in the merozoite compared to tachyzoites. One of these has an N-terminal domain with low similarity to a bacterial ribonuclease E family (e-value $<5 \times 10^{-8}$). Additional nonsynonymous mutations were identified in 17 genes expressed in the merozoite among other stages (ToxoDB, >25% percentile expression[169]). Four genes contained nonsynonymous SNPs that were overexpressed in sporozoites. These could augment the phenotype where oocyst shedding does not occur but would not explain the phenotype where the male and female gamete do not fuse. In T-263, also of particular interest, pertinent to the present manuscript, were a sodium-GABA symporter (TGME49_208420), an ATP binding domain-containing protein (TGME49_202850), and adenosine kinase (TGME49_250880). The former regulates movement of GABA, a downstream product of *Tg*O/GABA-AT when ornithine is the substrate, or the substrate of *Tg*O/GABA-AT. There are several known small molecule inhibitors, including commercially available anti-epileptic drugs, as well as the compounds presented herein. In the future, it will be particularly interesting to further characterize this SNP and others in the mutant. This is in light of our studies of *Tg*O/GABA-AT, because the literature suggests that OAT plays a role in the regulation of concentrations of GABA and glutamate. Glutamate is potentially important as a short-term energy source in *T. gondii*, as occurs in *Plasmodia*.[19] Adenosine kinase, another identified protein with non-synonymous SNPs in its gene in T-263, is a component in the redundant purine salvage pathway, with a characterized structure and known inhibitors.[199] These proteins, and the others that have been identified, are potentially targetable, either via small molecules or genetic technologies like CRISPR/Cas9,[187] as was the case in an interesting report in the HIV literature.[200] Should application of these technologies prove that one of these proteins is essential for the process of oocyst formation as was recently described for the microgamete gene, *HAP*, of unknown function in *T. gondii* but well known in plants and other species to be associated with fertilization,[64] it could be targeted directly to inhibit development or shedding of oocysts.

We did not find the fusogen HAP1,2 (reported to be present in both plasmodia and *T. gondii*) or LIKE1,2 or other known fusogens. The relationship of these genes to GABA, sodium channels and stress as some of the drivers of capacitation and PKA/Gs in gamete development and function are presented in Tables 2, 3, and 4. They unify our findings with *Tg*O/GABA-AT and GABA. Levels of GABA modulate capacitation through multiple steps. The sodium GABA symporter controls localization of GABA and sodium and this gene contains one of the T-263 mutations (Tables 2 and 3).

The work herein, in the context of multiple recent studies evaluating the molecular underpinnings of sexual development indicate that there are likely to be multiple genes important to this pathway (Figures 8, 9, 10, 11, 12, 13, 14, 15, and 16; Table S6) that also can be targeted.[64,201] The biological underpinning of sexual reproduction in the parasite represents a frontier in our understanding of eukaryotic parasites and *T. gondii*, more specifically and offers us a window into a potentially targetable pathway. Therefore, identification of genes critical for sexual development of the parasite and formation of zygotes studied including methods described herein[202–235] and newly described,[236] could facilitate public health interventions and interrupt environmental transmission. This would substantially reduce transmission to humans[1,4] and thus reduce the morbidity and mortality caused by this parasite.

Limitations of the study

Our characterizations, sequencing, and analyses of *Tg*O/GABA-AT and T-263 mutagenized *Toxoplasma* provide considerable insight into related molecular mechanisms critical in creation of *T. gondii* zygotes. One limitation is that background, haplotype, gene modifications, and different wild-type strains used in our different studies could have influenced results. Nonetheless, this work presents and develops foundational concepts, hypotheses to test, and empirical data. With the novel approaches and reagents that we and others have identified and created, future studies are needed to define which specific mutations in T-263 cause the block in capacitation to zygote formation in T-263*Toxoplasma*. The Rosetta stone T-263 mutations we have uncovered will inspire future studies to further fully define detailed mechanisms whereby the *T. gondii* ornithine-GABA pathway acts in merozoites and sporozoites with central roles in development or reduction of highly infectious oocysts, which widely contaminate the environment. The genes we have noted through the mutational analysis present a focused list of candidates associated with development of *T. gondii* feline stages. To fully identify the functions of selected and all relevant genes will require additional future studies. Nonetheless, genes and pathways identified reveal a process involved in capacitation, fertilization and formation of a *Toxoplasma* zygote. Even if they turn out not to be responsible for the T-263 phenotype they may with future experimentation prove to be critical for capacitation, fertilization and formation of the zygote, and have provided insights into the biology of GABA and *Tg*O/GABA-AT in these and other cellular processes.

Conclusions

*Tg*O/GABA-AT was found to utilize GABA and ornithine as substrates. Known aminotransferase inhibitors were screened against *Tg*O/GABA-AT, and many were found to inactivate *Tg*O/GABA-AT irreversibly. Importantly, compound **3** was found to be selective over other aminotransferase enzymes including GABA-AT and *h*OAT. From crystallography, known aminotransferase inhibitors gabaculine and **15** yielded predicable mechanisms of action against *Tg*O/GABA-AT. The phylogeny of *Tg*O/GABA-AT was determined and found to be conserved across taxa. A knockout parasite and a CRISPER/Cas9 knockout of *Tg*O/GABA-AT were made. *Tg*O/GABA-AT gene was found to be overexpressed in sporozoites and merozoites. *Tg*O/GABA-AT was not essential for the formation of oocysts in cats, nor was it critical for replication of tachyzoites, persistence of dormant cysts, or formation of cysts. A chemically mutagenized parasite, which has lost the capacity to make oocysts or to shed oocysts in the definitive feline host, called T-263, resulted in loss of function. When it was noted that T-263 could not progress beyond structurally normally appearing microgametes and macrogametes, mutations in merozoites (the pre-gamete stage) were considered most likely to be relevant since no mutations were noted in the microgamete or macrogamete. Based on the assumption that in nature a parasite would likely not be perpetuated, any mutation that was also present in any of the JCVI library of 100 isolates from throughout the world was excluded. This left 20 candidate mutations, 10 of which had genes with identifiable functions when searched by name and analyzed by PFAM. A search for whether those genes had been associated with infertility or involve steps known to occur in capacitation, triggering tyrosine phosphorylation, motility, membrane fusion, or fertility of gametes in other species revealed putative candidates for the mutations that are essential for conception of *Toxoplasma*. These mutations showed a putative pathway beginning with change in pH and ionicity derived from a sodium GABA symporter, leading to a change in cyclic AMP, PKA/PKG, and genes associated with motility and energy.[62, 76,79,83,87,124,126,167–169] These findings seemed to us similar to a Rosetta stone revealing the same critical genes for these processes that are key for conception in *Toxoplasma* as identified in other species. We note that GABA modulates these processes in all species studied, possibly providing an explanation for the overexpression of *Tg*O/GABA-AT in the life cycle stage where capacitation occurs, making possible the conception of *T. gondii*. These processes appear to be broadly conserved from plants to humans and might provide insights into how both medicines and vaccines could be developed to block these processes. For *Toxoplasma* this would be associated with the life stage of the cat that widely contaminates the environment.

STAR★METHODS

Detailed methods are provided in the online version of this paper and include the following:

- KEY RESOURCES TABLE
- RESOURCE AVAILABILITY
  - Lead contact
  - Materials availability
  - Data and code availability
- EXPERIMENTAL MODEL AND STUDY PARTICIPANT DETAILS
  - Animals
  - Dartmouth
  - Einstein
  - USDA
  - Italy
  - Human cell lines
  - Primary cell cultures
  - Microbe strains species/strain
- METHOD DETAILS
  - Multi-sequence alignment of ornithine aminotransferase
  - SNP analysis and phylogeny Construction
  - Cloning, expression, and purification
  - Enzyme activity assays
  - Variation of enzyme concentration of *Tg*O/GABA-AT
  - Determination of the K_m of ornithine against *Tg*O/GABA-AT
  - Measurement of kinetic constants of inhibitors and inactivators of *Tg*O/GABA-AT
  - Co-crystallization experiments
  - X-Ray data collection and structure determination
  - Measuring effect of *Tg*O/GABA-AT inactivators on *T. gondii in vitro*
  - Measuring effect of *Tg*O/GABA-AT inactivators on *P. falciparum in vitro*
  - *In vitro* and *In vivo* phenotypes of type II parasites deleted for *Tg*O/GABA-AT
  - Levels of *Tg*O/GABA-AT expression as a function of life cycle stage
  - Initial *Tg*O/GABA-AT antibody production using recombinant protein also studied in enzyme assays and with crystallography (called "antibody 1")

- Additional protein and antibody production; characterization with immunofluorescence assays for *Tg*O/GABA-AT (called "antibody 2")
- Production of anti-OAT antibodies and Western blot analysis
- Immunofluorescence
- Knockout of *Tg*O/GABA-AT in EGS-strain *T. gondii* followed by peroral infection of cat and evaluation of subsequent oocyst shedding
- Culture and sequencing of Frenkel Live Vaccine TS-Against*T. gondii*
- Genome sequencing of *T. gondii*T-263 and CTG strains
- Single nucleotide polymorphism (SNP) identification and annotation
- Analysis of putative cyclic-AMP dependent protein kinase
- CRISPR rescue of mutation in sodium GABA symporter
- Protein structures in mutated gene candidates predicted by AlphaFold
- Bioinformatics, identification by stage associated expression, presence of mutations in natural isolates, PFAM, literature search and systems analysis that reveal capacitation pathway modulated by GABA

- QUANTIFICATION AND STATISTICAL ANALYSIS

SUPPLEMENTAL INFORMATION

Supplemental information can be found online at https://doi.org/10.1016/j.isci.2023.108477.

ACKNOWLEDGMENTS

The data collection was performed at the LS-CAT at the Advanced Photon Source supported by the Argonne National Laboratory operated by University of Chicago Argonne, LLC, for the US Department of Energy, Office of Biological and Environmental Research under contract DE-AC02-06CH11357. The LS-CAT Sector 21 is supported by the Michigan Economic Development Corporation and the Michigan Technology Tri-Corridor (Grant 085P1000817). This project has been funded with Federal funds from the National Institute of Allergy and Infectious Diseases, National Institutes of Health, Department of Health and Human Services, under Contracts No. HHSN272200700058C and HHSN272201200026C (W.F.A.). This research was supported, in part, by NIH NIDDK grant #1T35DK062719-27 (to J.L.) and by NIH grant R01 DA030604 (to R.B.S.). This work was also supported by the Division of Microbiology and Infectious Diseases, National Institute of Allergy and Infectious Diseases (grant number U01AI082180-01,RMc), the Conte Center, and the National Institutes of Health (grant numbers 1P50MH094267 and U01HL108634-01). This work also was supported by NIH grant AI155603 (DJB) and NIH grant AI172811 (D.J.B.). We thank the Mann Cornwell family, Engel family (and "Taking Out Toxo"), Morel, Pritzker, Allen, Drago, VanDusen/Longfellow, Rodriguez and Rooney families for their support of this work. We thank Andrew Grose for assistance with references during manuscript preparation. We thank Michael Grigg for helpful discussion. We thank L. Knoll and B. Martorelli Di Genova for their early work with their model and image in Figure 7A. We thank Mario Falchi (Core Facilities, ISS) for confocal microscope analysis. We thank Mohamed-Ali Hakimi for advice concerning the MORC analysis and permission to include information from the data in that analysis.

AUTHOR CONTRIBUTIONS

Conception and design: R.L.M., R.B.S., H.A.L., L.M.W., D.B., J.L., J.P.D., E.V.F., T.T., B.A.F., D.B., and C.S.

Performed and/or interpreted experiments: Y.Z., M.J.M., H.V.L., E.V.F., W.A., S.D., H.A.L., S.W., C.W.R., P.L., M.H., B.F., K.E.B., F.S., C.H., P.L., M.H., M.M., J.P.D., M.M., S.V.R., K.F., K.E.B., K.M.W., S.D., C.H., S.P.M., M.M., and R.B.S.

Wrote manuscript: R.L.M., M.J.M., H.V.L., E.V.F., J.L., D.B., L.W., H.A.L., C.W.R., and R.B.S.

Revised manuscript: R.B.S., M.J.M., R.L.M., E.V.F., H.V.L., E.V.F., H.A.L., J.L., Y.Z., J.P.D., and C.W.R.

DECLARATION OF INTERESTS

H.V.L. is currently a program officer at the National Institute on Drug Abuse at the National Institutes of Health.

H.A.L. is currently a scientist working at National Institute of Diabetes, Digestive and Kidney Disease (NIDDK) at the National Institutes of Health. The findings and conclusions of this article are those of the authors and do not necessarily reflect the views of the National Institute on Drug Abuse, National Institute of Diabetes, Digestive and Kidney Diseases (NIDDK), the National Institutes of Health, nor the US Department of Health and Human Services.

R.B.S. and R.L.M., with H.V.L., submitted Patent Number: US 10,632,088 B2 INACTIVATORS OF TOXOPLASMA GONDII ORNITHINE AMINOTRANSFERASE FOR TREATING TOXOPLASMOSIS AND MALARIA through their Technology Transfer offices.

The authors declare no competing financial interest.

INCLUSION AND DIVERSITY

We support inclusion, diverse and equitable conduct of research.

Received: October 21, 2021
Revised: April 28, 2023
Accepted: November 13, 2023
Published: November 16, 2023

REFERENCES

1. McLeod, R., Cohen, W., Dovgin, S., Finkelstein, L., and Boyer, K.M. (2020). i Human *Toxoplasma* Infection. Chapter 4. In Toxoplasma gondii: The Model Apicomplexan, Third Edition, L.M. Weiss and K. Kim, eds. (Academic Press, Elsevier, London, Cambridge, San Diego, Oxford), pp. 117–227. http://www.sciencedirect.com/science/article/pii/B9780128150412000049).
2. Scallan, E., Hoekstra, R.M., Angulo, F.J., Tauxe, R.V., Widdowson, M.-A., Roy, S.L., Jones, J.L., and Griffin, P.M. (2011). Foodborne illness acquired in the United States—major pathogens. Emerg. Infect. Dis. *17*, 7–15.
3. Torgerson, P.R., and Mastroiacovo, P. (2013). The global burden of congenital toxoplasmosis: a systematic review. Bull. World Health Organ. *91*, 501–508.
4. Boyer, K., Hill, D., Mui, E., Wroblewski, K., Karrison, T., Dubey, J.P., Sautter, M., Noble, A.G., Withers, S., Swisher, C., et al. (2011). Unrecognized ingestion of Toxoplasma gondii oocysts leads to congenital toxoplasmosis and causes epidemics in North America. Clin. Infect. Dis. *53*, 1081–1089.
5. Dabritz, H.A., Miller, M.A., Atwill, E.R., Gardner, I.A., Leutenegger, C.M., Melli, A.C., and Conrad, P.A. (2007). Detection of Toxoplasma gondii-like oocysts in cat feces and estimates of the environmental oocyst burden. J. Am. Vet. Med. Assoc. *231*, 1676–1684.
6. Dubey, J.P. (1998). Toxoplasma gondii oocyst survival under defined temperatures. J. Parasitol. *84*, 862–865.
7. Frenkel, J.K., Ruiz, A., and Chinchilla, M. (1975). Soil survival of Toxoplasma oocysts in Kansas and Costa Rica. Am. J. Trop. Med. Hyg. *24*, 439–443.
8. Yilmaz, S.M., and Hopkins, S.H. (1972). Effects of different conditions on duration of infectivity of Toxoplasma gondii oocysts. J. Parasitol. *58*, 938–939.
9. Arnold, S.J., Kinney, M.C., McCormick, M.S., Dummer, S., and Scott, M.A. (1997). Disseminated toxoplasmosis. Unusual presentations in the immunocompromised host. Arch. Pathol. Lab. Med. *121*, 869–873.
10. Burrowes, D., Boyer, K., Swisher, C.N., Noble, A.G., Sautter, M., Heydemann, P., Rabiah, P., Lee, D., and McLeod, R.; the Toxoplasmosis Study Group (2012). Spinal cord lesions in congenital toxoplasmosis demonstrated with neuroimaging, including their successful treatment in an adult. J. Neuroparasitology *3*, 235533.
11. McLeod, R., Lykins, J., Gwendolyn Noble, A., Rabiah, P., Swisher, C.N., Heydemann, P.T., McLone, D., Frim, D., Withers, S., Clouser, F., and Boyer, K. (2014). Management of congenital toxoplasmosis. Curr. Pediatr. Rep. *2*, 166–194.
12. Felin, M.S., Wang, K., Moreira, A., Grose, A., Leahy, K., Zhou, Y., Clouser, F.A., Siddiqui, M., Leong, N., Goodall, P., et al. (2022). Building Programs to Eradicate Toxoplasmosis Part I: Introduction and Overview. Curr. Pediatr. Rep. *10*, 57–92.
13. Waxman, S., and Herbert, V. (1969). Mechanism of pyrimethamine-induced megaloblastosis in human bone marrow. N. Engl. J. Med. *280*, 1316–1319.
14. Caumes, E., Bocquet, H., Guermonprez, G., Rogeaux, O., Bricaire, F., Katlama, C., and Gentilini, M. (1995). Adverse cutaneous reactions to pyrimethamine/sulfadiazine and pyrimethamine/clindamycin in patients with AIDS and toxoplasmic encephalitis. Clin. Infect. Dis. *21*, 656–658.
15. McLeod, R., Khan, A.R., Noble, G.A., Latkany, P., Jalbrzikowski, J., and Boyer, K.; Toxoplasmosis Study Group (2006). Severe sulfadiazine hypersensitivity in a child with reactivated congenital toxoplasmic chorioretinitis. Pediatr. Infect. Dis. J. *25*, 270–272.
16. Neafsey, D.E. (2013). Genome sequencing sheds light on emerging drug resistance in malaria parasites. Nat. Genet. *45*, 589–590.
17. Rosenthal, P.J. (2013). The interplay between drug resistance and fitness in malaria parasites. Mol. Microbiol. *89*, 1025–1038.
18. Astegno, A., Maresi, E., Bertoldi, M., La Verde, V., Paiardini, A., and Dominici, P. (2017). Unique substrate specificity of ornithine aminotransferase from Toxoplasma gondii. Biochem. J. *474*, 939–955.
19. Srivastava, A., Philip, N., Hughes, K.R., Georgiou, K., MacRae, J.I., Barrett, M.P., Creek, D.J., McConville, M.J., and Waters, A.P. (2016). Stage-specific changes in Plasmodium metabolism required for differentiation and adaptation to different host and vector environments. PLoS Pathog. *12*, e1006094.
20. Agüero, F., Al-Lazikani, B., Aslett, M., Berriman, M., Buckner, F.S., Campbell, R.K., Carmona, S., Carruthers, I.M., Chan, A.W.E., Chen, F., et al. (2008). Genomic-scale prioritization of drug targets: the TDR Targets database. Nat. Rev. Drug Discov. *7*, 900–907.
21. Magariños, M.P., Carmona, S.J., Crowther, G.J., Ralph, S.A., Roos, D.S., Shanmugam, D., Van Voorhis, W.C., and Agüero, F. (2012). TDR Targets: a chemogenomics resource for neglected diseases. Nucleic Acids Res. *40*, D1118–D1127.
22. Baich, A. (1983). The effect of methionine on the accumulation of ornithine by Chinese hamster cells in culture. Biochim. Biophys. Acta *756*, 238–241.
23. Müller, S., Coombs, G.H., and Walter, R.D. (2001). Targeting polyamines of parasitic protozoa in chemotherapy. Trends Parasitol. *17*, 242–249.
24. Bacchi, C.J., and Yarlett, N. (2002). Polyamine metabolism as chemotherapeutic target in protozoan parasites. Mini Rev. Med. Chem. *2*, 553–563.
25. Birkholtz, L.M., Williams, M., Niemand, J., Louw, A.I., Persson, L., and Heby, O. (2011). Polyamine homoeostasis as a drug target in pathogenic protozoa: peculiarities and possibilities. Biochem. J. *438*, 229–244.
26. Roberts, S. (2013). Genetic manipulation of Leishmania parasites facilitates the exploration of the polyamine biosynthetic pathway as a potential therapeutic target. Faculty Scholarship (PHRM). http://commons.pacificu.edu/phrmfac/52.
27. Shih, V.E., Berson, E.L., Mandell, R., and Schmidt, S.Y. (1978). Ornithine ketoacid transaminase deficiency in gyrate atrophy of the choroid and retina. Am. J. Hum. Genet. *30*, 174–179.
28. Valle, D., Kaiser-Kupfer, M.I., and Del Valle, L.A. (1977). Gyrate atrophy of the choroid and retina: deficiency of ornithine aminotransferase in transformed lymphocytes. Proc. Natl. Acad. Sci. USA *74*, 5159–5161.
29. Lee, H., Juncosa, J.I., and Silverman, R.B. (2015). Ornithine aminotransferase versus GABA aminotransferase: implications for the design of new anticancer drugs. Med. Res. Rev. *35*, 286–305.
30. McCormick, D.A. (1989). GABA as an inhibitory neurotransmitter in human cerebral cortex. J. Neurophysiol. *62*, 1018–1027.
31. Doumlele, K., Conway, E., Hedlund, J., Tolete, P., and Devinsky, O. (2016). A case report on the efficacy of vigabatrin analogue (1S, 3S)-3-amino-4-difluoromethylenyl-1-cyclopentanoic acid (CPP-115) in a patient with infantile spasms. Epilepsy Behav. Case Rep. *6*, 67–69.
32. Silverman, R.B. (2012). The 2011 E. B. Hershberg Award for Important Discoveries in Medicinally Active Substances: (1S,3S)-3-Amino-4-difluoromethylenyl-1-cyclopentanoic acid (CPP-115), a GABA Aminotransferase Inactivator and New Treatment for Drug Addiction and Infantile Spasms. J. Med. Chem. *55*, 567–575.
33. Zigmond, E., Ya'acov, A.B., Lee, H., Lichtenstein, Y., Shalev, Z., Smith, Y., Zolotarov, L., Ziv, E., Kalman, R., Le, H.V., et al. (2015). Suppression of hepatocellular carcinoma by inhibition of overexpressed ornithine aminotransferase. ACS Med. Chem. Lett. *6*, 840–844.
34. Moschitto, M.J., Doubleday, P.F., Catlin, D.S., Kelleher, N.L., Liu, D., and Silverman, R.B. (2019). Mechanism of inactivation of ornithine aminotransferase by (1S,3S)-3-Amino-4-(hexafluoropropan-2-ylidenyl) cyclopentane-1-carboxylic acid. J. Am. Chem. Soc. *141*, 10711–10721.
35. Markova, M., Peneff, C., Hewlins, M.J.E., Schirmer, T., and John, R.A. (2005). Determinants of substrate specificity in ω-aminotransferases. J. Biol. Chem. *280*, 36409–36416.
36. Shah, S.A., Shen, B.W., and Brünger, A.T. (1997). Human ornithine aminotransferase complexed with L-canaline and gabaculine: structural basis for substrate recognition. Structure *5*, 1067–1075.
37. Shen, B.W., Hennig, M., Hohenester, E., Jansonius, J.N., and Schirmer, T. (1998).

Crystal structure of human recombinant ornithine aminotransferase. J. Mol. Biol. *277*, 81–102.
38. Storici, P., Capitani, G., Müller, R., Schirmer, T., and Jansonius, J.N. (1999). Crystal structure of human ornithine aminotransferase complexed with the highly specific and potent inhibitor 5-fluoromethylornithine. J. Mol. Biol. *285*, 297–309.
39. Gafan, C., Wilson, J., Berger, L.C., and Berger, B.J. (2001). Characterization of the ornithine aminotransferase from Plasmodium falciparum. Mol. Biochem. Parasitol. *118*, 1–10.
40. Vedadi, M., Lew, J., Artz, J., Amani, M., Zhao, Y., Dong, A., Wasney, G.A., Gao, M., Hills, T., Brokx, S., et al. (2007). Genome-scale protein expression and structural biology of Plasmodium falciparum and related Apicomplexan organisms. Mol. Biochem. Parasitol. *151*, 100–110.
41. Lykins, J.D., Filippova, E.V., Halavaty, A.S., Minasov, G., Zhou, Y., Dubrovska, I., Flores, K.J., Shuvalova, L.A., Ruan, J., El Bissati, K., et al. (2018). CSGID Solves Structures and Identifies Phenotypes for Five Enzymes in Toxoplasma gondii. Front. Cell. Infect. Microbiol. *8*, 352.
42. MacRae, J.I., Sheiner, L., Nahid, A., Tonkin, C., Striepen, B., and McConville, M.J. (2012). Mitochondrial metabolism of glucose and glutamine is required for intracellular growth of Toxoplasma gondii. Cell Host Microbe *12*, 682–692.
43. Fritz, H.M., Buchholz, K.R., Chen, X., Durbin-Johnson, B., Rocke, D.M., Conrad, P.A., and Boothroyd, J.C. (2012). Transcriptomic analysis of *Toxoplasma* development reveals many novel functions and structures specific to sporozoites and oocysts. PLoS One *7*, e29998.
44. Possenti, A., Fratini, F., Fantozzi, L., Pozio, E., Dubey, J.P., Ponzi, M., Pizzi, E., and Spano, F. (2013). Global proteomic analysis of the oocyst/sporozoite of Toxoplasma gondii reveals commitment to a host-independent lifestyle. BMC Genom. *14*, 183.
45. Kurata, S., Hiradate, Y., Umezu, K., Hara, K., and Tanemura, K. (2019). Capacitation of mouse sperm is modulated by GABA (gamma-aminobutyric acid) concentration. J. Reprod. Dev. *65*, 327–334.
46. Jortzik, E., Fritz-Wolf, K., Sturm, N., Hipp, M., Rahlfs, S., and Becker, K. (2010). Redox regulation of Plasmodium falciparum ornithine δ-aminotransferase. J. Mol. Biol. *402*, 445–459.
47. Lu, J.Z., Muench, S.P., Allary, M., Campbell, S., Roberts, C.W., Mui, E., McLeod, R.L., Rice, D.W., and Prigge, S.T. (2007). Type I and type II fatty acid biosynthesis in Eimeria tenella: enoyl reductase activity and structure. Parasitology *134*, 1949–1962.
48. Su, C., Khan, A., Zhou, P., Majumdar, D., Ajzenberg, D., Dardé, M.L., Zhu, X.-Q., Ajioka, J.W., Rosenthal, B.M., Dubey, J.P., and Sibley, L.D. (2012). Globally diverse Toxoplasma gondii isolates comprise six major clades originating from a small number of distinct ancestral lineages. Proc. Natl. Acad. Sci. USA *109*, 5844–5849.
49. Lu, H., and Silverman, R.B. (2006). Fluorinated conformationally restricted γ-aminobutyric acid aminotransferase inhibitors. J. Med. Chem. *49*, 7404–7412.
50. Juncosa, J.I., Takaya, K., Le, H.V., Moschitto, M.J., Weerawarna, P.M., Mascarenhas, R., Liu, D., Dewey, S.L., and Silverman, R.B. (2018). Design and mechanism of (S)-3-amino-4-(difluoromethylenyl)cyclopent-1-ene-1-carboxylic acid, a highly potent γ-aminobutyric acid aminotransferase inactivator for the treatment of addiction. J. Am. Chem. Soc. *140*, 2151–2164.
51. Fox, B.A., Falla, A., Rommereim, L.M., Tomita, T., Gigley, J.P., Mercier, C., Cesbron-Delauw, M.-F., Weiss, L.M., and Bzik, D.J. (2011). Type II Toxoplasma gondii KU80 knockout strains enable functional analysis of genes required for cyst development and latent infection. Eukaryot. Cell *10*, 1193–1206.
52. Fox, B.A., Rommereim, L.M., Guevara, R.B., Falla, A., Hortua Triana, M.A., Sun, Y., and Bzik, D.J. (2016). The Toxoplasma gondii rhoptry kinome is essential for chronic infection. mBio *7*. e001933-16.
53. Hortua Triana, M.A., Cajiao Herrera, D., Zimmermann, B.H., Fox, B.A., and Bzik, D.J. (2016). Pyrimidine pathway-dependent and -independent functions of the Toxoplasma gondii mitochondrial dihydroorotate dehydrogenase. Infect. Immun. *84*, 2974–2981.
54. Radke, J.B., Worth, D., Hong, D., Huang, S., Sullivan, W.J., Jr., Wilson, E.H., and White, M.W. (2018). Transcriptional repression by ApiAP2 factors is central to chronic toxoplasmosis. PLoS Pathog. *14*, e1007035.
55. McPhillie, M., Zhou, Y., El Bissati, K., Dubey, J., Lorenzi, H., Capper, M., Lukens, A.K., Hickman, M., Muench, S., Verma, S.K., et al. (2016). New paradigms for understanding and step changes in treating active and chronic, persistent apicomplexan infections. Sci. Rep. *6*, 29179.
56. Paredes-Santos, T.C., Martins-Duarte, E.S., Vitor, R.W.A., de Souza, W., Attias, M., and Vommaro, R.C. (2013). Spontaneous cystogenesis in vitro of a Brazilian strain of Toxoplasma gondii. Parasitol. Int. *62*, 181–188.
57. Paredes-Santos, T.C., Tomita, T., Yan Fen, M., de Souza, W., Attias, M., Vommaro, R.C., and Weiss, L.M. (2016). Development of dual fluorescent stage specific reporter strain of Toxoplasma gondii to follow tachyzoite and bradyzoite development *in vitro* and *in vivo*. Microbes Infect. *18*, 39–47.
58. Wadman, M. (2019). Scientists decry FDA's decision to end cat parasite research. Sci. AAAS. https://www.sciencemag.org/news/2019/04/scientists-decry-usdas-decision-end-cat-parasite-research).
59. Dubey, J.P. (1995). Duration of immunity to shedding of Toxoplasma gondii oocysts by cats. J. Parasitol. *81*, 410–415.
60. Dubey, J.P. (2009). Toxoplasmosis of Animals and Humans (CRC Press).
61. Dubey, J.P. (2005). Unexpected oocyst shedding by cats fed Toxoplasma gondii tachyzoites: *in vivo* stage conversion and strain variation. Vet. Parasitol. *133*, 289–298.
62. Farhat, D.C., Swale, C., Dard, C., Cannella, D., Ortet, P., Barakat, M., Sindikubwabo, F., Belmudes, L., De Bock, P.-J., Couté, Y., et al. (2020). A MORC-driven transcriptional switch controls Toxoplasma developmental trajectories and sexual commitment. Nat. Microbiol. *5*, 570–583.
63. Dubey, J.P. (2017). Schizogony and gametogony of oocyst-deficient T-263 strain of Toxoplasma gondii. Vet. Parasitol. *245*, 160–162.
64. Frenkel, J.K., and Smith, D.D. (1982). Immunization of cats against shedding of Toxoplasma oocysts. J. Parasitol. *68*, 744–748.
65. Frenkel, J.K., Dubey, J.P., and Miller, N.L. (1970). Toxoplasma gondii in cats: fecal stages identified as coccidian oocysts. Science *167*, 893–896.
66. Frenkel, J.K., Pfefferkorn, E.R., Smith, D.D., and Fishback, J.L. (1991). Prospective vaccine prepared from a new mutant of Toxoplasma gondii for use in cats. Am. J. Vet. Res. *52*, 759–763.
67. Freyre, A., Choromanski, L., Fishback, J.L., and Popiel, I. (1993). Immunization of cats with tissue cysts, bradyzoites, and tachyzoites of the T-263 strain of Toxoplasma gondii. J. Parasitol. *79*, 716–719.
68. Mateus-Pinilla, N.E., Dubey, J.P., Choromanski, L., and Weigel, R.M. (1999). A field trial of the effectiveness of a feline Toxoplasma gondii vaccine in reducing T. gondii exposure for swine. J. Parasitol. *85*, 855–860.
69. Pfefferkorn, E.R. (1978). Toxoplasma gondii: the enzymic defect of a mutant resistant to 5-fluorodeoxyuridine. Exp. Parasitol. *44*, 26–35.
70. Pfefferkorn, E.R., and Kasper, L.H. (1983). Toxoplasma gondii: genetic crosses reveal phenotypic suppression of hydroxyurea resistance by fluorodeoxyuridine resistance. Exp. Parasitol. *55*, 207–218.
71. Pfefferkorn, E.R., and Pfefferkorn, L.C. (1976). Toxoplasma gondii: isolation and preliminary characterization of temperature-sensitive mutants. Exp. Parasitol. *39*, 365–376.
72. Ramakrishnan, C., Maier, S., Walker, R.A., Rehrauer, H., Joekel, D.E., Winiger, R.R., Basso, W.U., Grigg, M.E., Hehl, A.B., Deplazes, P., and Smith, N.C. (2019). An experimental genetically attenuated live vaccine to prevent transmission of Toxoplasma gondii by cats. Sci. Rep. *9*, 1474.
73. Fenker, K.E., Hansen, A.A., Chong, C.A., Jud, M.C., Duffy, B.A., Norton, J.P., Hansen, J.M., and Stanfield, G.M. (2014). SLC6 family transporter SNF-10 is required for protease-mediated activation of sperm motility in C. elegans. Dev. Biol. *393*, 171–182.
74. Fenker, K.E., and Stanfield, G.M. (2015). SNF-10 connects male-derived signals to the onset of sperm motility in C. Elegans. Worm *4*, e1003002.
75. Rudnick, G., Krämer, R., Blakely, R.D., Murphy, D.L., and Verrey, F. (2014). The SLC6 transporters: perspectives on structure, functions, regulation, and models for transporter dysfunction. Pflugers Arch. *466*, 25–42.
76. Buffone, M.G., Wertheimer, E.V., Visconti, P.E., and Krapf, D. (2014). Central role of soluble adenyl cyclase and cAMP in sperm physiology. Biochim. Biophys. Acta *1842*, 2610–2620.
77. Pereira, R., Sá, R., Barros, A., and Sousa, M. (2017). Major regulatory mechanisms involved in sperm motility. Asian J. Androl. *19*, 5–14.
78. Bae, J.W., Yi, J.K., Jeong, E.J., Lee, W.J., Hwang, J.M., Kim, D.H., Ha, J.J., and Kwon, W.S. (2022). Ras-related proteins (Rab) play significant roles in sperm motility and capacitation status. Reprod. Biol. *22*, 100617.
79. Ambawat, S., Sharma, P., Yadav, N.R., and Yadav, R.C. (2013). MYB transcription factor genes as regulators for plant responses: an

overview. Physiol. Mol. Biol. Plants *19*, 307–321.
80. Puga Molina, L.C., Luque, G.M., Balestrini, P.A., Marín-Briggiler, C.I., Romarowski, A., and Buffone, M.G. (2018). Molecular basis of human sperm capacitation. Front. Cell Dev. Biol. *6*, 72.
81. Nixon, B., Johnston, S.D., Skerrett-Byrne, D.A., Anderson, A.L., Stanger, S.J., Bromfield, E.G., Martin, J.H., Hansbro, P.M., and Dun, M.D. (2019). Modification of crocodile spermatozoa refutes the tenet that post-testicular sperm maturation is restricted to mammals. Mol. Cell. Proteomics *18*, S58–S76.
82. Nixon, B., Bernstein, I.R., Cafe, S.L., Delehedde, M., Sergeant, N., Anderson, A.L., Trigg, N.A., Eamens, A.L., Lord, T., Dun, M.D., et al. (2019). A kinase anchor protein 4 is vulnerable to oxidative adduction in male germ cells. Cell Dev. Biol. *7*, 319.
83. El Bakkouri, M., Kouidmi, I., Wernimont, A.K., Amani, M., Hutchinson, A., Loppnau, P., Kim, J.J., Flueck, C., Walker, J.R., Seitova, A., et al. (2019). Structures of the cGMP-dependent protein kinase in malaria parasites reveal a unique structural relay mechanism for activation. Proc. Natl. Acad. Sci. USA *116*, 14164–14173.
84. Kurata, S., Umezu, K., Takamori, H., Hiradate, Y., Hara, K., and Tanemura, K. (2022). Exogenous gamma-aminobutyric acid addition enhances porcine sperm acrosome reaction. Anim. Sci. J. *93*, e13744.
85. Biancucci, M., Mattioli, R., Forlani, G., Funck, D., Costantino, P., and Trovato, M. (2015). Role of proline and GABA in sexual reproduction of angiosperms. Front. Plant Sci. *6*, 680.
86. Saxena, S., Sahu, S., Kaila, T., Nigam, D., Chaduvla, P.K., Rao, A.R., Sanand, S., Singh, N.K., and Gaikwad, K. (2020). Transcriptome profiling of differentially expressed genes in cytoplasmic male-sterile line and its fertility restorer line in pigeon pea (*Cajanus cajan* L.). BMC Plant Biol. *20*, 74.
87. Naz, R.K., and Rajesh, P.B. (2004). Role of tyrosine phosphorylation in sperm capacitation/acrosome reaction. Reprod. Biol. Endocrinol. *2*, 75.
88. Juárez, R., Ruiz, J.F., Nick McElhinny, S.A., Ramsden, D., and Blanco, L. (2006). A specific loop in human DNA polymerase mu allows switching between creative and DNA-instructed synthesis. Nucleic Acids Res. *34*, 4572–4582.
89. Yoo, H., Roth-Johnson, E.A., Bor, B., and Quinlan, M.E. (2015). Drosophila Cappuccino alleles provide insight into formin mechanism and role in oogenesis. Mol. Biol. Cell *26*, 1875–1886.
90. Leader, B., Lim, H., Carabatsos, M.J., Harrington, A., Ecsedy, J., Pellman, D., Maas, R., and Leder, P. (2002). Formin-2, polyploidy, hypofertility and positioning of the meiotic spindle in mouse oocytes. Nat. Cell Biol. *4*, 921–928.
91. Lorès, P., Dacheux, D., Kherraf, Z.E., Nsota Mbango, J.F., Coutton, C., Stouvenel, L., Ialy-Radio, C., Amiri-Yekta, A., Whitfield, M., Schmitt, A., et al. (2019). Mutations in TTC29, encoding an evolutionarily conserved axonemal protein, result in asthenozoospermia and male infertility. Am. J. Hum. Genet. *105*, 1148–1167.
92. Ohta, M., Ohyama, K., Asano, A., Yokota, S.I., Khalid, A.M., and Yamano, Y. (2012). Regulation of rat tetratricopeptide repeat domain 29 gene expression by follicle-stimulating hormone. Biosci. Biotechnol. Biochem. *76*, 1540–1543.
93. Xu, Y., Cao, J., Huang, S., Feng, D., Zhang, W., Zhu, X., and Yan, X. (2015). Characterization of tetratricopeptide repeat-containing proteins critical for cilia formation and function. PLoS One *10*, e0124378.
94. Wang, Z.T., Verma, S.K., Dubey, J.P., and Sibley, L.D. (2017). The aromatic amino acid hydroxylase genes AAH1 and AAH2 in Toxoplasma gondii contribute to transmission in the cat. PLoS Pathog. *13*, e1006272.
95. Hafidh, S., Potěšil, D., Fíla, J., Čapková, V., Zdráhal, Z., and Honys, D. (2016). Quantitative proteomics of the tobacco pollen tube secretome identifies novel pollen tube guidance proteins important for fertilization. Genome Biol. *17*, 81.
96. Zhang, X.L., Zhang, J., Guo, Y.H., Sun, P., Jia, H.X., Fan, W., Lu, M.Z., and Hu, J.J. (2016). Comparative Proteomic Analysis of Mature Pollen in Triploid and Diploid Populus deltoides. Int. J. Mol. Sci. *17*, 1475.
97. Gilkerson, J., Perez-Ruiz, J.M., Chory, J., and Callis, J. (2012). The plastid-localized pfkB-type carbohydrate kinases FRUCTOKINASE-LIKE 1 and 2 are essential for growth and development of *Arabidopsis thaliana*. BMC Plant Biol. *12*, 102.
98. Johnson, M.A., von Besser, K., Zhou, Q., Smith, E., Aux, G., Patton, D., Levin, J.Z., and Preuss, D. (2004). Arabidopsis hapless mutations define essential gametophytic functions. Genetics *168*, 971–982.
99. Jin, S.K., and Yang, W.X. (2017). Factors and pathways involved in capacitation: how are they regulated? Oncotarget *8*, 3600–3627. https://www.oncotarget.com/article/12274/text/.
100. Johnson, S.L., and Yund, P.O. (2004). Remarkable longevity of dilute sperm in a free-spawning colonial ascidian. Biol. Bull. *206*, 144–151.
101. Liu, D.Y., Clarke, G.N., and Baker, H.W.G. (2006). Tyrosine phosphorylation on capacitated human sperm tail detected by immunofluorescence correlates strongly with sperm-zona pellucida (ZP) binding but not with the ZP-induced acrosome reaction. Hum. Reprod. *21*, 1002–1008.
102. Liu, D.Y., Clarke, G.N., and Baker, H.W.G. (2006). Hyper-osmotic condition enhances protein tyrosine phosphorylation and zona pellucida binding capacity of human sperm. Hum. Reprod. *21*, 745–752.
103. Massonnet, M., Cochetel, N., Minio, A., Vondras, A.M., Lin, J., Muyle, A., Garcia, J.F., Zhou, Y., Delledonne, M., Riaz, S., et al. (2020). The genetic basis of sex determination in grapes. Nat. Commun. *11*, 2902.
104. Lin, Y.N., and Matzuk, M.M. (2014). Genetics of male fertility. Methods Mol. Biol. *1154*, 25–37.
105. Werner, E.R., Keller, M.A., Sailer, S., Lackner, K., Koch, J., Hermann, M., Coassin, S., Golderer, G., Werner-Felmayer, G., Zoeller, R.A., et al. (2020). The *TMEM189* gene encodes plasmanylethanolamine desaturase which introduces the characteristic vinyl ether double bond into plasmalogens. Proc. Natl. Acad. Sci. USA *117*, 7792–7798.
106. Zhang, X., Shen, Y., Wang, X., Yuan, G., Zhang, C., and Yang, Y. (2016). A novel homozygous *CFAP65* mutation in humans causes male infertility with multiple morphological abnormalities of the sperm flagella. Clin. Genet. *96*, 541–548.
107. Lalanne, E., Michaelidis, C., Moore, J.M., Gagliano, W., Johnson, A., Patel, R., Howden, R., Vielle-Calzada, J.-P., Grossniklaus, U., and Twell, D. (2004). Highlights the diversity of mechanisms underlying male progamic development in *Arabidopsis*. Genetics *167*, 1975–1986.
108. Jin, J.Y., Chen, W.Y., Zhou, C.X., Chen, Z.H., Yu-Ying, Y., Ni, Y., Chan, H.C., and Shi, Q.X. (2009). Activation of GABAAreceptor/Cl-channel and capacitation in rat spermatozoa: HCO3- and Cl- are essential. Syst. Biol. Reprod. Med. *55*, 97–108.
109. de Jong, R.M., Tebeje, S.K., Meerstein-Kessel, L., Tadesse, F.G., Jore, M.M., Stone, W., and Bousema, T. (2020). Immunity against sexual stage Plasmodium falciparum and Plasmodium vivax parasites. Immunol. Rev. *293*, 190–215.
110. Kumar, S., Haile, M.T., Hoopmann, M.R., Tran, L.T., Michaels, S.A., Morrone, S.R., Ojo, K.K., Reynolds, L.M., Kusebauch, U., Vaughan, A.M., et al. (2021). Plasmodium falciparum calcium-dependent protein kinase 4 is critical for male gametogenesis and transmission to the mosquito vector. mBio *12*, e0257521.
111. Kumar, S., Abatiyow, B.A., Haile, M.T., Oualim, K.M.Z., Leeb, A.S., Vaughan, A.M., and Kappe, S.H. (2022). A putative plasmodium RNA-binding protein plays a critical role in female gamete fertility and parasite transmission to the Mosquito. Front. Cell Dev. Biol. *10*, 825247.
112. Guttery, D.S., Roques, M., Holder, A.A., and Tewari, R. (2015). Commit and Transmit: Molecular Players in Plasmodium Sexual Development and Zygote Differentiation. Trends Parasitol. *31*, 676–685.
113. Baker, M.A., Hetherington, L., Ecroyd, H., Roman, S.D., and Aitken, R.J. (2004). Analysis of the mechanism by which calcium negatively regulates the tyrosine phosphorylation cascade associated with sperm capacitation. J. Cell Sci. *117*, 211–222.
114. Chen, Y., Cann, M.J., Litvin, T.N., Iourgenko, V., Sinclair, M.L., Levin, L.R., and Buck, J. (2000). Soluble adenylyl cyclaseas an evolutionarily conserved bicarbonate sensor. Science *289*, 625–628.
115. Joshi, M., Sethi, S., Mehta, P., Kumari, A., and Rajender, S. (2023). Small RNAs, spermatogenesis, and male infertility: a decade of retrospect. Reprod. Biol. Endocrinol. *21*, 106.
116. Gromenko, Y.Y., Galimov, K.S., Gilyazova, I.R., Galimova, E.F., Bulygin, K.V., Ryagin, S.N., Galimov, S.N., Litvitskiy, P.F., Piavchenko, G.A., and Pavlov, V.N. (2023). Single nucleotide polymorphism rs527236194 of the cytochrome B gene (MT-CYB) is associated with alterations in sperm parameters. Mol. Biol. Rep. *50*, 10131–10136.
117. Zhao, J., Zhang, C., Li, S., Yuan, M., Mu, W., Yang, J., Ma, Y., Guan, C., and Ma, C. (2023). Changes in m^{6}A RNA methylation are associated with male sterility in wolfberry. BMC Plant Biol. *23*, 456.
118. Kopanja, D., Roy, N., Stoyanova, T., Hess, R.A., Bagchi, S., and Raychaudhuri, P. (2011). Cul4A is essential for spermatogenesis and male fertility. Dev. Biol. *352*, 278–287.
119. Nomikos, M. (2015). Novel signaling mechanism and clinical applications of

sperm-specific PLCζ. Biochem. Soc. Trans. *43*, 371–376.
120. Nomikos, M., Sanders, J.R., Parthimos, D., Buntwal, L., Calver, B.L., Stamatiadis, P., Smith, A., Clue, M., Sideratou, Z., Swann, K., and Lai, F.A. (2015). Essential Role of the EF-hand Domain in Targeting Sperm Phospholipase Cζ to Membrane Phosphatidylinositol 4,5-Bisphosphate (PIP2). J. Biol. Chem. *290*, 29519–29530.
121. Nomikos, M., Sanders, J.R., Kashir, J., Sanusi, R., Buntwal, L., Love, D., Ashley, P., Sanders, D., Knaggs, P., Bunkheila, A., et al. (2015). Functional disparity between human PAWP and PLCζ in the generation of Ca2+ oscillations for oocyte activation. Mol. Hum. Reprod. *21*, 702–710.
122. Shawki, H.H., Ishikawa-Yamauchi, Y., Kawashima, A., Katoh, Y., Matsuda, M., Al-Soudy, A.S., Minisy, F.M., Kuno, A., Gulibaikelamu, X., Hirokawa, T., et al. (2019). EFCAB2 is a novel calcium-binding protein in mouse testis and sperm. PLoS One *14*, e0214687.
123. Kumar, S., Valansi, C., Haile, M.T., Li, X., Flyak, K., Dwivedy, A., Abatiyow, B.A., Leeb, A.S., Kennedy, S.Y., Camargo, N.M., et al. (2022). Malaria parasites utilize two essential plasma membrane fusogens for gamete fertilization. Cell. Mol. Life Sci. *79*, 549.
124. Dey, S., Brothag, C., and Vijayaraghavan, S. (2019). Signaling enzymes required for sperm maturation and fertilization in mammals. Front. Cell Dev. Biol. *7*, 341.
125. Li, Y., Qin, T., Wei, C., Sun, J., Dong, T., Zhou, R., Chen, Q., and Wang, Q. (2019). Using transcriptome analysis to screen for key genes and pathways related to cytoplasmic male sterility in cotton (Gossypium hirsutum L.). Int. J. Mol. Sci. *20*, 5120.
126. Ferris, P.J., Waffenschmidt, S., Umen, J.G., Lin, H., Lee, J.-H., Ishida, K., Kubo, T., Lau, J., and Goodenough, U.W. (2005). Plus and minus sexual agglutinins from Chlamydomonas reinhardtii. Plant Cell *17*, 597–615.
127. Silflow, C.D., and Lefebvre, P.A. (2001). Assembly and motility of eukaryotic cilia and flagella. Lessons from Chlamydomonas reinhardtii. Plant Physiol. *127*, 1500–1507.
128. Aitken, R.J., and Drevet, J.R. (2020). The Importance of Oxidative Stress in Determining the Functionality of Mammalian Spermatozoa: A Two-Edged Sword. Antioxidants (Basel) *9*, 111.
129. Baker, M.A., Hetherington, L., and Aitken, R.J. (2006). Identification of SRC as a key PKA-stimulated tyrosine kinase involved in the capacitation-associated hyperactivation of murine spermatoa. J. Cell Sci. *119*, 3182–3192.
130. Begcy, K., Nosenko, T., Zhou, L.Z., Fragner, L., Weckwerth, W., and Dresselhaus, T. (2019). Male Sterility in Maize after Transient Heat Stress during the Tetrad Stage of Pollen Development. Plant Physiol. *181*, 683–700.
131. Cannarella, R., Condorelli, R.A., Mongioì, L.M., La Vignera, S., and Calogero, A.E. (2020). Molecular Biology of Spermatogenesis: Novel Targets of Apparently Idiopathic Male Infertility. Int. J. Mol. Sci. *21*, 1728.
132. Dix, D.J., Allen, J.W., Collins, B.W., Mori, C., Nakamura, N., Poorman-Allen, P., Goulding, E.H., and Eddy, E.M. (1996). Targeted gene disruption of Hsp70-2 results in failed meiosis, germ cell apoptosis, and male infertility. Proc. Natl. Acad. Sci. USA *93*, 3264–3268.
133. Griffiths, A.J.F., Miller, J.H., Suzuki, D.T., and Freeman, W.H. (2000). Cytoplasmic male sterility. An Introduction to Genetic Analysis, 7th edition (W. H. Freeman). https://www.ncbi.nlm.nih.gov/books/NBK22015/.
134. Gunes, S., Al-Sadaan, M., and Agarwal, A. (2015). Spermatogenesis, DNA damage and DNA repair mechanisms in male infertility. Reprod. Biomed. Online *31*, 309–319.
135. Hamada, A., Esteves, S.C., Nizza, M., and Agarwal, A. (2012). Unexplained male infertility: diagnosis and management. Int. Braz J. Urol. *38*, 576–594.
136. Huang, J., Cheng, Z., Wang, C., Hong, Y., Su, H., Wang, J., Copenhaver, G.P., Ma, H., and Wang, Y. (2015). Formation of interference-sensitive meiotic cross-overs requires sufficient DNA leading-strand elongation. Proc. Natl. Acad. Sci. USA *112*, 12534–12539.
137. Huang, L., Dong, H., Zhou, D., Li, M., Liu, Y., Zhang, F., Feng, Y., Yu, D., Lin, S., and Cao, J. (2018). Systematic identification of long non-coding RNAs during pollen development and fertilization in Brassica rapa. Plant J. *96*, 203–222.
138. Islam, M.S., Studer, B., Møller, I.M., and Asp, T. (2014). Genetics and biology of cytoplasmic male sterility and its applications in forage and turf grass breeding. Plant Breed. *133*, 299–312.
139. Jensen, M., Leffers, H., Petersen, J.H., Nyboe Andersen, A., Jørgensen, N., Carlsen, E., Jensen, T.K., Skakkebaek, N.E., and Rajpert-De Meyts, E. (2004). Frequent polymorphism of the mitochondrial DNA polymerase gamma gene (POLG) in patients with normal spermiograms and unexplained subfertility. Hum. Reprod. *19*, 65–70.
140. Jiang, J., Jiang, J., Qiu, L., Miao, Y., Yao, L., and Cao, J. (2013). Identification of gene expression profile during fertilization in Brassica campestris subsp. chinensis. Genome *56*, 39–48.
141. Zuo, J., and Li, J. (2014). Molecular dissection of complex agronomic traits of rice: a team effort by Chinese scientists in recent years. Natl. Sci. Rev. *1*, 253–276.
142. Kobayashi, Y., Watanabe, M., Okada, Y., Sawa, H., Takai, H., Nakanishi, M., Kawase, Y., Suzuki, H., Nagashima, K., Ikeda, K., and Motoyama, N. (2002). Hydrocephalus, situs inversus, chronic sinusitis, and male infertility in DNA polymerase lambda-deficient mice: possible implication for the pathogenesis of immotile cilia syndrome. Mol. Cell Biol. *22*, 2769–2776.
143. Kotchoni, S.O., Jimenez-Lopez, J.C., Gachomo, E.W., and Seufferheld, M.J. (2010). A new and unified nomenclature for male fertility restorer (RF) proteins in higher plants. PLoS One *5*, e15906.
144. Kraus, D.M., Elliott, G.S., Chute, H., Horan, T., Pfenninger, K.H., Sanford, S.D., Foster, S., Scully, S., Welcher, A.A., and Holers, V.M. (2006). CSMD1 is a novel multiple domain complement-regulatory protein highly expressed in the central nervous system and epithelial tissues. J. Immunol. *176*, 4419–4430.
145. Lee, A.S., Rusch, J., Lima, A.C., Usmani, A., Huang, N., Lepamets, M., Vigh-Conrad, K.A., Worthington, R.E., Mägi, R., Wu, X., et al. (2019). Rare mutations in the complement regulatory gene CSMD1 are associated with male and female infertility. Nat. Commun. *10*, 4626.
146. Mukherjee, S., Ridgeway, A.D., and Lamb, D.J. (2010). DNA mismatch repair and infertility. Curr. Opin. Urol. *20*, 525–532.
147. Liu, C., He, X., Liu, W., Yang, S., Wang, L., Li, W., Wu, H., Tang, S., Ni, X., Wang, J., et al. (2019). Bi-allelic Mutations in TTC29 Cause Male Subfertility with Asthenoteratospermia in Humans and Mice. Am. J. Hum. Genet. *105*, 1168–1181.
148. Liu, Y., Tewari, R., Ning, J., Blagborough, A.M., Garbom, S., Pei, J., Grishin, N.V., Steele, R.E., Sinden, R.E., Snell, W.J., and Billker, O. (2008). The conserved plant sterility gene HAP2 functions after attachment of fusogenic membranes in Chlamydomonas and Plasmodium gametes. Genes Dev. *22*, 1051–1068.
149. Lopes, F.R., Carazzolle, M.F., Pereira, G.A.G., Colombo, C.A., and Carareto, C.M.A. (2008). Transposable elements in *Coffea* (Gentianales: Rubiacea) transcripts and their role in the origin of protein diversity in flowering plants. Mol. Genet. Genomics. *279*, 385–401.
150. Mori, T., Hirai, M., Kuroiwa, T., and Miyagishima, S.Y. (2010). The functional domain of GCS1-based gamete fusion resides in the amino terminus in plant and parasite species. PLoS One *5*, e15957.
151. Mounkes, L.C., Jones, R.S., Liang, B.C., Gelbart, W., and Fuller, M.T. (1992). A Drosophila model for xeroderma pigmentosum and Cockayne's syndrome: haywire encodes the fly homolog of ERCC3, a human excision repair gene. Cell *71*, 925–937.
152. Ogawa, T., Nishimura, K., Aoki, T., Takase, H., Tomizawa, K.I., Ashida, H., and Yokota, A. (2009). A phosphofructokinase B-type carbohydrate kinase family protein, NARA5, for massive expressions of plastid-encoded photosynthetic genes in Arabidopsis. Plant Physiol. *151*, 114–128.
153. Rovio, A.T., Marchington, D.R., Donat, S., Schuppe, H.C., Abel, J., Fritsche, E., Elliott, D.J., Laippala, P., Ahola, A.L., McNay, D., et al. (2001). Mutations at the mitochondrial DNA polymerase (POLG) locus associated with male infertility. Nat. Genet. *29*, 261–262.
154. Ryley, D.A., Wu, H.H., Leader, B., Zimon, A., Reindollar, R.H., and Gray, M.R. (2005). Characterization and mutation analysis of the human formin-2 (FMN2) gene in women with unexplained infertility. Fertil. Steril. *83*, 1363–1371.
155. Schnable, P., and Wise, R.P. (1998). The molecular basis of cytoplasmic male sterility and fertility restoration. Trends Plant Sci. *3*, 175–180.
156. Shamsi, M.B., Imam, S.N., and Dada, R. (2011). Sperm DNA integrity assays: diagnostic and prognostic challenges and implications in management of infertility. J. Assist. Reprod. Genet. *28*, 1073–1085.
157. Singh, S.P., Srivastava, R., and Kumar, J. (2015). Male sterility systems in wheat and opportunities for hybrid wheat development. Acta Physiol. Plant. *37*, 1713.
158. Sugi, T., Ma, Y.F., Tomita, T., Murakoshi, F., Eaton, M.S., Yakubu, R., Han, B., Tu, V., Kato, K., Kawazu, S., et al. (2016). *Toxoplasma gondii* Cyclic AMP-Dependent Protein Kinase Subunit 3 Is Involved in the Switch from Tachyzoite to Bradyzoite Development. mBio *27*. e00755-16.
159. Sun, C.Q., Chen, F.D., Teng, N.J., Yao, Y.M., Shan, X., and Dai, Z.L. (2019). Transcriptomic and proteomic analysis reveals mechanisms of low pollen-pistil compatibility during

water lily cross breeding. BMC Plant Biol. *19*, 542.
160. Tan, Y., Xu, X., Wang, C., Cheng, G., Li, S., and Liu, X. (2015). Molecular characterization and application of a novel cytoplasmic male sterility-associated mitochondrial sequence in rice. BMC Genet. *16*, 45.
161. Tu, Z., Cohen, M., Bu, H., and Lin, F. (2010). Tissue distribution and functional analysis of Sushi domain-containing protein 4. Am. J. Pathol. *176*, 2378–2384.
162. Tuteja, R., Saxena, R.K., Davila, J., Shah, T., Chen, W., Xiao, Y.L., Fan, G., Saxena, K.B., Alverson, A.J., Spillane, C., et al. (2013). Cytoplasmic male sterility-associated chimeric open reading frames identified by mitochondrial genome sequencing of four Cajanus genotypes. DNA Res. *20*, 485–495.
163. Van Tang, H., Pring, D.R., Muza, F.R., and Yan, B. (1996). Sorghum mitochondrial orf25 and a related chimeric configuration of a male-sterile cytoplasm. Curr. Genet. *29*, 265–274.
164. Weider, C., Stamp, P., Christov, N., Hüsken, A., Foueillassar, X., Camp, K.-H., and Munsch, M. (2009). Stability of Cytoplasmic Male Sterility in Maize under Different Environmental Conditions. Crop Sci. *49*, 77–84.
165. Whitford, R., Fleury, D., Reif, J.C., Garcia, M., Okada, T., Korzun, V., and Langridge, P. (2013). Hybrid breeding in wheat: technologies to improve hybrid wheat seed production. J. Exp. Bot. *64*, 5411–5428.
166. Sigrell, J.A., Cameron, A.D., Jones, T.A., and Mowbray, S.L. (1998). Structure of Escherichia coli ribokinase in complex with ribose and dinucleotide determined to 1.8 A resolution: insights into a new family of kinase structures. Structure *6*, 183–193.
167. Yang, F., Scarbrough, C., Sisson, J.H., and Wirschell, M. (2019). PKA, PP1 and DC1 phosphorylation mediate alcoholinducedciliary dysfunction in Chlamydomonas reinhardtii. Alcohol *75*, 31–38.
168. Kidaka, T., Sugi, T., Hayashida, K., Suzuki, Y., Xuan, X., Dubey, J.P., and Yamagishi, J. (2022). TDD-seq of Toxoplasma gondii sporozoites revealed a novel motif in stage-specific promoters, Infection, Genetics and Evolution. Infect. Genet. Evol. *98*, 105213. Contents lists available at Science Direct Infection, Genetics and Evolution www.elsevier.com/locate/meegid https://doi.org/10.1016/j.meegid.2022.105213 Note:also see 43.
169. Hehl, A.B., Basso, W.U., Lippuner, C., Ramakrishnan, C., Okoniewski, M., Walker, R.A., Grigg, M.E., Smith, N.C., and Deplazes, P. (2015). Asexual expansion of Toxoplasma gondii merozoites is distinct from tachyzoites and entails expression of non-overlapping gene families to attach, invade, and replicate within feline enterocytes. BMC Genom. *16*, 66.
170. Sugi, T., Tomita, T., Kidaka, T., Kawai, N., Hayashida, K., Weiss, L.M., and Yamagishi, J. (2022). Single Cell Transcriptomes of In Vitro Bradyzoite Infected Cells Reveals Toxoplasma gondii Stage Dependent Host Cell Alterations. Front. Cell. Infect. Microbiol. *12*, 848693.
171. Su, C., Shwab, E.K., Zhou, P., Zhu, X.Q., and Dubey, J.P. (2010). Moving towards an integrated approach to molecular detection and identification of Toxoplasma gondii. Parasitology *137*, 1–11.
172. Goodenough, U.W., Armbrust, E.V., Campbell, A.M., and Ferris, P.J. (1995). Molecular genetics of sexuality in Chlamydomonas. Annu. Rev. Plant Phys. *46*, 21–44.
173. Ferguson, D.J. (2002). *Toxoplasma gondii* and sex: essential or optional extra? Trends Parasitol. *18*, 351–355.
174. Gibrat, J.F., Madej, T., and Bryant, S.H. (1996). Surprising similarities in structure comparison. Curr. Opin. Struct. Biol. *6*, 377–385.
175. Penmatsa, A., Wang, K.H., and Gouaux, E. (2013). X-ray structure of dopamine transporter from Drosophila elucidates antidepressant mechanism. Nature *503*, 85–90.
176. Scanlon, S.M., Williams, D.C., and Schloss, P. (2001). Membrane cholesterol modulates serotonin transporter activity. Biochemistry *40*, 10507–10513.
177. North, P., and Fleischer, S. (1983). Alteration of synaptic membrane cholesterol/phospholipid ratio using a lipid transfer protein. Effect on γ-aminobutyric acid uptake. J. Biol. Chem. *258*, 1242–1253.
178. Hong, W.C., and Amara, S.G. (2010). Membrane cholesterol modulates the outward facing conformation of the dopamine transporter and alters cocaine binding. J. Biol. Chem. *285*, 32616–32626.
179. Martorelli Di Genova, B., Wilson, S.K., Dubey, J.P., and Knoll, L.J. (2019). Intestinal delta-6-desaturase activity determines host range for Toxoplasma sexual reproduction. PLoS Biol. *17*, e3000364.
180. Christen, P., and Metzler, D.E. (1985). Transaminases (Wiley).
181. Mehta, P.K., Hale, T.I., and Christen, P. (1993). Aminotransferases: demonstration of homology and division into evolutionary subgroups. Eur. J. Biochem. *214*, 549–561.
182. Liu, W., Peterson, P.E., Carter, R.J., Zhou, X., Langston, J.A., Fisher, A.J., and Toney, M.D. (2004). Crystal structures of unbound and aminooxyacetate-bound Escherichia coli γ-aminobutyrate aminotransferase. Biochemistry *43*, 10896–10905.
183. Berman, H.M., Bhat, T.N., Bourne, P.E., Feng, Z., Gilliland, G., Weissig, H., and Westbrook, J. (2000). The protein data bank and the challenge of structural genomics. Nat. Struct. Biol. *7*, 957–959.
184. Baugh, L., Phan, I., Begley, D.W., Clifton, M.C., Armour, B., Dranow, D.M., Taylor, B.M., Muruthi, M.M., Abendroth, J., Fairman, J.W., et al. (2015). Increasing the structural coverage of tuberculosis drug targets. Tuberculosis *95*, 142–148.
185. Silverman, R.B. (1995). Mechanism-based enzyme inactivators. In Methods in Enzymology, *249* (Academic Press), pp. 240–283.
186. Singh, J., Petter, R.C., Baillie, T.A., and Whitty, A. (2011). The resurgence of covalent drugs. Nat. Rev. Drug Discov. *10*, 307–317.
187. Fu, M., and Silverman, R.B. (1999). Isolation and characterization of the product of inactivation of γ-aminobutyric acid aminotransferase by gabaculine. Bioorg. Med. Chem. *7*, 1581–1590.
188. Rando, R.R. (1977). Mechanism of the irreversible inhibition of γ-aminobutyric acid-α-ketoglutaric acid transaminase by the neurotoxin gabaculine. Biochemistry *16*, 4604–4610.
189. Le, H.V., Hawker, D.D., Wu, R., Doud, E., Widom, J., Sanishvili, R., Liu, D., Kelleher, N.L., and Silverman, R.B. (2015). Design and mechanism of tetrahydrothiophene-Based γ-aminobutyric acid aminotransferase inactivators. J. Am. Chem. Soc. *137*, 4525–4533.
190. Bönnighausen, J., Gebhard, D., Kröger, C., Hadeler, B., Tumforde, T., Lieberei, R., Bergemann, J., Schäfer, W., and Bormann, J. (2015). Disruption of the GABA shunt affects mitochondrial respiration and virulence in the cereal pathogen Fusarium graminearum. Mol. Microbiol. *98*, 1115–1132.
191. Sharma, J., Rodriguez, P., Roy, P., and Guiton, P.S. (2020). Transcriptional ups and downs: patterns of gene expression in the life cycle of Toxoplasma gondii. Microb. Infect. *22*, 525–533.
192. Coppin, A., Varré, J.S., Lienard, L., Dauvillée, D., Guérardel, Y., Soyer-Gobillard, M.-O., Buléon, A., Ball, S., and Tomavo, S. (2005). Evolution of plant-like crystalline storage polysaccharide in the protozoan parasite Toxoplasma gondii argues for a red alga ancestry. J. Mol. Evol. *60*, 257–267.
193. Dzierszinski, F., Popescu, O., Toursel, C., Slomianny, C., Yahiaoui, B., and Tomavo, S. (1999). The protozoan parasite Toxoplasma gondii expresses two functional plant-like glycolytic enzymes Implications for evolutionary origin of apicomplexans. J. Biol. Chem. *274*, 24888–24895.
194. Dzierszinski, F., Mortuaire, M., Dendouga, N., Popescu, O., and Tomavo, S. (2001). Differential expression of two plant-like enolases with distinct enzymatic and antigenic properties during stage conversion of the protozoan parasite Toxoplasma gondii. J. Mol. Biol. *309*, 1017–1027.
195. Miranda, K., Pace, D.A., Cintron, R., Rodrigues, J.C.F., Fang, J., Smith, A., Rohloff, P., Coelho, E., de Haas, F., de Souza, W., et al. (2010). Characterization of a novel organelle in Toxoplasma gondii with similar composition and function to the plant vacuole. Mol. Microbiol. *76*, 1358–1375.
196. Dubey, J.P., Cerqueira-Cézar, C.K., Murata, F.H.A., Kwok, O.C.H., Yang, Y.R., and Su, C. (2020). All about toxoplasmosis in cats: the last decade. Vet. Parasitol. *283*, 109145.
197. Kirkman, L.A., Weiss, L.M., and Kim, K. (2001). Cyclic nucleotide signaling in Toxoplasma gondii bradyzoite differentiation. Infect. Immun. *69*, 148–153.
198. Kurokawa, H., Kato, K., Iwanaga, T., Sugi, T., Sudo, A., Kobayashi, K., Gong, H., Takemae, H., Recuenco, F.C., Horimoto, T., and Akashi, H. (2011). Identification of Toxoplasma gondii cAMP dependent protein kinase and its role in the tachyzoite growth. PLoS One *6*, e22492.
199. Schumacher, M.A., Scott, D.M., Mathews, I.I., Ealick, S.E., Roos, D.S., Ullman, B., and Brennan, R.G. (2000). Crystal structures of Toxoplasma gondii adenosine kinase reveal a novel catalytic mechanism and prodrug binding. J. Mol. Biol. *298*, 875–893.
200. Wang, Z., Pan, Q., Gendron, P., Zhu, W., Guo, F., Cen, S., Wainberg, M.A., and Liang, C. (2016). CRISPR/Cas9-derived mutations both inhibit HIV-1 replication and accelerate viral escape. Cell Rep. *15*, 481–489.
201. Sweasy, J.B., Lauper, J.M., and Eckert, K.A. (2006). DNA polymerases and human diseases. Radiat. Res. *166*, 693–714.
202. Aslanidis, C., and de Jong, P.J. (1990). Ligation-independent cloning of PCR

products (LIC-PCR). Nucleic Acids Res. *18*, 6069–6074.
203. Silverman, R.B., Bichler, K.A., and Leon, A.J. (1996). Mechanisms of inactivation of γ-aminobutyric acid aminotransferase by 4-amino-5-fluoro-5-hexenoic acid. J. Am. Chem. Soc. *118*, 1241–1252.
204. Minor, W., Cymborowski, M., Otwinowski, Z., and Chruszcz, M. (2006). HKL-3000: the integration of data reduction and structure solution – from diffraction images to an initial model in minutes. Acta Crystallogr. D Biol. Crystallogr. *62*, 859–866.
205. McCoy, A.J., Grosse-Kunstleve, R.W., Adams, P.D., Winn, M.D., Storoni, L.C., and Read, R.J. (2007). Phaser crystallographic software. J. Appl. Crystallogr. *40*, 658–674.
206. Winn, M.D., Ballard, C.C., Cowtan, K.D., Dodson, E.J., Emsley, P., Evans, P.R., Keegan, R.M., Krissinel, E.B., Leslie, A.G.W., McCoy, A., et al. (2011). Overview of the CCP4 suite and current developments. *Acta Crystallogr.* D Biol. Crystallogr. *67*, 235–242.
207. Morris, R.J., Perrakis, A., and Lamzin, V.S. (2003). Enzymology. In Vol. 374 of Macromolecular Crystallography, Part D, B.-M., ed. (Academic Press), pp. 229–244. http://www.sciencedirect.com/science/article/pii/S0076687903740117).
208. Emsley, P., and Cowtan, K. (2004). Coot: model-building tools for molecular graphics. Acta Crystallogr. D Biol. Crystallogr. *60*, 2126–2132.
209. Emsley, P., Lohkamp, B., Scott, W.G., and Cowtan, K. (2010). Features and development of Coot. Acta Crystallogr. D Biol. Crystallogr. *66*, 486–501.
210. Murshudov, G.N., Skubák, P., Lebedev, A.A., Pannu, N.S., Steiner, R.A., Nicholls, R.A., Winn, M.D., Long, F., and Vagin, A.A. (2011). REFMAC5 for the refinement of macromolecular crystal structures. Acta Crystallogr. D Biol. Crystallogr. *67*, 355–367.
211. Painter, J., and Merritt, E.A. (2006). Optimal description of a protein structure in terms of multiple groups undergoing TLS motion. Acta Crystallogr. D Biol. Crystallogr. *62*, 439–450.
212. Painter, J., and Merritt, E.A. (2006). TLSMD web server for the generation of multi-group TLS models. J. Appl. Crystallogr. *39*, 109–111.
213. Davis, I.W., Leaver-Fay, A., Chen, V.B., Block, J.N., Kapral, G.J., Wang, X., Murray, L.W., Arendall, W.B., Snoeyink, J., Richardson, J.S., and Richardson, D.C. (2007). MolProbity: all-atom contacts and structure validation for proteins and nucleic acids. Nucleic Acids Res. *35*, W375–W383.
214. Chen, V.B., Arendall, W.B., Headd, J.J., Keedy, D.A., Immormino, R.M., Kapral, G.J., Murray, L.W., Richardson, J.S., and Richardson, D.C. (2010). MolProbity: all-atom structure validation for macromolecular crystallography. Acta Crystallogr. D Biol. Crystallogr. *66*, 12–21.
215. Holm, L., and Rosenström, P. (2010). Dali server: conservation mapping in 3D. Nucleic Acids Res. *38*, W545–W549.
216. Laskowski, R.A., Watson, J.D., and Thornton, J.M. (2005). ProFunc: a server for predicting protein function from 3D structure. Nucleic Acids Res. *33*, W89–W93.
217. Madej, T., Lanczycki, C.J., Zhang, D., Thiessen, P.A., Geer, R.C., Marchler-Bauer, A., and Bryant, S.H. (2014). MMDB and VAST+: tracking structural similarities between macromolecular complexes. Nucleic Acids Res. *42*, D297–D303.
218. McNicholas, S., Potterton, E., Wilson, K.S., and Noble, M.E.M. (2011). Presenting your structures: the CCP4mg molecular-graphics software. Acta Crystallogr. D Biol. Crystallogr. *67*, 386–394.
219. Johnson, J.D., Dennull, R.A., Gerena, L., Lopez-Sanchez, M., Roncal, N.E., and Waters, N.C. (2007). Assessment and continued validation of the malaria SYBR Green I-based fluorescence assay for use in malaria drug screening. Antimicrob. Agents Chemother. *51*, 1926–1933.
220. Plouffe, D., Brinker, A., McNamara, C., Henson, K., Kato, N., Kuhen, K., Nagle, A., Adrián, F., Matzen, J.T., Anderson, P., et al. (2008). In silico activity profiling reveals the mechanism of action of antimalarials discovered in a high-throughput screen. Proc. Natl. Acad. Sci. USA *105*, 9059–9064.
221. Rommereim, L.M., Hortua Triana, M.A., Falla, A., Sanders, K.L., Guevara, R.B., Bzik, D.J., and Fox, B.A. (2013). Genetic manipulation in Δku80 strains for functional genomic analysis of Toxoplasma gondii. J. Vis. Exp. e50598.
222. Schindelin, J., Arganda-Carreras, I., Frise, E., Kaynig, V., Longair, M., Pietzsch, T., Preibisch, S., Rueden, C., Saalfeld, S., Schmid, B., et al. (2012). Fiji: an open-source platform for biological-image analysis. Nat. Methods *9*, 676–682.
223. Shen, B., Brown, K.M., Lee, T.D., and Sibley, L.D. (2014). Efficient gene disruption in diverse strains of toxoplasma gondii using CRISPR/CAS9. mBio *5*. e01114-14.
224. Kim, K., Soldati, D., and Boothroyd, J.C. (1993). Gene replacement in Toxoplasma gondii with chloramphenicol acetyltransferase as selectable marker. Science *262*, 911–914.
225. Upadhya, R., Kim, K., Hogue-Angeletti, R., and Weiss, L.M. (2011). Improved techniques for endogenous epitope tagging and gene deletion in Toxoplasma gondii. J. Microbiol. Methods *85*, 1–24.
226. Watts, E., Zhao, Y., Dhara, A., Eller, B., Patwardhan, A., and Sinai, A.P. (2015). Novel approaches reveal that Toxoplasma gondii bradyzoites within tissue cysts are dynamic and replicating entities *in vivo*. mBio *6*. e01155-15.
227. Fritz, H.M., Bowyer, P.W., Bogyo, M., Conrad, P.A., and Boothroyd, J.C. (2012). Proteomic analysis of fractionated *Toxoplasma* oocysts reveals clues to their environmental resistance. PLoS One *7*, e29955.
228. Goodenough, U., and Heitman, J. (2014). Origins of Eukaryotic Sexual Reproduction. Cold Spring Harb. Perspect. Biol. *6*, a016154.
229. Tomasina, R., and Francia, M.E. (2020). The Structural and Molecular Underpinnings of Gametogenesis in Toxoplasma gondii. Front. Cell. Infect. Microbiol. *10*, 608291.
230. Ferguson, D.J.P., Henriquez, F.L., Kirisits, M.J., Muench, S.P., Prigge, S.T., Rice, D.W., Roberts, C.W., and McLeod, R.L. (2005). Maternal inheritance and stage-specific variation of the apicoplast in Toxoplasma gondii during development inthe intermediate and definitive host. Eukaryot. Cell *4*, 814–826.
231. Castillo, J., Bogle, O.A., Jodar, M., Torabi, F., Delgado-Dueñas, D., Estanyol, J.M., Ballescà, J.L., Miller, D., and Oliva, R. (2019). Proteomic changes in human sperm during sequential *in vitro* capacitation and acrosome reaction. Front. Cell Dev. Biol. *7*, 295.
232. Schuermann, J.P., Jiang, J., Cuellar, J., Llorca, O., Wang, L., Gimenez, L.E., Jin, S., Taylor, A.B., Demeler, B., Morano, K.A., et al. (2008). Structure of the Hsp110:Hsc70 nucleotide exchange mashine. Mol. Cell *31*, 232–243.
233. Lorenzi, H., Khan, A., Behnke, M.S., Namasivayam, S., Swapna, L.S., Hadjithomas, M., Karamycheva, S., Pinney, D., Brunk, B.P., Ajioka, J.W., et al. (2016). Local admixture of amplified and diversified secreted pathogenesis determinants shapes mosaic Toxoplasma gondii genomes. Nat. Commun. *7*, 10147.
234. McLeod, R., Lorenzi, H., Pepert, R., and Zhou, Y. (2012). McLeod White Paper 06152012Human and Toxoplasma gondii Genetics and Cellular/Molecular Interactions. JCVI White paper. pp.1-23. https://www.jcvi.org/sites/default/files/assets/projects/gcid/parasite/Human_and_Toxoplasma_gondii_Genetics_and_CellularMolecular_Interactions/Toxoplasma_gondii_06152012.pdf.
235. Galal, L., Ariey, F., Gouilh, M.A., Dardé, M.L., Hamidović, A., Letourneur, F., Prugnolle, F., and Mercier, A. (2022). A uniqueToxoplasma gondii haplotypeaccompanied the global expansion of cats. Nat. Commun. *13*, 5778–5790.
236. Antunes, A.V., Shahinas, M., Swale, C., Farhat, D.C., Ramakrishnan, C., Bruley, C., Cannella, D., Rober, t.M.G., Corrao, C., Couté, Y., et al. (2024). *In vitro* production of cat-restricted *Toxoplasma* pre-sexual stages. Nature *13*, 1–11.

STAR★METHODS

KEY RESOURCES TABLE

REAGENT or RESOURCE	SOURCE	IDENTIFIER
Antibodies		
Anti-SAG1 (D61S)	This paper	N/A
Anti-BAG1	This paper	N/A
Anti-TgO/GABA-AT	This paper	N/A
Anti-GRA1 mAb Tg17.43	https://doi.org/10.1016/0014-4894(90)90014-4	N/A
Anti-AMA1	This paper	N/A
Bacterial and virus strains		
E. coli BL21(DE3)	Sigma-Aldrich	CMC0016
Chemicals, peptides, and recombinant proteins		
Isopropyl ß-D-1-thiogalactopyranoside (IPTG)	Sigma-Aldrich	CAS # 367-93-1
Terrific Broth - Novagen	Sigma-Aldrich	Product# 71754-M
Trizma Base	Sigma-Aldrich	CAS # 77-86-1
Sodium Chloride	Sigma-Aldrich	CAS# 7647-14-5
Ammonium Sulfate	Sigma-Aldrich	CAS# 7783-20-2
Sodium Phosphate	Sigma-Aldrich	CAS# 7601-54-9
Citric Acid	Sigma-Aldrich	CAS# 77-92-9
Glycerol	Sigma-Aldrich	CAS# 56-81-5
Imidazole	Sigma-Aldrich	CAS# 288-32-4
N-Dodecyl β-D-Maltoside (DDM)	Sigma-Aldrich	CAS# 69227-93-6
β-mercaptoethanol (BME)	Sigma-Aldrich	CAS# 60-24-2
Gabaculine	Santa Cruz Animal Health	CAS# 59556-17-1
Pyridoxal Phosphate (PLP)	Sigma-Aldrich	CAS# 853645-22-4
Bis-Tris	Sigma-Aldrich	CAS# 6976-37-0
Polyethylene Glycol 3350	Millipore Sigma	CAS# 25322-68-3
L-Glutathione Oxidized	Sigma-Aldrich	CAS# 27025-41-8
mycophenolic acid	Sigma-Aldrich	Cas: 24280-93-1
xanthine	Sigma-Aldrich	Cas: 69-89-6
GABase (succinic semialdehyde)	Sigma Aldrich	G7509-10UN
Pyrrolidine 5- carboxylate reductase (PYCR1)	Creative Biomart	PYCR1-935H
beta-Nicotinamide adenine dinucleotide reduced disodium salt	Thermo-Fisher	AAJ6163803
Deposited data		
Crystal structure of TgO/GABA-AT with PLP bound to Lys286	This paper	PDB: 4ZLV
Crystal structure of *Tg*O/GABA-AT in unliganded state	This paper	PDB: 5EAV
Crystal structure of gabaculine-inactivated *Tg*O/GABA-AT	This paper	PDB: 5DJ9
Crystal structure of **15**-inactivated *Tg*O/GABA-AT in intermediate state of reaction	This paper	PDB: 5E3K
Crystal structure of **15**-inactivated *Tg*O/GABA-AT in final state of reaction	This paper	PDB: 5E5I

(*Continued on next page*)

Continued

REAGENT or RESOURCE	SOURCE	IDENTIFIER
Experimental models: Cell lines		
HFF cells	ATCC	SCRC-1041
HFF cells	ATCC	CRL-1634
Human erythrocytes	Valley Biomedical	HB1005
Experimental models: Organisms/strains		
BALB/c-Ifng	Jackson Laboratory	C.129S7(B6)-Ifngtm1Ts/J
Swiss Webster	NIH, Bethesda	N/A
Cat	USDA inhouse	N/A
C57BL/6	Jackson Laboratory	000664
CD1	Charles River Laboratory	CD-1® IGS Mouse strain 022
T. gondii RH	https://www.nature.com/articles/ncomms10147#article-info	N/A
T. gondii C56	Dubey P[63]	N/A
T. gondii Me49	https://www.nature.com/articles/ncomms10147#article-info	N/A
T. gondii Pru	https://www.nature.com/articles/ncomms10147#article-info	N/A
T. gondii Pru-Ku80	This paper	N/A
T. gondii EGS	ATCC	PRA-396 ™
T. gondii T-263	Dubey P[63]	N/A
P. falciparum TM91C235	WRAIR, Thailand	N/A
P. falciparum W2	CDC/Indochina III	N/A
Oligonucleotides		
Table S4B	This paper	N/A
Recombinant DNA		
pMCSG28	Novo Pro	V010689
pCas9-CAT	Gift from Dr. Lourido, S and Dr. Weiss, L	N/A
Software and algorithms		
Graphpad Prism	Graph Pad	https://www.graphpad.com/scientific-software/prism/
Other		
Algorhithm for downselection and snp data	This paper Tables 2, 3, and 4 and Figure 8.	N/A
Code	This paper	https://github.com/TriLab-bioinf/McLeod_T263_manuscript

RESOURCE AVAILABILITY

Lead contact

Further information and requests for resources and reagents should be directed to and will be fulfilled by the lead contact, Dr. Rima McLeod (rmcleod@uchicago.edu).

Materials availability

A putative OAT from *T. gondii ME49* clone or protein are available to order free of charge for scientific community from the Center for Structural Genomics of Infectious Disease at Northwestern University (Chicago, IL) repository (https://csgid.org/). Inhibitors and inactivators of *Tg*O/GABA-AT were generated in Dr. Richard B. Silverman laboratory and could be obtained upon request (r-silverman@northwestern.edu).

Data and code availability

Sequences of proteins from *T. gondii ME49* used this study are available at ToxoDBdatabase (https://toxodb.org/toxo/app). Code for down selection of genes with mutations is at: https://github.com/TriLab-bioinf/McLeod_T263_manuscript. Original blots are at https://data.mendeley.com. All determined crystal structures with original codes (listed in method details) are deposited into the Protein DataBank (https://www.rcsb.org/). All data reported in this paper will be shared by the lead contact upon request. Generated structure models by AlphaFold2 reported in this paper will be shared by the lead contact upon request.

EXPERIMENTAL MODEL AND STUDY PARTICIPANT DETAILS

List of all experimental models used in this study:

Animals

(species/strain, genotype, age/developmental stage, sex (and gender if reported for human studies), maintenance, and care, including institutional permission and oversight information for the studies the experimental animal/human study):

Dartmouth

Cyst burden and virulence assays were performed in 7–8 week old female C57BL/6 mice housed under standard conditions and fed standard mouse food using protocols approved by the Laboratory Animal Use and Care Committee. IACUC protocol approval number is 00002108.Dartmouth's AAALAC accreditation number is 398 and Animal Welfare Assurance number is D16-0016 (A3259-01).

Einstein

In the Weiss laboratory, CD1 female mice were used and were from Charles River Laboratory age 5 to 6 weeks Catalog number CD-1 IGS Mouse strain 022. IACUC from 2015 to 2018 was 20150908. For experiments in the time frame of 2012–2015 it was #20121104.

USDA

For these and other studies herein, overall, four cats, 88–103 days old, 2 males, 2 females from the USDA in-house-colony were utilized; Cats were fed pelleted Purina cat chow.

At the USDA, overall description of mouse source and care is as follows: The KO mice were 8–12 week-old females, BALB/c-Ifnγ from Jackson Laboratory, Bar Harbor, Maine. The outbred Swiss Webster mice were 10–12 weeks old females from NIH, Bethesda, MD. Mice were fed pelleted mouse chow. BAACUC Protocol No.: # 12–016 is the protocol number for animal use.

Italy

BALB/c female mice were housed in standard conditions and fed standard laboratory mouse food. The animal work has been authorized by the Italian Ministry of Health, according to Legislative Decree 116/92, which implemented the European Directive 86/609/EEC on laboratory animal protection. Animals used in this study were housed at the Istituto Superiore di Sanità and treated according to Legislative Decree 116/92 guidelines.

Human cell lines

In the Weiss laboratory for these and other studies herein, HFF human foreskin fibroblasts were from ATCC laboratory Cat SCRC-1041 and also have been HFF ATCC CRL-1634.

Primary cell cultures

Human erythrocytes for malaria inhibition assay were from Valley Biomedical (HB1005).

Microbe strains species/strain

At Walter Reed Army Instiute (WRAIR) D6 (CDC/Sierra Leone), TM91C235 (WRAIR, Thailand), and W2 (CDC/Indochina III) laboratory strains of *P. falciparum* were utilized.

At Dartmouth, KU80 knockout background,[191] the Type II *Tg*O/GABA-AT gene locus (TGME49_269110) was deleted in the PruΔ *ku80*Δ*hxgprt* (this paper).

T. gondii Pru (https://www.nature.com/articles/ncomms10147#article-info)

EGS strain *T. gondii* is ATCC PRA-396 .

RH strain *T. gondii* (https://www.nature.com/articles/ncomms10147#article-info).

Me49 strain *T. gondii* (https://www.nature.com/articles/ncomms10147#article-info)

C56 strain *T. gondii* (Dubey JP[63]).

T-263 strain *T. gondi* (Dubey JP[6]).

Details of use of each of these models in each of the specific studies are presented under the corresponding section.

METHOD DETAILS

Multi-sequence alignment of ornithine aminotransferase

In the first instance, a small amino acid sequence alignment was performed with Clustal Omega on close homologues (*Hammondia hammondi*, *Neospora caninum* & *P. falciparum*), and the more distant, but important in the context of this work, *Felis catus*, and *Homo sapiens* OAT structures (accession numbers *T. gondii* (XP_002365604.1), *H. hammondi* (XP_008882303.1), *N. caninum* (XP_003883978.1), *P. falciparum* (CAG25330.1), *F. catus* (XP_003994548.1), and *H. sapiens* (AAA59957.1)). Then, a second, more extensive sequence alignment was performed in Consurf with 499 sequences identified.

SNP analysis and phylogeny Construction

Nucleic acid sequences for *Toxoplasma gondii* ornithine aminotransferase were extracted from the ToxoDBwebsite (http://toxodb.org/) for all available isolates. Sequences were formatted and exported as a FASTA file for analysis. Using PHYLIP (PHYLogeny Inference Package, v3.696) programs included in the Seaview phylogeny interface (http://doua.prabi.fr/software/seaview), 1000 pseudoreplicate datasets were created and an unrooted bootstrap consensus tree was constructed by parsimony analysis.

Cloning, expression, and purification

Gene (GI: 237832613) of a putative OAT from *T. gondii* ME49 (*Tg*O/GABA-AT truncated construct (residues 17–441); *Tg*O/GABA-AT(17–441)) was PCR-amplified and cloned into the IPTG (isopropyl β-D-1-thiogalactopyranoside)-inducible pMCSG28 vector by the ligation-independent-cloning.[202] The pMCSG28 vector possesses the C-terminal 6×His affinity tag and Tobacco Etch Virus (TEV) protease cleavage site. *Escherichia coli* (E. coli) BL21(DE3)/pMagic cells harboring the *Tg*O/GABA-AT-pMCSG28 plasmid were grown in the Terrific Broth (TB) medium to OD600 = 0.6 at 37°C followed by 1 mM IPTG induction at 25°C overnight. Incubated cells were collected by centrifugation (6,000 rpm, 4°C, 10 min) and lysed by sonication in 10 mM Tris-HCl pH 8.3 buffer containing 250 mM NaCl, 100 mM (NH4)2SO4, 43.6 mM Na3PO4, 3.25 mM citric acid, 10% glycerol, 5 mM imidazole and 0.08% n-dodecyl β-D-maltoside (DDM), and 5 mM β-mercaptoethanol (BME) on ice. The soluble fraction and cell debris were separated by centrifugation at 19,000 rpm, 4°C for 40 min. The supernatant was applied onto a 5-mLNi-NTA column (GE Healthcare, Piscataway, NJ), and impurities were washed out using 10 mM Tris-HCl buffer at pH 8.3, with 500 mM NaCl, 5 mM BME, and 25 mM imidazole. *Tg*O/GABA-AT was eluted with 500 mM imidazole in 10 mM Tris-HCl pH 8.3 buffer containing 500 mM NaCl and 5 mM BME and further purified by size exclusion chromatography on a HiLoad 26/60 Superdex 200 column (GE Healthcare, Piscataway, NJ). All purification steps were carried out on the ÄKTAxpress (GE Healthcare Life Sciences, Piscataway, NJ) high-throughput purification system at 4°C. Final purity of the protein was assayed by SDS-PAGE.

Enzyme activity assays

GABA, *L*-ornithine, PLP, α-ketoglutarate, NADH, and $NADP^+$ were purchased from Sigma–Aldrich or Alfa Aesar. Human recombinant pyrroline 5-carboxylate reductase 1 (PYCR1) was purchased from Creative Biomart. Succinic semialdehyde dehydrogenase (SSDH) was purified from GABase, a commercially available mixture of SSDH and GABA-AT, using a known procedure.[203] Ultraviolet (UV) absorption was measured using a Synergy H1 hybrid multimode microplate reader (BioTek, USA) with transparent 96-well plates or 384-well plates (Greiner Bio-One, USA). Compounds **1**-**15** were previously synthesized, characterized, and tested against human ornithine aminotransferase and used without further manipulation in the TgO/GABA-AT assay procedure.[33]

Variation of enzyme concentration of *Tg*O/GABA-AT

For GABA assays, microplate wells were loaded with 60 μL of an assay mixture containing 100 mM potassium pyrophosphate buffer at pH 8.0, 11.1 mM α-ketoglutarate, 1.11 mM GABA, 1.11 mM $NADP^+$, and 1 μL of SSDH. For *L*-ornithine assays, microplate wells were loaded with 60 μL of an assay mixture containing 100 mM potassium pyrophosphate at pH 8.0, 11.1 mM α-ketoglutarate, 1.11 mM NADH, 0.028 mM PLP, 11.1 mM L-ornithine, and 2.5 ng of PYCR1. 30 μL of potassium pyrophosphate buffer was added to each well. After incubating the mixture at 37°C for 10 min, 10 μL of various concentrations of *Tg*O/GABA-AT in 100 mM potassium pyrophosphate at pH 8.0 was added. The plate was shaken at 37°C for 1 min, and absorbance was measured at 340 nm every 10 s for 90 min. All assays were performed in duplicate. Absorbance was plotted as a function of time in GraphPad Prism as shown in Figures S3A and S3D.

Determination of the K_m of ornithine against *Tg*O/GABA-AT

For GABA assays, microplate wells were loaded with 60 μL of an assay mixture containing 100 mM potassium pyrophosphate buffer at pH 8.0, 11.1 mM α-ketoglutarate, 1.11 mM $NADP^+$, 1 μL of SSDH, and varying concentrations of GABA. For *L*-ornithine assays, microplate wells were loaded with 60 μL of an assay mixture containing 100 mM potassium pyrophosphate at pH 8.0, 11.1 mM α-ketoglutarate, 1.11 mM NADH, 0.028 mM PLP, 2.5 ng of PYCR1, and varying concentrations of ornithine. 30 μL of potassium pyrophosphate buffer was added to each well. After incubating the mixture at 37°C for 10 min, 10 μL of *Tg*O/GABA-AT (0.15 mg/mL for GABA assay and 1.0 mg/mL for ornithine assays in 100 mM potassium pyrophosphate buffer at pH 8.0) was added. The plate was shaken at 37°C for 1 min, and the absorbance was measured at 340 nm every 10 s for 90 min. All assays were performed in duplicate. Relative velocity was determined from the slope of the linear portion (t = 750–1500 s for GABA and 2000–4000 s for ornithine) a plot of absorbance versus time. The K_m was then obtained by plotting GABA or

ornithine concentration versus relative velocity (Figures S3C and S3F) and fitting to the Michaelis-Menton Equation in GraphPad Prism where $v = (V_{max}\,[S])/(K_M + [S])$ where v is relative velocity and [S] is the concentration of GABA or ornithine.

Measurement of kinetic constants of inhibitors and inactivators of *Tg*O/GABA-AT

Curve fitting method – GABA: Microplate wells were loaded with 80 μL of an assay mixture containing 100 mM potassium pyrophosphate at pH 8.0, 11.1 mM α-ketoglutarate, 11.1 mM GABA, 1.11 mM $NADP^+$, and 1 μL of SSDH. Varying concentrations of inhibitors were added to each well, and the plate was preheated at 37°C for 10 min. 10 μL of *Tg*O/GABA-AT (0.15 mg/mL in 100 mM potassium pyrophosphate buffer at pH 8.0) was added via a multichannel pipette. The plate was shaken for 5 s at 37°C, and the absorbance was measured at 340 nm every 10 s for 30 min. All assays were performed in duplicate.

Curve fitting method – ornithine: For *L*-ornithine assays, microplate wells were loaded with 60 μL of an assay mixture containing 100 mM potassium pyrophosphate buffer at pH 8.0, GABA, 11.1 mM α-ketoglutarate, 1.11 mM NADH, 0.028 mM PLP, 11.1 mM L-ornithine, and 2.5 ng of PYCR1. Varying concentrations of inhibitors were added to each well, and the plate was preheated at 37°C for 10 min. 10 μL of *Tg*O/GABA-AT (1.0 mg/mL in 100 mM potassium pyrophosphate buffer at pH 8.0) was added via a multichannel pipette. The plate was shaken for 30 s at 37°C, and the absorbance was measured at 340 nm every 10 s for 90 min. All assays were performed in duplicate.

Curve fitting method – calculations: Absorbance data were fitted according to a previous procedure.[50] Absorbance data were fitted to Equation 1, where v_i is the initial velocity, v_s is the steady state velocity, t is time, and a_0 is the initial absorbance. K_{obs} is then fitted to Equation 2 where [*I*] is the inactivator concentration and S is substrate (ornithine) concentration.

$$\text{Absorbance} = \frac{v_i - v_s}{k_{obs}}\left[1 - \exp(-k_{obs}t)\right] + v_s t + a_0 \qquad \text{(Equation 1)}$$

$$k_{obs} = \frac{k_{inact}[I]}{k_I\left(1+\frac{S}{K_m}\right)+[I]} \qquad \text{(Equation 2)}$$

Time-dependent assay method – GABA: Microplate wells were loaded with 5 μL of varying inhibitor concentrations and 11.1 mM α-ketoglutarate in 100 mM potassium pyrophosphate buffer at pH 8. At time points of 0, 10, 20, and 25 min, 5 μL of *Tg*O/GABA-AT (0.15 mg/mL) was added to each inhibitor concentration. After 30 min, 40 μL of an assay solution (preheated at 37°C for 10 min) containing 11.1 mM α-ketoglutarate, 11.1 mM GABA, 1.11 mM $NADP^+$, and 1 μL of SSDH was added. The plate was shaken at 37°C for 60 s, and the absorbance was read at 340 nm for 30 min.

Time-dependent assay method – ornithine: Microplate wells were loaded with 5 μL of varying inhibitor concentrations and 11.1 mM α-ketoglutarate in 100 mM potassium pyrophosphate buffer at pH 8. At time points of 0, 10, 20, and 25 min, 5 μL of *Tg*O/GABA-AT (1.0 mg/mL) was added to each inhibitor concentration. After 30 min, 40 μL of an assay solution (preheated at 37°C for 10 min) containing 11.1 mM α-ketoglutarate, 11.1 mM ornithine, 1.11 mM NADH, 0.028 mM PLP, and 0.5 μL of PYCR1 was added. The plate was shaken at 37°C for 60 s, and the absorbance was read at 340 nm for 60 min.

Time-dependent assay method – calculations: GABA and ornithine data were fitted according to a literature procedure.[33] Briefly, initial velocities are calculated from the slope of a plot of absorbance versus time at each concentration and for each preincubation time. Initial velocity for each concentration and preincubation time is then converted into percent inhibition by considering the positive (No inhibitor) and negative (no inhibitor, no enzyme) controls. Log (Percent inhibition) is then plotted versus preincubation time for each concentration of inhibitor tested. The slope of this plot yields k_{obs}. k_{inact} and K_I are obtained from a plot of k_{obs} and the concentration of each inhibitor and fitted in GraphPad Prism to the equation $k_{obs} = (k_{inact} \times [I])/(K_I + [I])$ where [I] is the inhibitor concentration.

Co-crystallization experiments

The *Tg*O/GABA-AT protein at a concentration of 7 mg/mL was crystallized in the presence of gabaculine and *Tg*O/GABA-AT-specific inactivators (compounds **1**, **2**, **3**, and **15**) by the sitting-drop vapor-diffusion technique at 295 K. The crystal of *Tg*O/GABA-AT with PLP covalently bound to Lys286 was obtained from co-crystallization of *Tg*O/GABA-AT with 2 mM PLP followed by overnight (14–15 h) incubation. The crystal of *Tg*O/GABA-AT in complex with gabaculine was obtained by co-crystallization with 5 mM gabaculine and 2 mM PLP. The above crystals were grown under similar conditions containing 200 mM $(NH_4)_2SO_4$, 100 mM Bis-Tris pH 5.5 and 25% (w/v) PEG3350. The crystals of *Tg*O/GABA-AT in complex with compound **15** in an intermediate state and final inactivated state were obtained by co-crystallization with 5 mM compound **15** and 2 mM PLP under conditions containing 0.2 M $(NH_4)_2SO_4$, 0.1 M Bis-Tris pH 6.5, and 25% (w/v) PEG3350 followed by an incubation period at 4°C for 4 h and overnight (14–15 h), respectively. To oxidize protein and attempt to promote disulfide bond formation, we dialyzed *Tg*O/GABA-AT enzyme in a buffer containing 10 mM Tris-HCl pH 8.3, 500 mM NaCl, 2 mM PLP and 0.5 mM oxidized glutathione. Therefore, the crystal of *Tg*O/GABA-AT in an unliganded state was obtained under conditions containing 0.2 M $(NH_4)_2SO_4$, 0.1 M Bis-Tris pH 5.5, and 25% (w/v) PEG3350. Prior to data collection, all crystals were soaked in well solution for cryoprotection and then flash frozen in liquid nitrogen.

X-Ray data collection and structure determination

Monochromatic X-ray diffraction oscillation data from all crystals were collected at the Life Sciences Collaborative Access Team (LS-CAT) beamlines at Argonne National Laboratory (ANL), Advanced Photon Source (APS). Data were processed with *HKL*-3000.[204] The structures were determined by the molecular replacement method using *Phaser*[205] from the *CCP4* suite.[206] The crystal structure of the related *P. falciparum* OAT (Protein DataBank (PDB) code 3lg0[46]) was used as a search model for the *Tg*O/GABA-AT structure with PLP in the unbound state that was later used to solve the structures of *Tg*O/GABA-AT with PLP in a bound state, gabaculine-inactivated, and **15**-inactivated *Tg*O/GABA-AT states. The initial structure solution for all determined structures was rebuilt using *ARP/wARP*.[207] Water molecules, manual structure inspection, and alteration of the rebuilt structural models were done in *Coot*[208,209] and *REFMAC*,[210] respectively. The Translation-Libration-Screw (TLS) refinement (TLS groups were identified on TLSMD server http://skuld.bmsc.washington.edu/~tlsmd/[211,212] was introduced at the final stages of refinement. The final model of structures was validated with the *MolProbity*[213,214] http://molprobity.biochem.duke.edu/). The structures were deposited in the PDB under the accession code 4zlv (*Tg*O/GABA-AT with PLP bound to Lys286), 5eav (*Tg*O/GABA-AT in unliganded state), 5dj9 (gabaculine-inactivated *Tg*O/GABA-AT), 5e3k (**15**-inactivated *Tg*O/GABA-AT in intermediate state of reaction), 5e5i (**15**-inactivated *Tg*O/GABA-AT in final state of reaction), Table S2 contains detailed crystallographic data of deposited structures. The structural comparison between *Tg*O/GABA-AT and its homologues was done using web servers DALI, VAST, and ProFunc.[213,214] All figures presenting *Tg*O/GABA-AT structures were prepared in graphical program CCP4mg.[218]

Measuring effect of *Tg*O/GABA-AT inactivators on *T. gondii in vitro*

Human foreskin fibroblasts (HFFs) were grown to confluence in black, flat-bottomed 96-well microplates. HFFs were infected with 2000 Type I RH parasites expressing yellow fluorescent protein (YFP). The parasites were incubated with the cells for 1 h to allow sufficient time for invasion of HFFs and were then treated with several of the *Tg*O/GABA-AT-specific GABA analogues, including compounds **1**, **2**, **3** and **15**. Control triplicates with only fibroblasts and with pyrimethamine and sulfadiazine (the current standard of treatment of *T. gondii* infection) were also conducted. The cells and parasites were then incubated at 37°C for 72 h. Fluorescence was measured using a Bio-Tek Synergy H4 Hybrid Multi-Mode Microplate Reader.

Measuring effect of *Tg*O/GABA-AT inactivators on *P. falciparum in vitro*

The Malaria SYBR Green I - Based Fluorescence (MSF) Assay is a microtiter plate drug sensitivity assay that uses the presence of malarial DNA as a measure of parasitic proliferation in the presence of antimalarial drugs or experimental compounds. As the intercalation of SYBR Green I dye and its resulting fluorescence is relative to parasite growth, a test compound that inhibits the growth of the parasite will result in a lower fluorescence. D6 (CDC/Sierra Leone), TM91C235 (WRAIR, Thailand), and W2 (CDC/Indochina III) laboratory strains of *P. falciparum* were used for each drug sensitivity assessment. The parasite strains were maintained continuously in long-term cultures as previously described.[208] Predosed microtiter drug plates for use in the MSF assay were produced using sterile 384-well black optical bottom tissue culture plates containing quadruplicate 12 2-fold serial dilutions of each test compound or mefloquine hydrochloride (Sigma-Aldrich Co., Catalog #M2319) suspended in dimethyl sulfoxide. The final concentration range tested was 0.5–10000 ng/mL for all assays. Pre-dosed plates were stored at 4°C until used, not to exceed five days. No difference was seen in drug sensitivity determinations between stored or fresh drug assay plates (data not shown). A batch control plate using chloroquine (Sigma-Aldrich Co., Catalog #C6628) at a final concentration of 2000 ng/mL was used to validate each assay run. The Tecan Freedom Evo liquid handling system (Tecan US, Inc., Durham, NC) was used to produce all drug assay plates. Based on modifications of previously described methods by Plouffe et al. and Johnson et al., *P. falciparum* strains in late-ring or early-trophozoite stages were cultured in the pre-dosed 384-well microtiter drug assay plates in 38 μL culture volume per well at a starting parasitemia of 0.3% and a hematocrit of 2%.[219,220] The cultures were then incubated at 37°C within a humidified atmosphere of 5% CO_2, 5% O_2 and 90% N_2, for 72 h. Lysis buffer (38 μL per well), consisting of 20 mM Tris HCl, 5 mM EDTA, 1.6% Triton X-, 0.016% saponin, and SYBR green I dye at a 20x concentration (Invitrogen, Catalog #S-7567) was then added to the assay plates for a final SYBR Green concentration of 10x. The Tecan Freedom Evo liquid handling system was used to dispense malaria cell culture and lysis buffer. The plates were then incubated in the dark at room temperature for 24 h and examined for the relative fluorescence units (RFU) per well using the Tecan Genios Plus (Tecan US, Inc., Durham, NC). Each drug concentration was transformed into Log[X] and plotted against the RFU values. The 50% and 90% inhibitory concentrations (IC_{50}s and IC_{90}s, respectively) were then generated with GraphPad Prism (GraphPad Software Inc., San Diego, CA) using the nonlinear regression (sigmoidal dose-response/variable slope) equation.

In vitro and *In vivo* phenotypes of type II parasites deleted for *Tg*O/GABA-AT

Using efficient gene targeting in the KU80 knockout background, the Type II *Tg*O/GABA-AT gene locus (TGME49_269110) was deleted in the PruΔ*ku80*Δ*hxgprt* strain using previously described methods.[51] The *Tg*O/GABA-AT knockout plasmid was assembled using recombinational cloning from PCR products using the oligonucleotide primers shown in Table S4A and the targeting plasmid was verified by DNA sequencing. Following transfection of linearized *Tg*O/GABA-AT targeting plasmid, Type II *Tg*O/GABA-AT knockouts were selected in 50 μg/mL mycophenolic acid and 50 μg/mL xanthine and parasites cloned by limiting dilution three weeks after transfection. *Tg*O/GABA-AT (Δ*oat*) knockouts were validated using previously described genotype analysis in PCR assays to measure in PCR 1 the targeted deletion of the *Tg*O/GABA-AT coding region (DF and DR primers), in PCR 2 the targeted 5′ integration (CXF & 5′DHFRCXR primers), and in PCR 3 the targeted 3′ integration (3′DHFRCXF and CXR primers) of HXGPRT to replace the deleted *Tg*O/GABA-AT gene (validation primers shown in Table S3B).[51,221] The

replication rate of Type II Δ*oat* tachyzoites in primary vacuoles (parasites/vacuole) was measured using previously described methods, and the size of 12 day Δ*oat* plaques was measured in comparison to the size of 12 day PruΔ*ku80* plaques by scoring the area of 40 randomly chosen plaques (in triplicate assays) using arbitrary pixel units determined with FIJI software.[222] Cyst burden and virulence assays were performed in 7–8 week old C57BL/6 mice using protocols approved by the Laboratory Animal Use and Care Committee (Dartmouth College 00002108) using previously established methods.[51,52] Brain cyst burdens of mice infected with parental PruΔ*ku80* or Δ*oat* parasites were scored by counting GFP^+ cysts at a total magnification of 150X, and scoring the number of cysts in 20% of each brain.[51]

Levels of *Tg*O/GABA-AT expression as a function of life cycle stage

ToxoDb was used to assess transcription levels of *Tg*O/GABA-AT expression in different life cycle stages.

Initial *Tg*O/GABA-AT antibody production using recombinant protein also studied in enzyme assays and with crystallography (called "antibody 1")

Mice were injected with 50 μg of recombinant *Tg*O/GABA-AT, subcutaneously. The protein was formulated with an NISV (nonionic surfactant vesicle) preparation to act as an adjuvant. The vesicles were made by melting mono-palmitoyl glycerol, cholesterol, and dicetyl-phosphate (All from Sigma, UK) in a molar ratio of 5:4:1. Vesicles formed following the addition of 37°C PBS pH 7.4 and vigorously vortexed for 2 min. Vesicle preparations were lyophilized and subsequently rehydrated with the appropriate protein dilutions. These preparations were stored at −20°C until use and heated to 37°C just prior to injection. Mice were given 2 injections of the preparations, 2 weeks apart. Ten days after the final injection, the mice were euthanized by CO_2 inhalation, and blood was obtained by cardiac puncture. Blood samples were centrifuged at 13,000 rpm for 10 min at 4°C. Serum was collected and stored at −20°C prior to testing.

Additional protein and antibody production; characterization with immunofluorescence assays for *Tg*O/GABA-AT (called "antibody 2")

Parasites

Toxoplasma gondii oocysts of the ME49 strain (genotype II) were recovered from the feces of experimentally infected cats housed at the United States Department of Agriculture Laboratory, Beltsville, Maryland, USA and purified by sucrose flotation, as previously described.[54]

Production of anti-OAT antibodies and Western blot analysis

To raise anti-*Tg*O/GABA-AT mouse antisera, BALB/c female mice were immunized at 3–4 weeks intervals by intraperitoneal injection with 50 μg of purified recombinant protein in complete (first immunization) or incomplete (first boost) Freund's adjuvant. Individual sera were collected 2 weeks after the second boost (soluble antigen in PBS). The animal work has been authorized by the Italian Ministry of Health, according to Legislative Decree 116/92, which implemented the European Directive 86/609/EEC on laboratory animal protection. Animals used in this study were housed at the Istituto Superiore di Sanità and treated according to Legislative Decree 116/92 guidelines.

Total protein extracts from ME49 bradyzoites (kindly provided by Manlio Di Cristina, University of Perugia, Italy), tachyzoites and sporozoites were quantified with a Qubit fluorometer (Invitrogen) and equal amounts of the three samples were resolved by SDS–PAGE on a 12% NuPage Novex Bis-Tris gel (Invitrogen). Following transfer to nitrocellulose, the blots were blocked with 5% w/v skimmed milk in 1X Tris Borate Saline Tween (TBST; 50 mM Tris pH 8.0, 150 mM NaCl, 1% Tween 20) and probed for 1 h with a mouse anti-OAT antiserum (1:1000) or with a rabbit anti-GRA1 control serum. Anti-GRA1 mAb Tg17.43; dilution employed 1:2000 Ref. https://doi.org/10.1016/0014-4894(90)90014-4. After 30 min incubation with the appropriate anti-IgG secondary antibody conjugated to horseradish peroxidase (BioRad), reactive protein bands were revealed by chemiluminescence with LiteAblot Plus (EuroClone, Italy). Originals of blots are at https://data.mendeley.com.

Immunofluorescence

Freshly excysted ME49 sporozoites were air dried on multispot glass slides and fixed for 5 min in cold 95% ethanol/5% acetic acid. samples were blocked with 2% fetal bovine serum in PBS and double stained for 1 h with anti-TgOAT mouse antibodies (1:100) and a rabbit anti-AMA1 serum (1:1000). Anti-GRA1 serum (1:200,000) was also used. Following 30 min incubation with anti-mouse and anti-rabbit IgG secondary antibodies conjugated to Alexa Fluor 488 and Alexa Fluor 594, respectively, samples were mounted in SlowFade Antifade reagent (Invitrogen) and observed under a Zeiss Axioplan 2 epifluorescence microscope using a 100× oil immersion objective. Images were collected with an Axiocam digital camera using the Zeiss Axiovision 4.8 software.

For MitoTracker and anti *Tg*O/GABA-AT co-localization, and deconvolution, ME49 oocysts were excysted in 1.5% sodium taurocholate in Hank's balanced salt solution (HBSS) supplemented with 500 nM MitoTracker™ Red CMXRos (Thermo Fisher Scientific). Freshly excysted sporozoites were washed twice in HBSS and seeded in 8-well Nunc Lab-Tek glass chamber slides (Thermo Fisher Scientific) previously coated with Cell-Tak (Corning). Tachyzoites were processed the same way. Following centrifugation at 700 rpm for 2 min, immobilized parasites were fixed with 4% paraformaldehyde, permeabilized with 0.5% Triton X-100 in PBS, and blocked with 2% fetal bovine serum in PBS for 1 h. Samples were then stained for 1 h with anti-*Tg*O/GABA-AT mouse antibodies (1:50) followed by 30 min incubation with anti-mouse IgG secondary antibodies conjugated to Alexa Fluor 488 and DAPI. Samples were mounted in SlowFade Antifade reagent (Thermo Fisher Scientific) and epifluorescence images were taken using the EVOS™ FL Imaging System (Thermo Fisher Scientific) using a 100X oil immersion objective.

Confocal images with an optical thickness of 0.12 microns were taken by a Zeiss LSM 980 microscope using a planapo objective 60x oil A.N. 1,42.

Knockout of *Tg*O/GABA-AT in EGS-strain *T. gondii* followed by peroral infection of cat and evaluation of subsequent oocyst shedding

Insertion of the drug selection marker in the *Tg*O/GABA-AT coding sequence was performed. First, CRISPR/Cas9 mediated targeting construct pCAS9-GFP::sgRNA-*Tg*O/GABA-AT was made by replacing the sgRNA-UPRT to sgRNA-*Tg*O/GABA-AT. Primers sgRNA-R 5′-AACTTGACATCCCCATTTAC-3′ and 172F 5′-AAGGTAAAGGTGCTCGCGTTGTTTTAGAGCTAGAAATAGC-3′ or 183F 5′-GCTCGCGTTTGGGATATCAAGTTTTAGAGCTAGAAATAGC-3′ (underlined sequence are gRNA target sequence) was used to replace the 20 bp target sequence from pCAS9-GFP::sgRNA-UPRT (*114*) to pCAS9-GFP::sgRNA-172 and 183, respectively. Chloramphenicol acetyl-transferase (CAT) flanked by the tubulin promoter and SAG1 terminator (CAT cassette)[224] was used as a drug selectable marker. CAT cassette was PCR amplified from the pTUB/CAT[224] (kindly provided by Dr. K. Kim) with primers M13_20 forward 5′-GTAAAACGACGGCCAGT-3′and M13_reverese 5′-GGAAACAGCTATGACCATG-3′ and used for the transfection. For the control exogenous DNA, sfGFP sequences flanked with promoter of sporoSAG1 or sporoMUC1 and gra2 3′UTR were amplified from pDHFR-sporoSAG1-sfGFP or pDHFR-sporoMUC1-sfGFP with primers sporoSAG_F or sporoMUC_F and M13_Reverse. PCR products were cut with DpnI to remove the residual plasmid template and used for transfection. 1 μg CAT cassette (1.7 kbp) was mixed with either of 12 μg sporoSAG1-sfGFP cassette (3 kbp), 12 μg sporoMUC1-sfGFP cassette (3kbp), 20 μg pCAS9- GFP::sgRNA178 (9.7 kbp) or 20 μg pCAS9-GFP::sgRNA183 (9.7 kbp) and transfected into EGS strain 10^6 freshly purified tachyzoites in 100 μL cytomix using T16 nucleofection as described elsewhere.[225] Transfected parasites were inoculated to HFF cells and 25 uM chloramphenicol selection was started immediately after transfection. Parasites were subcloned and target loci were verified with primers *Tg*O/GABA-AT_996F CTGTGCGACTGATTCAGGGT and CAT_CDS_R GCCATCACAAACGGCATGATG. From the pCAS9-GFP::sgRNA183 transfectants, we used the insertional knock-out line EGS/183-KO to infect mice to produce brain cyst. CD1 mice were injected intraperitoneally with 100 tachyzoites and treated with 400 mg/L sodium sulfadiazine in the drinking water beginning 4 days after injection. When mice had symptoms of acute toxoplasmosis, 0.8 mg sodium sulfadiazine / mouse was injected daily subcutaneously. Similar methods have been utilized previously to use CRISPR/Cas9 for investigations in *Toxoplasma*.[223] Four weeks after injection, infected brains were collected and brain cysts were purified as described.[226]

T. gondii infected mouse brains from 10 mice infected with (EGS-*Tg*O/GABA-AT KO—cat 04) and EGS-spGFP (cat 05) were homogenized by syringe and fed to two female, 141 and 144-day old, coccidia-free cats from the USDA's cat colony by placing them at the back of the tongue. All feces for each cat were collected daily after feeding infected mouse brains, and examined for *T. gondii* oocysts. Screening and harvesting of *T. gondii* oocysts were done between 3 to 21 days after infection by following procedures as described previously.[59,60] Cats were euthanized on day 21 post infection and blood was collected to do modified agglutination tests (MAT) to test for immunological reactivity to *T. gondii* antigens. Oocysts were collected by floatation methods using sucrose solution with a specific gravity of 1.15 or higher. Concentrated oocyst pellets were suspended in an aqueous solution containing 2% H_2SO_4, and aerated on the shaker for 7 days at room temperature (20°C–22°C) to allow for oocyst sporulation. For these and other studies herein, overall, four cats, 88–103 days old, 2 males, 2 females from the USDA in-house-colony were utilized; Cats were fed pelleted Purina cat chow.

To confirm durability and persistence of CRISPR mutation, 5 mL of oocyst suspension was neutralized with equal vol. of 3.3% NaOH and centrifuged at 2000 rpm 10 min. Sediments were resuspended into 1 mL with 0.9% NaCl with 1% penicillin and streptomycin. 200 μL suspension/mouse was injected into 6 BALB/c mice subcutaneously. Mice were observed daily until they showed symptoms of ruff coat and peritoneal inflammation; then they were euthanized. Lungs from the euthanized mice were homogenized and incubated with HFF host cells to recover tachyzoites. Genomic DNA from the tissue culture parasites was used for genotyping of the parasite progeny pool.

At the USDA in the Dubey laboratory, in this study and overall description of mouse source and care is as follows: The KO mice were 8–12 week-old females, BALB/c-Ifnγ from Jackson Laboratory, Bar Harbor, Maine The outbred Swiss Webster mice were 10–12 weeks old females from NIH, Bethesda, MD. Mice were fed pelleted mouse chow. In the Weiss laboratory, CD1 Mice were used and were from Charles River Laboratory age 5 to 6 weeks Catalog number CD-1® IGS Mouse strain 022.

In the Weiss laboratory for these and other studies herein, HFF human foreskin fibroblasts were from ATCC laboratory Cat SCRC-1041 and also have been HFF ATCC CRL-1634; EGS strain *T. gondii* is ATCC PRA-396 ™.

Culture and sequencing of Frenkel Live Vaccine TS-Against*T. gondii*

T-263 was thawed and grown in HFF. DNA was isolated as previously described.[224]

Genome sequencing of *T. gondii*T-263 and CTG strains

For each strain a single Illumina paired-end barcoded library was prepared from tachyzoite gDNA with Illumina TrueSeq library preparation kit. The libraries were then sequenced using 150 bp paired-end reads with an Illumina NextSeq machine to generate ~50 millon paired-end sequencing reads per genome.

Single nucleotide polymorphism (SNP) identification and annotation

Illumina genome sequencing reads from T-263 parasites and from its parental wild-type strain, CTG, were aligned to the *T. gondii* ME49 reference genome assembly (ABPA02000000, ToxoDBS31 release 13.0) with Bowtie2 and realigned around gaps using the GATK toolkit. SNP calls were done simultaneously on both strains with samtools utility mpileup, requiring a minimum SNP coverage of 5 reads and an alternative allele frequency of 0.8 or higher, given the haploid nature of these genomes. Thereafter, SnpEff and a gff3 file containing the annotation of *T. gondii* ME49 downloaded from ToxoDBv13.0 were used to classify the different types of mutations identified in each strain. Allelic variants that were different between T-263 and both CTG and ME49 were considered T-263-specific.

Analysis of putative cyclic-AMP dependent protein kinase

A change in pH and ionicity activates male gamete Cyclic-AMP and PKA that then phosphorylates tyrosines in proteins is a fundamental process in fertilization in a variety of species and a 23% homologous enzyme was noted in plasmodia.

CRISPR rescue of mutation in sodium GABA symporter

Homologue of a sodium GABA symporter has a likely functional mutation. This gene is overexpressed in merozoites. This mutation was rescued in the T-263 mutant successfully with Crispr cas9 as presented in Figure 10.

Protein structures in mutated gene candidates predicted by AlphaFold

AlphaFold version 2.0 colab has been used to predict the effect of mutations on structure and function of proteins listed in Table 4 including sodium GABA symporter (TGME49_208420), SAG-related sequence containing protein SRS 15C (TGME49_320230), AP2 domain containing transcription factor AP2V-2 (TGME49_285895), cAMP-dependent protein kinase (TGME49_209985), DNA directed DNA polymerase (TGME49_216140) and adenosine kinase (TGME_250880) from *Toxoplasma gondii*. AlphaFold2 interface that runs structure prediction pipeline is available at https://colab.research.google.com/github/sokrypton/ColabFold/blob/main/AlphaFold2.ipynb. AlphaFold code license is available at https://www.apache.org/licenses/LICENSE-2.0. Protein sequences for model predictions were downloaded from ToxoDBdatabase at https://toxodb.org/toxo/app. First 200 and 132 N-terminal residues comprising disordered region of the predicted sodium GABA_Tg symporter and DNA-directed DNA polymerase, respectively, were omitted from the sequence for the model prediction of the mutated variant. The structural comparison between predicted structures and their homologues was done using web servers DALI[215] and VAST.[205] Structure figures were made in graphical program CCP4mg.[218]

Bioinformatics, identification by stage associated expression, presence of mutations in natural isolates, PFAM, literature search and systems analysis that reveal capacitation pathway modulated by GABA

Initial stage specific expression of genes with mutations was determined. Meta data had been collected for 100 isolates. Analysis of those identified genes expressed in merozoites that were not found in any natural isolates used code for algorhithm at https://github.com/TriLab-bioinf/McLeod_T263_manuscript.

PFAM analysis was performed on these then AlphaFold2 as above. Each of those genes were searched in Google Google Scholar and PubMed using additional terms capacitation, conception, fertility, infertility which revealed genes associated with capacitation. These were also considered in the context of what is known about the *T. gondii* sexual cycle in the literature.[227–235]

QUANTIFICATION AND STATISTICAL ANALYSIS

All kinetic experiments were performed in duplicates. All statistical details could be found on Figures. No additional methods were used to determine whether the data met assumptions of the statistical approach.